

MARIE CURIE RESEARCH TRAINING NETWORK



SPICE



SEISMIC WAVE **P**ROPAGATION AND **I**MAGING
IN **C**OMPLEX MEDIA: A **E**UROPEAN NETWORK

COORDINATOR: HEINER IGEL

THE FINITE-DIFFERENCE METHOD FOR SEISMOLOGISTS

AN INTRODUCTION

BY

PETER MOCZO, JOZEF KRISTEK,
AND LADISLAV HALADA

COMENIUS UNIVERSITY
BRATISLAVA

The Finite-Difference Method for Seismologists

An Introduction

by

Peter MOCZO , Jozef KRISTEK ,
and Ladislav HALADA

Comenius University Bratislava
2004

Preparation of the publication was supported by the
Marie Curie Research Training Network SPICE Contract No MRTN-CT-2003-504267

© 2004, Peter Moczo, Jozef Kristek, Ladislav Halada

ISBN 80-223-2000-5

The Finite-Difference Method for Seismologists

An Introduction

by

Peter MOCZO

Professor of Physics; Faculty of Mathematics, Physics and Informatics, Comenius University
Bratislava, Slovak Republic

Jozef KRISTEK

Senior Researcher; Faculty of Mathematics, Physics and Informatics, Comenius University
Bratislava, Slovak Republic

Ladislav HALADA

Associate Professor of Mathematics; Institute of Informatics, Slovak Academy of Sciences
Bratislava, Slovak Republic

Reference:

Moczo, P., J. Kristek, and L. Halada, 2004. The Finite-Difference Method for Seismologists. An Introduction. *Comenius University, Bratislava*.
(ISBN: 80-223-2000-5)

Available at:

<http://www.spice-rtn.org>

<ftp://ftp.seismology.sk/pub/papers/FDM-Intro-SPICE.pdf>

Contents

Preface.....	vii
Introduction.....	1
A Brief Introduction	1
The Principle of the Finite-difference (FD) Method	3
Grid	3
The FD Approximations to Derivatives	4
Properties of the FD Equation	7
Explicit and Implicit FD Schemes	9
Homogeneous and Heterogeneous FD Schemes.....	9
Formulations of the Equations, Grids and FD Schemes	10
1D Elastic Problem	13
Coordinate System and Basic Quantities.....	13
Equation of Motion and Hooke's Law	13
Velocity-stress FD Schemes.....	14
Von Neumann's Analysis of Stability.....	22
Material Grid Parameters.....	29
Staggered-grid FD Schemes – A Summary	30
Contact of Two Media – A Material Discontinuity.....	33
Welded interface between two halfspaces	35
Simple physical model	36
Heterogeneous formulation of the equation of motion and Hooke's law	39
Heterogeneous FD schemes	40
Free Surface.....	43
Wave Excitation	46
Boundaries of the Grid	47
Incorporation of the Realistic Attenuation	51
Stress-Strain Relation in Viscoelastic Medium	51
Conversion of the Convolutory Stress-Strain Relation into a Differential Form.....	54

The GZB and GMB-EK Rheological Models	55
GMB-EK.....	58
GZB.....	59
The Relation between the GZB and GMB-EK.....	60
Introduction of the Anelastic Functions	62
Equations for the 1D Case – A Summary	66
An FD Scheme for the Anelastic Functions	67
Contact of Two Viscoelastic Media – A Material Discontinuity.....	69
FD Schemes for the 1D Case – A Summary	70
Equations and Considerations for the 3D Case	72
Notes on the accuracy and computational efficiency	74
 Program Package 1DFD.....	 77
Introduction.....	77
Program 1DFD_DS.....	79
Program 1DFD_DVS	87
Program 1DFD_VS.....	95
Program MODEL_PREP_1D.....	103
Program SOURTF	109
 Numerical Examples	 113
Unbounded Homogeneous Elastic Medium.....	113
Single Layer over Halfspace	121
Unbounded Homogenous Viscoelastic Medium.....	129
 References	 139

Preface

The primary goal of the presented text is to provide basics of the finite-difference method and its application to the numerical modeling of seismic wave propagation and earthquake motion. The text was written for participants of the Research and Training Workshop of the Marie Curie Research Training Network SPICE held in Venice, Italy, September 25 – October 2, 2004. It may be useful also for seismologists who are not familiar with the finite-difference method, or those who are interested in some particular topics explained and analyzed in the text.

This introduction covers neither all aspects of the finite-difference method nor all applications of the method in seismology. It is focused primarily on the 1D problem. The 1D problem itself is not fully analyzed. The references probably do not include all relevant contributions, though we tried to include many of them.

It is important to realize that the understanding of the 1D problem is just the beginning. It is, however, important and useful because it considerably helps in learning the full 3D problem.

The text also contains a user's guide to the FORTRAN 95 program package 1DFD which is intended as a training tool for beginners in development and application of the finite-difference method. Numerical examples – model configurations, input data, and results – are also included.

Though the text is introductory, it includes some material which probably cannot be found elsewhere.

We would like to stress at the very beginning that a user of the finite-difference method should understand basics of the method. Many computer codes based on the method almost always give some results but not necessarily results which are reasonable, sufficiently accurate or at the level of the state-of-the-art.

The user of the finite-difference method and particularly of some available computer codes should not be misled by the user-friendly simplicity of the algorithm, code and input-data preparation. The ease in using a particular code cannot guarantee sufficient quality.

Therefore, users of the finite-difference method should be aware of both, advantages and problems of the method.

Introduction

A Brief Introduction

The Earth's interior is considerably laterally heterogeneous with complex geometry of the interfaces between different material layers and blocks as well as smoothly spatially varying material parameters inside the layers and blocks. Analytical methods do not provide solutions of the equation of motion (elastodynamic equation) for complex or sufficiently realistic models of the Earth's interior. Therefore, approximate numerical methods have to be used. A numerical method transforms an original differential problem into a system of algebraic equations. In the numerical method, a continuous function in the differential equation has to be represented by a finite set of numbers. The set of numbers has to be stored in a computer memory. Each numerical method is specific in a way how it represents a solution using a finite set of numbers and how it approximates derivatives.

In modeling seismic wave propagation and seismic motion, a numerical method should allow for heterogeneity of the medium (including material discontinuities and gradients), realistic attenuation (to account for attenuation), free-surface topography, and sufficient frequency range. In modeling the earthquake faulting, a numerical method should also allow for realistic geometry of the fault surface, heterogeneity of the initial stress, and friction law. At the same time, a numerical method has to be computationally efficient (efficient in terms of the computer memory and time). One can intuitively guess that there is hardly one single method which would be the best from the point of view of all the above requirements. The choice of the suitable numerical method should be, in general, a problem-dependent.

The finite-difference method belongs to the so-called grid-point methods. In the grid-point methods a computational domain is covered by a space-time grid and each function is represented by its values at grid points. The space-time distribution of the grid points may be, in principle, arbitrary, but it significantly affects the accuracy of the approximation. Usually, no assumption is made about the values in-between the grid points. A derivative of a function is approximated by the so-called finite-difference formula which uses values of the function at a specified set of the grid points.

It is useful to understand the basics of the finite-difference method even if one does not use the method to solve the differential equation. This is because the time-dependence of the functions is often approximated by the finite-difference formulas also in other numerical methods.

Due to its definition, the finite-difference method is one of the most important numerical methods in seismology and certainly still dominant method in earthquake ground motion modeling. In particular, this is due to the fact, that, formally it is applicable to complex models, relatively accurate and computationally efficient. Moreover, it is relatively easy to encode. Because the finite-difference operators are local, the method enables parallelization.

At the same time, many users, especially those who are not familiar with the method, overestimate the accuracy of the very simple finite-difference schemes because they are not aware of the properties and limitations of the method. Moreover, due to inherent limitations of the method, mainly the difficulty to implement boundary conditions, its application to complex models still requires much more elaboration.

Many users decide for one of relatively many finite-difference schemes and corresponding computer codes simply because they find the code simpler for the use than other codes (for example in terms of the theory behind or simplicity of the model preparation). Some of them do not realize that friendly or simply looking features of the finite-difference scheme and the computer code may be far from the sufficiently accurate modeling for a given problem.

If the finite-difference method is used as the black-box method, which, unfortunately, is not so unusual case, the method can give considerably inaccurate results.

More detailed introduction into the finite-difference method as well as a systematic exposition of the method for solving different types of the differential problem can be found in the mathematical textbooks or the topic-oriented monographs as, for example, Forsythe and Wasow (1960), Isaacson and Keller (1966), Richtmyer and Morton (1967), Mitchell and Griffiths (1994), Morton and Mayers (1994), Durrant (1999).

An introductory text on the application of the FD method to the seismic wave propagation and seismic motion modeling can be found in Moczo (1998).

In this text we will include only **the time-domain finite-difference modeling**. An alternative approach, the frequency-domain finite-difference modeling, has not become so widely used in seismology.

The Principle of the Finite-difference (FD) Method

The application of the method to a particular differential problem includes the following steps:

- a. Construction of a discrete finite-difference model of the problem:
 - coverage of the computational domain by a space-time grid,
 - approximations to derivatives, functions, initial and/or boundary condition - all at the grid points,
 - construction of a system of the finite-difference (i.e., algebraic) equations
- b. Analysis of the finite-difference model:
 - consistency and order of the approximation
 - stability
 - convergence
- c. Numerical computations

Grid

Consider a computational domain in the four-dimensional space of variables (x, y, z, t) . Cover this space by a **grid** of discrete points

$$(x_I, y_K, z_L, t_m)$$

given by

$$x_I = x_0 + I\Delta x, \quad y_K = y_0 + K\Delta y, \quad z_L = z_0 + L\Delta z, \quad t_m = t_0 + m\Delta t,$$

$$\begin{aligned} I, K, L &= 0, \pm 1, \pm 2, \dots \\ m &= 0, 1, 2, \dots \end{aligned}$$

Here, Δx , Δy and Δz are usually called **grid spacings**, and Δt is called **time step** since t usually represents time. If x, y and z are Cartesian coordinates, the corresponding spatial grid is a rectangular grid.

At the grid points a function $u(x, y, z, t)$ is to be approximated by a grid function $U(x_I, y_K, z_L, t_m)$. A value of $u(x_I, y_K, z_L, t_m)$ can be denoted by $u_{I,K,L}^m$ while approximation to $u_{I,K,L}^m$ can be denoted by $U_{I,K,L}^m$.

A spatial grid that is the most appropriate for the problem under consideration should be chosen. In many applications, the **regular (uniform) rectangular grid** with the grid spacings $\Delta x = \Delta y = \Delta z = h$ is a natural and reasonable choice. Other types of grids, including **non-uniform** grids, for example, grids with a varying size of the grid spacing, discontinuous or combined grids with sudden change in size of the grid spacing, are used if they better accommodate geometry of the problem (e.g., shapes of material discontinuities) or if they simplify the finite-difference approximations to derivatives. We also recognize **structured** and **unstructured** grids. At a grid point of the structured grids we always know the neighboring grid points (for example, using some mathematical rule). At each grid point of the unstructured grid we need some additional information about the neighboring grid points.

The FD Approximations to Derivatives

Consider a function $\Phi(x)$ which has a continuous first derivative. Then the following three expressions for the first derivative will give the same value of the derivative:

$$\begin{aligned}\frac{d\Phi}{dx}(x_0) &= \lim_{h \rightarrow 0} \frac{\Phi(x_0 + h) - \Phi(x_0)}{h} \\ \frac{d\Phi}{dx}(x_0) &= \lim_{h \rightarrow 0} \frac{\Phi(x_0) - \Phi(x_0 - h)}{h} \\ \frac{d\Phi}{dx}(x_0) &= \lim_{h \rightarrow 0} \frac{\Phi(x_0 + h) - \Phi(x_0 - h)}{2h}.\end{aligned}\tag{1}$$

Because, however, in the finite-difference grid the size of h is bounded by the size of the grid spacing (distance between two neighboring grid points in the x -direction in this case), the limits cannot be evaluated and a difference between the functional values at the grid points divided by the distance between the two points only approximates the value of the derivative. Obviously, in general, the three differences (finite differences or finite-difference formulas) will give different approximate values for the same derivative. Moreover, the use of a particular difference formula leads to a particular finite-difference (algebraic) equation.

While the two approximations, the so-called **forward-difference formula**

$$\frac{d\Phi}{dx}(x_0) \doteq \frac{\Phi(x_0 + h) - \Phi(x_0)}{h} \quad (2)$$

and the so-called **backward-difference formula**

$$\frac{d\Phi}{dx}(x_0) \doteq \frac{\Phi(x_0) - \Phi(x_0 - h)}{h} \quad (3)$$

are the 1st-order approximations to the first derivative, the **central-difference formula**

$$\frac{d\Phi}{dx}(x_0) \doteq \frac{\Phi(x_0 + h) - \Phi(x_0 - h)}{2h} \quad (4)$$

is the 2nd-order approximation to the first derivative (because it is centered about the point at which the derivative is approximated). The three formulas can be easily obtained using Taylor expansions of functional values $\Phi(x_0 + h)$ and $\Phi(x_0 - h)$ about the point x_0 . The order of approximation is determined by the **truncation error** (approximation error). For example, the 2nd-order approximation means that the leading term of the truncation error is proportional to h^2 .

It is possible to find higher-order approximations to derivatives. The procedure may be as follows (for example, Durran 1999):

1. Choose the derivative (for example, the first derivative).
2. Choose the grid points around the grid point at which the derivative is to be approximated (for example, x_0 - grid point at which the derivative is to be approximated, $x_0 - 2\Delta x, x_0 - \Delta x, x_0 + \Delta x, x_0 + 2\Delta x$ - grid points you want to use to approximate the derivative).
3. Choose the order of the approximation (for example, the 4th-order).
In the chosen example, this means that the approximation should be

$$\begin{aligned} \Phi'(x_0) = & \\ & a \Phi(x_0 + 2\Delta x) + b \Phi(x_0 + \Delta x) + c \Phi(x_0) + d \Phi(x_0 - \Delta x) + e \Phi(x_0 - 2\Delta x) \quad (5) \\ & + O[(\Delta x)^4] \end{aligned}$$

with the unknown coefficients a, b, c, d, e . The coefficients have to be determined so that the sum on the right-hand side eliminates all derivatives except the first derivative of function $\Phi(x)$.

4. Write down a Taylor expansion for a point whose position differs from x_0 by increment h :

$$\Phi(x_0 + h) = \Phi(x_0) + h \Phi'(x_0) + \frac{h^2}{2} \Phi''(x_0) + \frac{h^3}{6} \Phi'''(x_0) + \frac{h^4}{24} \Phi''''(x_0) + O[h^5] . \quad (6)$$

5. Apply $2\Delta x, \Delta x, 0, -\Delta x, -2\Delta x$ as values of h and construct a table

<i>coefficient</i>	<i>value of h</i>	h^0	h^1	$h^2 / 2$	$h^3 / 6$	$h^4 / 24$
a	$2\Delta x$	1	2	4	8	16
b	Δx	1	1	1	1	1
c	0	1	0	0	0	0
d	$-\Delta x$	1	-1	1	-1	1
e	$-2\Delta x$	1	-2	4	-8	16

6. Equate coefficients for equal powers of the argument increment and get equations for the unknown coefficients:

$$\begin{aligned} h^0 & : a + b + c + d + e = 0 \\ h^1 & : 2a + b - d - 2e = 1/\Delta x \\ h^2 / 2 & : 4a + b + d + 4e = 0 \\ h^3 / 6 & : 8a + b - d - 8e = 0 \\ h^4 / 24 & : 16a + b + d + 16e = 0 \end{aligned} \quad (7)$$

7. Solve the system of equations and get

$$a = -\frac{1}{12\Delta x} \quad b = \frac{2}{3\Delta x} \quad c = 0 \quad d = -\frac{2}{3\Delta x} \quad e = \frac{1}{12\Delta x} . \quad (8)$$

The finite-difference formula (5) can be written in the form

$$\begin{aligned} \Phi'(x_0) = & \\ & \frac{1}{\Delta x} \left\{ -\frac{1}{12} [\Phi(x_0 + 2\Delta x) - \Phi(x_0 - 2\Delta x)] + \frac{2}{3} [\Phi(x_0 + \Delta x) - \Phi(x_0 - \Delta x)] \right\} . \quad (9) \\ & + O[(\Delta x)^4] \end{aligned}$$

For higher-order FD approximations and FD approximations on arbitrary spaced grids see also Dablain (1986) and Fornberg (1988), respectively.

Properties of the FD Equation

The objective of the finite-difference method for solving an ordinary differential equation (ODE) or a partial differential equation (PDE) is to transform ODE or PDE into a finite-difference equation (FDE, also FD scheme) or a system of FDE (i.e., to approximate ODE/PDE by FDE).

The most important properties of the FDE are consistency, stability and convergence. These notions cover different aspects of the relation between the PDE and FDE, and the exact and numerical solutions of the PDE.

First, consider the concept of consistency. Because the FDE is only an approximation to the PDE, the following property is required.

*An FDE is **consistent** with a PDE if the difference between the FDE and the PDE (i.e., the truncation error) vanishes as the sizes of the time step and spatial grid spacing go to zero independently.*

Note that no conditions on the time step and spatial grid spacing are required. The statement can be briefly written as

$$|PDE - FDE| \rightarrow 0 \quad \text{if} \quad \Delta t \rightarrow 0, \quad h \rightarrow 0 . \quad (10)$$

It may happen that the above condition is fulfilled only when certain relationship is satisfied between the size of the time step and the spatial grid spacing. We will say in such a case that the FDE is **conditionally consistent**. Obviously, if the truncation errors of the finite difference approximation to the exact derivatives in the PDE are known, then the proof of consistency is straightforward.

Next, consider the concept of stability. If the exact solution of the PDE is unbounded, then the numerical solution must be unbounded too. If the exact solution of the PDE is bounded, it is reasonable to require that the numerical solution will be bounded too. Therefore, the concept of the stability can be defined as follows.

*An FDE is **stable** if it produces a bounded solution when the exact solution is bounded, and is **unstable** if it produces an unbounded solution when the exact solution is bounded.*

Briefly speaking, we know that the solution of the most physical problems is bounded. This can be proved analytically. Therefore, in such cases the solution of the FDE also must be bounded. If the solution of the FDE is bounded for all values of the grid spacing, then the FDE is **unconditionally stable**. If the solution of the FDE is bounded only for certain values of the grid spacing, then the FDE is **conditionally stable**. The worst case is the last possibility: if the solution of the FDE is unbounded for all values of the grid spacing then the FDE is **unconditionally unstable**.

The stability analysis can be performed only for a linear PDE. A nonlinear PDE must be first linearized locally. The FDE of the linearized PDE can be analyzed for stability. The most used method for the stability analysis is the von Neumann method.

The last analyzed property of the FDE is the convergence.

*An FDE is **convergent** if the solution of the FDE approaches the exact solution of the PDE as the sizes of the time step and spatial grid spacing go to zero independently.*

Let us denote the solutions obtained by the PDE and FDE as u_{PDE} and u_{FDE} , respectively. Then the convergence property can be expressed as

$$|u_{PDE} - u_{FDE}| \rightarrow 0 \quad \text{if} \quad \Delta t \rightarrow 0, h \rightarrow 0. \quad (11)$$

Note that consistency is property of the FDE. It relates the FDE to the PDE. The stability and convergence are properties of the numerical solution of the FDE. They relate to the method (scheme, algorithm) used to obtain the numerical solution. This is an important difference between the consistency on one hand, and the stability and convergence on the other.

The proof of the convergence of an FDE solution is not a trivial problem, in general. Fortunately, the convergence is related to the consistency and the stability. It follows from **Lax equivalence theorem** that if the FDE is consistent and stable, then

the finite-difference method is convergent. Thus, the proof of the consistency and the stability is a sufficient condition for the convergence of an FDE solution.

Further, we will use FD scheme instead of FDE.

Explicit and Implicit FD Schemes

In general, an FD scheme solving the equation of motion may be explicit or implicit. In the explicit schemes, the function (motion) at a given spatial grid point and time level is calculated only from the functional values (motion) at previous time levels and coefficients (material grid parameters). In the implicit schemes, the function at a given time level is calculated simultaneously at all spatial grid points from the functional values at previous time levels and coefficients using an inverse matrix. As pointed out, e.g., already by Kelly et al. (1976), the explicit schemes are computationally simpler. For example, all recent earthquake ground motion modeling studies use the explicit FD schemes.

Homogeneous and Heterogeneous FD Schemes

Motion in a smoothly heterogeneous elastic or viscoelastic continuum is governed by the equation of motion. The equation can be solved by a proper finite-difference scheme.

As already mentioned, models of the Earth's interior and surface geological structures have to include layers/blocks of different materials and thus also interfaces between them (that is, material discontinuities). If the medium contains a material discontinuity, i.e., an interface between two homogeneous or smoothly heterogeneous media, at which density and elastic moduli change discontinuously, the equation of motion still governs motion outside the discontinuity but boundary conditions apply at the discontinuity. Then a natural or, say, classical approach is to apply

- a) an FD scheme for the smoothly heterogeneous medium at grid points outside the material discontinuity,
- b) an FD scheme obtained by a proper discretization of the boundary conditions at grid points at or near the material discontinuity.

Such an approach is called **homogeneous**. As already stressed by Boore (1972) and Kelly et al. (1976), a homogeneous FD scheme is specific for a particular problem. While it may be suitable for simple geometry of the material discontinuities, its application to complex models with curved material discontinuities is difficult and

therefore impractical. In any case, the approach requires stable and sufficiently accurate FD approximation to the boundary conditions which, in fact, is not a trivial problem.

In the alternative **heterogeneous** approach only one FD scheme is used for all interior grid points (points not lying on boundaries of a grid), no matter what their positions are with respect to the material discontinuity. The presence of the material discontinuity is accounted for only by values of elastic moduli and density. Therefore, the heterogeneous approach has been much more popular since the beginning of seventies. There are, however, two fundamental questions in the heterogeneous approach:

- 1) Is the heterogeneous approach justified? In other words, is it possible to find a heterogeneous formulation of the equation of motion, that is, the same form of the equation both for a point outside the material discontinuity and for a point at the material discontinuity?
- 2) How should values be of the material parameters at grid points at and near the discontinuity determined? Strictly speaking, this question has sense only if there is a positive answer to the first question.

Because recent seismology has to address structurally as realistic models of the Earth's interior as possible, the problem of the heterogeneous FD schemes is of the fundamental importance. Surprisingly, it has not been addressed correspondingly until very recently. We will review the history of development in this respect later.

Formulations of the Equations, Grids and FD Schemes

The equation of motion and Hooke's law (the stress-strain relation, constitutive law) together with the initial and/or boundary conditions fully describe a problem of seismic wave propagation and motion. If we keep the equation of motion separately from Hooke's law, we can speak of the **displacement-stress** formulation. If we use particle velocity in the equation of motion, keep Hooke's law, and add the definition of the particle velocity, we get the **displacement-velocity-stress** formulation. If we apply time derivative to Hooke's law (instead of adding the particle-velocity definition), we have the **velocity-stress** formulation. In the fourth alternative we eliminate the stress-tensor components by inserting Hooke's law into the equation of motion. We obtain **displacement** formulation – the only one of the four with the second spatial derivatives.

The most natural choice of the FD grid for the displacement formulation is the **conventional** grid in which all displacement and body-force components are located at each grid point. The most natural choice for the three other formulations is the **staggered** grid in which each displacement/particle-velocity component and each shear

stress-tensor component has its own grid position. The only but easily understandable exception is the same grid position for the three diagonal stress-tensor components.

There are particular applications, e.g. anisotropic media or source dynamics, in which different grid positions for different stress-tensor components pose a considerable problem. Therefore, a **partly-staggered** grid has been also used. In this type of grid all displacement components share the same grid position and all the stress-tensor components share some other grid position.

The conventional grid had been used for more than ten years (for example, Alterman and Karal 1968, Kelly et al. 1976, and many others). The conventional-grid displacement FD schemes had problems with instabilities and grid dispersion in media with high Poisson's ratio. The staggered grid was introduced by Madariaga (1976) who used it for the dynamic modeling of the earthquake rupture. A major progress in modeling of seismic wave propagation was done by Virieux (1984, 1986) who applied the staggered grid to the wave propagation problem. Bayliss et al. (1986) and Levander (1988) introduced the 4th-order staggered-grid FD schemes which are in 2D four times and in 3D eight times less memory requiring than the 2nd-order schemes. The staggered-grid FD schemes have become the dominant type of schemes in the 3D FD modeling of seismic wave propagation and earthquake motion – for example Olsen and Schuster (1992), Graves (1993), Rodrigues (1993), Yomogida and Etgen (1993),

Luo and Schuster (1990) suggested a parsimonious staggered-grid FD scheme for the P-SV wave, that is, the displacement-stress FD scheme. The displacement-stress scheme in 3D needs only 75% of the memory required by the velocity-stress FD scheme because the stress-tensor components are temporary quantities which are not stored in core memory. The displacement-stress FD scheme was then used by Rodrigues (1993), and Yomogida and Etgen (1993) who used the 8th-order approximation in space. Ohminato and Chouet (1997) applied the 2nd-order while Moczo et al. (2000, 2002) the 4th-order approximations.

Saenger et al. (2000) and Saenger and Bohlen (2004) have recently promoted the use of the partly-staggered grid to account for heterogeneity and anisotropy. They called the grid rotated staggered grid because they obtained the FD spatial operator by the rotation of the standard staggered-grid operator. The term 'rotated staggered grid' can be a little bit misleading. If we assume one spatial grid position for the stress tensor and other position for the displacement vector, it is possible to find a variety of FD schemes - depending on the order of approximation. Only in one particular case the spatial FD operator can be obtained by the rotation of the standard staggered-grid operator, though it is also easy to obtain it without explicit consideration of the rotation.

In seismology, the partly-staggered grid was probably first used by Andrews (1973) in his traction-at-split-node method for the fault rupture. Magnier et al. (1994) used the same grid as Andrews (1973) to develop an alternative (to the standard staggered-grid)

FD approximation to the spatial derivatives. Their intention was to solve limitations of the staggered grid FD schemes in the anisotropic media. Later, Zhang (1997) used the partly-staggered grid in his 2D velocity-stress FD modeling.

While the reason to use the partly-staggered grid for the anisotropic media is obvious (all stress-tensor components located at the same grid position), the application of the grid to heterogeneous media requires more elaboration.

Cruz-Atienza and Virieux (2004) applied an FD scheme for the partly-staggered grid to a problem of rupture propagation in 2D.

The rectangular grid with a varying size of the grid spacings was first used by Boore (1970) in the 1D case. Mikumo and Miyatake (1987) used a grid with varying size of the grid spacing in the 3D case in a homogeneous medium. Moczo (1989), and Moczo and Bard (1993) applied the grid to the SH case in the laterally heterogeneous medium. The use of the spatial grid with varying size of the grid spacing in 3D was then promoted by Pitarka (1999) in the 4th-order staggered-grid velocity-stress modeling, and by Opršal and Zahradník (1999) in the 2nd-order conventional-grid displacement formulation.

Jastram and Behle (1992), Falk et al. (1996), Moczo et al. (1996), Robertsson and Holliger (1997), Kristek et al. (1999), Aoi and Fujiwara (1999), and Hayashi et al. (2001) introduced discontinuous grids. A clever approach to combine two grids with different size of grid spacings was presented by Wang et al. (2001).

In fact, the concept of the discontinuous grid is not restricted to the spatial grid. Falk et al. (1998) and Tessmer (2000) introduced a combined grid whose one part is solved using a smaller time step and the other by a larger time step. Kang and Baag (2004a,b) combined the concepts of spatial discontinuous grid and variable time step. They developed an efficient velocity-stress 2D and 3D velocity-stress FD schemes in which smaller time step is used in the finer spatial grid and larger time step in the three times coarser spatial grid. The proportionality of the time step to the grid spacing is due to the overlapping of the two grids in medium with a higher speed. An advantage of the approach by Kang and Baag (2004a,b) is that a finer grid can cover a rectangular region which may have a planar free surface. This makes it possible to efficiently model sedimentary basins or other localized surface soft inclusions.

Let us at least briefly mention the approach of Geller and his co-workers although it deserves, in fact, a special chapter. Geller and Takeuchi (1995) developed a general criterion for optimally accurate numerical operators. The criterion was a basis for an optimally accurate time-domain FD scheme for 1D problem presented by Geller and Takeuchi (1998). Takeuchi and Geller (2000) then developed optimally accurate time-domain FD operators for 2D and 3D problems.

1D Elastic Problem

Coordinate System and Basic Quantities

Although we start with the 1D problem here, we can specify a 3D coordinate system. In most cases a Cartesian coordinate system (x_1, x_2, x_3) is used, possibly with the x_1 -axis horizontal and positive to the right, and the x_3 -axis positive downward. Let $\rho(x_i)$; $i \in \{1, 2, 3\}$ be density, $\kappa(x_i)$ bulk modulus, and $\mu(x_i)$ shear modulus. Alternatively, moduli $\lambda(x_i)$ and $\mu(x_i)$ may be used. Let $\vec{u}(x_i, t)$ be displacement vector, t time, $\vec{f}(x_i, t)$ body force per unit volume, $\tau_{ij}(x_k, t)$; $i, j, k \in \{1, 2, 3\}$ stress-tensor, and $\varepsilon_{ij}(x_k, t)$; $i, j, k \in \{1, 2, 3\}$ strain-tensors. (Further, x_1, x_2, x_3 and x, y, z will be used interchangeably; similarly, 1, 2, 3 and x, y, z in the subscripts of the stress-tensor components.) Here we use τ for the stress. In the chapter on viscoelastic medium we will use σ instead.

Equation of Motion and Hooke's Law

Consider a perfectly elastic isotropic medium with density ρ and Lamé's elastic coefficients μ and λ being continuous functions of x . Then a plane wave propagation in the x -direction is described by the equation of motion and Hooke's law in the

displacement-stress formulation

$$\rho \ddot{d} = \tau_{,x} + f \quad , \quad \tau = C d_{,x} \quad (12)$$

where either $d(x, t)$ is the x -component of the displacement $\vec{u}(d, 0, 0)$, $\tau(x, t)$ the xx -component of the stress tensor, $f(x, t)$ the x -component of the body force per unit volume $\vec{f}(f, 0, 0)$ and $C(x) = \lambda(x) + 2\mu(x)$ in the case of P wave, or $d(x, t)$ is the y -component of the displacement $\vec{u}(0, d, 0)$, $\tau(x, t)$ the xy -component of the stress tensor, $f(x, t)$ the y -component of the body force per unit volume $\vec{f}(0, f, 0)$ and

$C(x) = \mu(x)$ in the case of the SH wave (since the coordinate system can always be rotated so that the S wave could be the SH wave). The dot above the symbol means the time derivative. The subscript x in $\tau_{,x}$ and $d_{,x}$ means the spatial derivative.

As already indicated, the two equations (12) can be called the displacement-stress formulation of the equation of motion and the stress-strain relation. In developing a FD scheme for some problems it may be more advantageous to use one of the alternative formulations:

displacement-velocity-stress formulation

$$\rho \dot{v} = \tau_{,x} + f \quad , \quad v = \dot{d} \quad , \quad \tau = C d_{,x} \quad (13)$$

velocity-stress formulation

$$\rho \dot{v} = \tau_{,x} + f \quad , \quad \dot{\tau} = C v_{,x} \quad (14)$$

displacement formulation

$$\rho \ddot{d} = (C d_{,x})_{,x} + f \quad (15)$$

with v denoting the particle velocity.

Velocity-stress FD Schemes

Equations (12) - (15) can be solved by the finite-difference method. Let h and Δt be the grid spacing and time step. Let D_I^m , V_I^m , T_I^m and F_I^m be the discrete approximations to $d_I^m = d(Ih, m\Delta t)$, $v_I^m = v(Ih, m\Delta t)$, $\tau_I^m = \tau(Ih, m\Delta t)$ and $f_I^m = f(Ih, m\Delta t)$.

Consider first the velocity-stress formulation (14) and omit for simplicity the body-force term:

$$\dot{v} = \frac{1}{\rho} \tau_{,x} \quad , \quad \dot{\tau} = C v_{,x} \quad (16)$$

Here we closely follow the example given by Aki and Richards (1980). In addition to the example, we will also explain the von Neumann's method of the stability analysis.

Denoting also $\rho_I = \rho(Ih)$ and $C_I = C(Ih)$, using the forward difference formula for the time derivative and the central difference formula for the spatial derivative we can approximate equations (16) by the following FD scheme:

$$\frac{1}{\Delta t} (V_I^{m+1} - V_I^m) = \frac{1}{\rho_I} \frac{1}{2h} (T_{I+1}^m - T_{I-1}^m), \quad (17)$$

$$\frac{1}{\Delta t} (T_I^{m+1} - T_I^m) = C_I \frac{1}{2h} (V_{I+1}^m - V_{I-1}^m). \quad (18)$$

It is easy to check consistency of the scheme in the homogeneous medium. Check, for example, equation (17). Consider FD and differential operators

$$L_\Delta = \frac{1}{\Delta t} (v_I^{m+1} - v_I^m) - \frac{1}{\rho_I} \frac{1}{2h} (\tau_{I+1}^m - \tau_{I-1}^m),$$

$$L = \dot{v}(Ih, m\Delta t) - \frac{1}{\rho_I} \tau_{,x}(Ih, m\Delta t).$$

Substituting Taylor's expansions for v_I^{m+1} , v_I^m , τ_{I+1}^m and τ_{I-1}^m about $(Ih, m\Delta t)$ in L_Δ we get

$$L_\Delta = \dot{v}(Ih, m\Delta t) - \frac{1}{\rho_I} \tau_{,x}(Ih, m\Delta t) + O(\Delta t) + O(h^2)$$

and

$$L - L_\Delta = -O(\Delta t) - O(h^2) \rightarrow 0 \quad \text{when} \quad h, \Delta t \rightarrow 0.$$

Similarly we could check consistency of equation (18).

The FD scheme given by equations (17) and (18) is consistent with the differential equations (16). The scheme is 1st-order accurate in time and 2nd-order accurate in space.

Let us check now stability of the scheme. Assume V and T in the form

$$T_I^m = A \exp(-i\omega m\Delta t + i k Ih) \quad (19)$$

and

$$V_I^m = B \exp(-i\omega m\Delta t + i k I h) \quad (20)$$

and investigate their propagation in the grid. Substitute equations (19) and (20) into the FD equations (17) and (18):

$$\begin{aligned} B [\exp(-i\omega\Delta t) - 1] &= \frac{\Delta t}{2\rho_I h} A 2i \sin kh, \\ A [\exp(-i\omega\Delta t) - 1] &= \frac{C_I \Delta t}{2h} B 2i \sin kh. \end{aligned}$$

Eliminating B and A gives

$$\begin{aligned} [\exp(-i\omega\Delta t) - 1]^2 &= -\frac{C_I}{\rho_I} \left(\frac{\Delta t}{h}\right)^2 (\sin kh)^2, \\ \exp(-i\omega\Delta t) &= 1 \pm i \left(\frac{C_I}{\rho_I}\right)^{1/2} \frac{\Delta t}{h} \sin kh, \\ |\exp(-i\omega\Delta t)| &= \left| 1 \pm i \left(\frac{C_I}{\rho_I}\right)^{1/2} \frac{\Delta t}{h} \sin kh \right| > 1. \end{aligned}$$

It follows from the inequality that ω is complex. This means that the assumed solution grows exponentially with time. In other words, the FD scheme given by equations (17) and (18) is unstable.

Try now to approximate \dot{v} and $\dot{\tau}$ in equations (16) by the central-difference formula. We obtain

$$\frac{1}{2\Delta t} (V_I^{m+1} - V_I^{m-1}) = \frac{1}{\rho_I} \frac{1}{2h} (T_{I+1}^m - T_{I-1}^m) \quad (21)$$

and

$$\frac{1}{2\Delta t} (T_I^{m+1} - T_I^{m-1}) = C_I \frac{1}{2h} (V_{I+1}^m - V_{I-1}^m). \quad (22)$$

The spatial positions of the particle velocity and stress are illustrated in Figure 1.

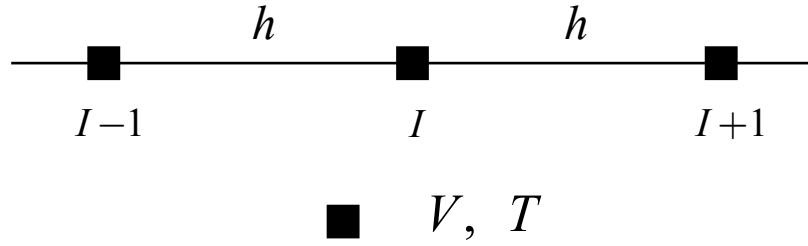


Figure 1. Conventional spatial grid for the velocity-stress FD scheme (21)-(22); positions of the particle velocity V and stress T .

Substitute equations (19) and (20) into the FD equations (21) and (22), and obtain

$$\begin{aligned}
 -i 2B \sin \omega \Delta t &= \frac{\Delta t}{\rho_I h} A 2 i \sin k h \\
 -i 2A \sin \omega \Delta t &= \frac{C_I \Delta t}{h} B 2 i \sin k h \\
 (\sin \omega \Delta t)^2 &= \frac{C_I}{\rho_I} \left(\frac{\Delta t}{h} \right)^2 (\sin k h)^2 \\
 \sin \omega \Delta t &= \pm \left(\frac{C_I}{\rho_I} \right)^{1/2} \frac{\Delta t}{h} \sin k h .
 \end{aligned}$$

Assume now that

$$\left(\frac{C_I}{\rho_I} \right)^{1/2} \frac{\Delta t}{h} \leq 1.$$

Then

$$|\sin \omega \Delta t| \leq 1$$

and consequently ω is real. This means that the assumed solutions (19) and (20) do not grow with time. The FD scheme given by equations (21) and (22) is stable under condition

$$\Delta t \leq \frac{h}{c_I} \tag{23}$$

where

$$c_I = \left(\frac{C_I}{\rho_I} \right)^{1/2}.$$

Condition (23) is called the **stability condition**.

The FD scheme given by equations (21) and (22) is the velocity-stress FD scheme on a conventional grid. In view of the common FD schemes and the scheme's properties such a scheme is not the most natural and certainly not the best – as it will be clear from the further exposition.

Try now to use the central-difference formula over smaller grid distances - h and Δt instead of $2h$ and $2\Delta t$, respectively. We get first

$$\frac{1}{\Delta t} (V_I^{m+1/2} - V_I^{m-1/2}) = \frac{1}{\rho_I} \frac{1}{h} (T_{I+1/2}^m - T_{I-1/2}^m). \quad (24)$$

The approximation leads to the **staggered-grid FD scheme**: the grid position for T is shifted with respect to the grid position for V by $h/2$ in space and by $\Delta t/2$ in time. Then equation (24) implies

$$\frac{1}{\Delta t} (T_{I+1/2}^m - T_{I+1/2}^{m-1}) = C_{I+1/2} \frac{1}{h} (V_{I+1}^{m-1/2} - V_I^{m-1/2}). \quad (25)$$

The spatial positions of the particle velocity and stress are illustrated in Figure 2.

The differencing over twice smaller grid distances implies that the leading term of the approximation error is now four times smaller than that in the scheme given by equations (21) and (22). In this case the stability analysis gives the relation

$$\sin \frac{\omega \Delta t}{2} = \left(\frac{C_{I+1/2}}{\rho_I} \right)^{1/2} \frac{\Delta t}{h} \sin \frac{k h}{2}. \quad (26)$$

This means that the stability condition is the same as for the scheme given by equations (21) and (22).

The physical meaning of the stability condition (23) is clear: The time step cannot be larger than the time necessary for any disturbance to propagate over the distance h .

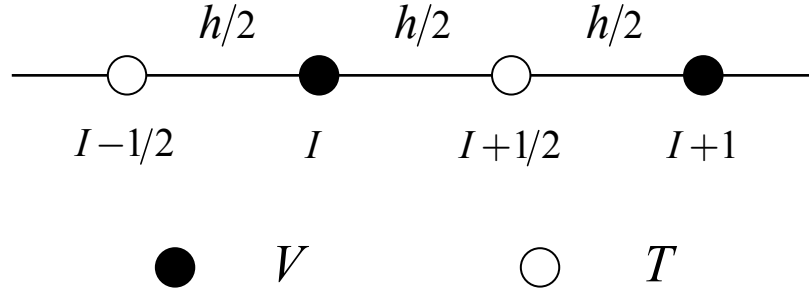


Figure 2. Staggered spatial grid for the velocity-stress FD scheme (24)-(25); positions of the particle velocity V and stress T .

Investigate now equation (26) since it gives the relation between ω and k (angular frequency and wavenumber). Assume Δt and h small enough for the approximations

$$\sin \frac{\omega \Delta t}{2} \doteq \frac{\omega \Delta t}{2} \quad , \quad \sin \frac{k h}{2} \doteq \frac{k h}{2} \quad .$$

Then it follows from (26) that

$$\frac{\omega}{k} = \left(\frac{C_{I+1/2}}{\rho_I} \right)^{1/2} = c_0 \quad . \quad (27)$$

This means that for a small time step Δt and grid spacing h , equation (26) determines a correct local value of the phase velocity. The question is how small h should be in order to justify the approximate relation (27). Obviously h has to be related to a wavelength for which approximation (27) should be valid.

Using $k = 2\pi/\lambda$ we get from (26) relations for the actual **grid phase** and **group velocities**:

$$c^{grid} = \frac{\omega}{k} = \frac{h}{\pi \Delta t} \frac{\lambda}{h} \arcsin \left(c_0 \frac{\Delta t}{h} \sin \frac{\pi h}{\lambda} \right) ,$$

$$v_g^{grid} = \frac{\partial \omega}{\partial k} = \frac{c_0 \cos \frac{\pi h}{\lambda}}{\left[1 - \left(c_0 \frac{\Delta t}{h} \sin \frac{\pi h}{\lambda} \right)^2 \right]^{1/2}} .$$

Assuming a homogeneous medium with phase velocity c_0 , it is easy to see the dependence of c^{grid} and v_g^{grid} on a spatial sampling ratio h/λ and stability ratio $c_0 \Delta t/h$, i. e., the so-called **grid dispersion**, by plotting both velocities normalized by c_0 as it is illustrated in Figure 3.

It is clear from Figure 3 that c^{grid} and v_g^{grid} are close to the true phase and group velocities if $h/\lambda < 0.1$. This means that at least 10 grid spacings h should be used to sample the wavelength λ in order to avoid the grid dispersion of the phase and group velocities for the wavelength λ . Relation

$$h < \frac{\lambda}{10} \quad (28)$$

may be called a **spatial sampling criterion**. Let v_{min} be a minimum velocity in a medium. Then, if we want to have our finite-difference computation sufficiently accurate up to the frequency f_{ac} , the grid spacing h has to satisfy the sampling criterion

$$h < \frac{v_{min}}{10 f_{ac}} . \quad (29)$$

It is important to remind that the above sampling criterion has been obtained for the FD scheme which is just 2nd-order accurate in space. Approximation of spatial derivatives by a 4th-order FD formula would lead to a less severe sampling criterion – requiring approximately only five or six grid spacings per wavelength.

Of course, the above considerations about the spatial sampling are not rigorous. The reason is obvious. If the grid velocity for some value of the spatial sampling ratio differs from the true velocity in the physical medium, the effect of the difference on the wave propagation is cumulative - it is proportional to the distance the wave has traveled. As a consequence, one has to quantitatively analyze the grid dispersion and determine a proper value of the spatial sampling ratio according to the travel distance that is to be included in simulation and a desired/necessary level of accuracy in terms of

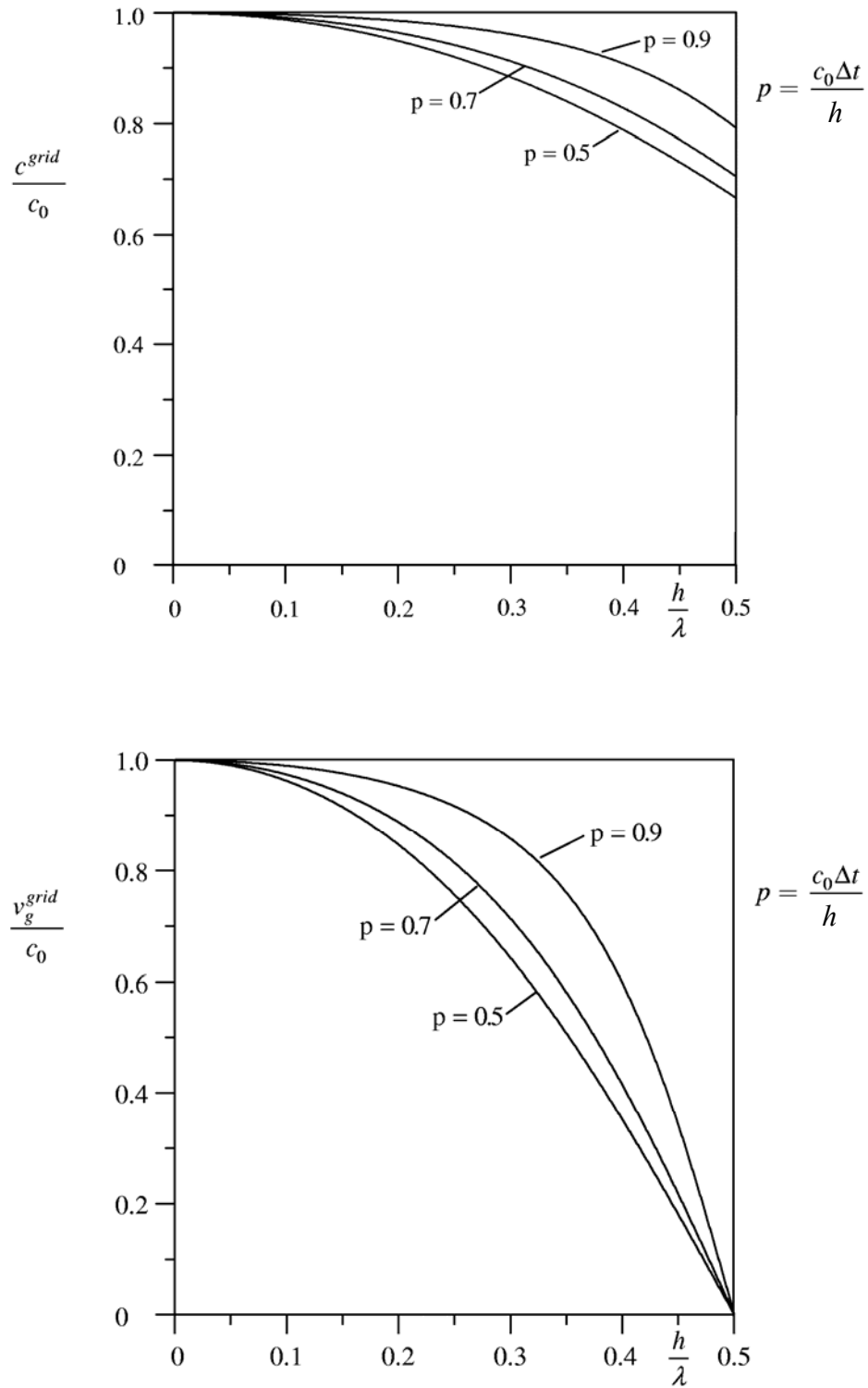


Figure 3. Grid-dispersion curves for the velocity-stress FD scheme (24)-(25).

the grid dispersion. The above ‘visually guessed’ values are typical for recent earthquake ground motion modeling.

For a detailed analysis of stability and grid dispersion in 2D and 3D cases see, for example, papers by Crase et al. (1992), Igel et al. (1995), Moczo et al. (2000).

Von Neumann’s Analysis of Stability

The way we investigated the stability of the FD schemes in the previous section is acceptable but does not give a possibility to quantify a measure of (in)stability. This is possible with the von Neumann’s method. Because the stability is the key concept we will illustrate the von Neumann’s method on three examples:

- a. The unstable velocity-stress FD scheme on a conventional grid given by equations (17) and (18),
- b. The stable velocity-stress FD scheme on a conventional grid given by equations (21) and (22),
- c. The stable velocity-stress FD scheme on a staggered grid given by equations (24) and (25).

The method investigates the local stability – stability at one grid point. Von Neumann’s method assumes representation of a discrete solution at a time $m\Delta t$ and spatial point Ih by a finite Fourier series and examination of the stability of a Fourier component. The solution is stable if and only if each Fourier component is stable. The analysis is applicable to linear FDE with constant coefficients. A periodicity of the spatial domain is assumed for the finite Fourier series but the analysis can give a useful result even if this condition is not met.

Example a. Recall the FD scheme (17)-(18):

$$\begin{aligned}\frac{1}{\Delta t}(V_I^{m+1} - V_I^m) &= \frac{1}{\rho_I} \frac{1}{2h}(T_{I+1}^m - T_{I-1}^m) \\ \frac{1}{\Delta t}(T_I^{m+1} - T_I^m) &= C_I \frac{1}{2h}(V_{I+1}^m - V_{I-1}^m).\end{aligned}\tag{30}$$

Assume

$$\begin{aligned}V_I^m &= A \exp i(-\omega m \Delta t + k I h) \\ T_I^m &= B \exp i(-\omega m \Delta t + k I h).\end{aligned}\tag{31}$$

Equations (30) yield an explicit FD scheme for the unknown quantities V_I^{m+1} and T_I^{m+1} . In Von Neumann's analysis we have to express unknown quantities using the known ones. From equations (31) we have

$$\begin{aligned} T_{I+1}^m - T_{I-1}^m &= T_I^m (\exp(ikh) - \exp(-ikh)) \\ &= T_I^m 2i \sin kh \end{aligned} \quad (32)$$

and, similarly,

$$V_{I+1}^m - V_{I-1}^m = V_I^m 2i \sin kh . \quad (33)$$

Inserting equations (32) and (33) into equations (30) gives

$$\begin{aligned} V_I^{m+1} &= V_I^m + \frac{1}{\rho_I} \frac{\Delta t}{h} T_I^m i \sin kh \\ T_I^{m+1} &= T_I^m + C_I \frac{\Delta t}{h} V_I^m i \sin kh \end{aligned}$$

which may be rewritten as

$$\begin{aligned} V_I^{m+1} &= V_I^m + \frac{1}{\rho_I} \Delta i S T_I^m \\ T_I^{m+1} &= T_I^m + C_I \Delta i S V_I^m \end{aligned} \quad (34)$$

where

$$\Delta = \frac{\Delta t}{h}, \quad S = \sin kh . \quad (35)$$

Define vector U_I^m

$$\mathbf{U}_I^m = \begin{bmatrix} V_I^m \\ T_I^m \end{bmatrix} \quad (36)$$

and matrix \mathbf{G}

$$\mathbf{G} = \begin{bmatrix} 1 & \Delta i S / \rho_I \\ C_I \Delta i S & 1 \end{bmatrix} . \quad (37)$$

Then equations (34) may be written in the matrix form

$$\mathbf{U}_I^{m+1} = \mathbf{G} \mathbf{U}_I^m . \quad (38)$$

\mathbf{G} is an amplification factor. It is determined by the form of the FD scheme. Because we deal with the FD scheme with constant coefficients, the amplification factor does not change with time. We can write

$$\mathbf{U}_I^{m+1} = \mathbf{G}^{m+1} \mathbf{U}_I^0 . \quad (39)$$

Because

$$\|\mathbf{U}_I^{m+1}\| = \|\mathbf{G}^{m+1} \mathbf{U}_I^0\| \leq \|\mathbf{G}\|^{m+1} \|\mathbf{U}_I^0\|$$

the discrete solution will be bounded if

$$\|\mathbf{G}\| \leq 1 . \quad (40)$$

Here, $\|\cdot\|$ means a norm of a matrix. Equation (40) is the sufficient condition for stability of the FD scheme (34). The von Neumann necessary condition of stability can be formulated using an absolute value of eigenvalues Λ_1, Λ_2 of the matrix \mathbf{G} :

$$\max_{j=1,2} |\Lambda_j| \leq 1 .$$

Λ is an eigenvalue of the matrix \mathbf{G} if and only if the characteristic equation

$$\det[\mathbf{G} - \Lambda \mathbf{1}] = 0 \quad (41)$$

is satisfied. From equation (41) we get

$$(1 - \Lambda)^2 - i^2 \Delta^2 \frac{C_I}{\rho_I} S^2 = 0$$

and

$$|1 - \Lambda| = i \Delta \left(\frac{C_I}{\rho_I} \right)^{1/2} S .$$

Then the eigenvalues of the matrix \mathbf{G} are

$$\Lambda_{1,2} = 1 \pm i \left(\frac{\Delta t}{h} \right) \left(\frac{C_I}{\rho_I} \right)^{1/2} \sin kh . \quad (42)$$

It is clear from the equation that for any $\frac{\Delta t}{h}$ there is $|\Lambda_{1,2}| > 1$. This means that FD scheme (30) is **unconditionally unstable**.

Example b. Recall the FD scheme (21)-(22):

$$\begin{aligned} \frac{1}{2\Delta t} (V_I^{m+1} - V_I^{m-1}) &= \frac{1}{\rho_I} \frac{1}{2h} (T_{I+1}^m - T_{I-1}^m) \\ \frac{1}{2\Delta t} (T_I^{m+1} - T_I^{m-1}) &= C_I \frac{1}{2h} (V_{I+1}^m - V_{I-1}^m) . \end{aligned} \quad (43)$$

Assuming again V_I^m and T_I^m in the forms given by equations (31) we can substitute the right-hand sides of equations (43) by the expressions given by equations (32) and (33). We get

$$\begin{aligned} V_I^{m+1} &= V_I^{m-1} + \frac{1}{\rho_I} \Delta 2i S T_I^m \\ T_I^{m+1} &= T_I^{m-1} + C_I \Delta 2i S V_I^m \end{aligned} \quad (44)$$

with Δ and S given by equations (35). Comparing equations (44) with equations (34) we can see that now the two unknown quantities V_I^{m+1} and T_I^{m+1} depend on four known quantities V_I^{m-1} , V_I^m , T_I^{m-1} and T_I^m . In order to get a convenient matrix form as that in equation (38) we can consider two additional equations

$$V_I^m = V_I^m \quad \text{and} \quad T_I^m = T_I^m .$$

We can consider the following system of equations:

$$\begin{aligned}
 V_I^{m+1} &= V_I^{m-1} + \frac{1}{\rho_I} \Delta 2iS T_I^m \\
 V_I^m &= V_I^m \\
 T_I^{m+1} &= T_I^{m-1} + C_I \Delta 2iS V_I^m \\
 T_I^m &= T_I^m .
 \end{aligned} \tag{45}$$

Define vector \mathbf{U}_I^m

$$\mathbf{U}_I^m = \begin{bmatrix} V_I^m \\ V_I^{m-1} \\ T_I^m \\ T_I^{m-1} \end{bmatrix} \tag{46}$$

and matrix \mathbf{G}

$$\mathbf{G} = \begin{bmatrix} 0 & 1 & \frac{1}{\rho_I} \Delta 2iS & 0 \\ 1 & 0 & 0 & 0 \\ C_I \Delta 2iS & 0 & 0 & 1 \\ 0 & 0 & 1 & 0 \end{bmatrix} . \tag{47}$$

Then system of equations can be written in the matrix form

$$\mathbf{U}_I^{m+1} = \mathbf{G} \mathbf{U}_I^m . \tag{48}$$

Similarly to the case of the equation (38) for the FDE (30) we get the characteristic equation

$$1 - 2\Lambda^2 + 4\Delta^2 \frac{C_I}{\rho_I} S^2 \Lambda^2 + \Lambda^4 = 0 . \tag{49}$$

Denoting

$$a = \Delta^2 \frac{C_I}{\rho_I} S^2 \tag{50}$$

and

$$Z = \Lambda^2 \quad (51)$$

we can rewrite the above equation in the form

$$1 + (4a - 2)Z + Z^2 = 0$$

from which we get

$$Z_{1,2} = (1 - 2a) \pm 2(a^2 - a)^{1/2}. \quad (52)$$

If $0 < a \leq 1$ then $|Z_{1,2}| \leq 1$. Referring to equation (50) we see that the necessary condition of stability of the scheme (45) is

$$\Delta^2 \frac{C_I}{\rho_I} S^2 \leq 1.$$

Substituting Δ and S from equations (35) we get for the time step Δt condition, that is, the stability condition

$$\Delta t \leq \left(\frac{\rho_I}{C_I} \right)^{1/2} h. \quad (53)$$

The FD scheme (43) is **conditionally stable**.

Example c. Recall the FD scheme (24) and (25):

$$\begin{aligned} \frac{1}{\Delta t} (V_I^{m+1/2} - V_I^{m-1/2}) &= \frac{1}{\rho_I} \frac{1}{h} (T_{I+1/2}^m - T_{I-1/2}^m) \\ \frac{1}{\Delta t} (T_{I+1/2}^{m+1} - T_{I+1/2}^m) &= C_{I+1/2} \frac{1}{h} (V_{I+1}^{m+1/2} - V_I^{m+1/2}). \end{aligned} \quad (54)$$

Let again V_I^m and T_I^m have the form given by (31). Then we get

$$\begin{aligned} T_{I+1/2}^m - T_{I-1/2}^m &= T_I^m 2i \sin \frac{kh}{2} \\ V_{I-1}^{m+1/2} - V_I^{m+1/2} &= V_{I+1/2}^{m+1/2} 2i \sin \frac{kh}{2}. \end{aligned}$$

Applying these equation to (54) we get

$$\begin{aligned} V_I^{m+1/2} &= V_I^{m-1/2} + \frac{1}{\rho_I} \frac{\Delta t}{h} T_I^m 2i \sin \frac{kh}{2} \\ T_{I+1/2}^{m+1} &= T_{I+1/2}^m + C_{I+1/2} \frac{\Delta t}{h} V_{I+1/2}^{m+1/2} 2i \sin \frac{kh}{2}. \end{aligned} \quad (55)$$

Because von Neumann's analysis investigates the amplification factor of a function (scalar, vector or tensor) at the same grid point, we have to express the value of the particle velocity and stress at one grid point. This means that we have to reformulate the second equation of (55) as follows

$$T_I^{m+1/2} = T_I^{m-1/2} + C_I \frac{\Delta t}{h} V_I^m 2i \sin \frac{kh}{2}.$$

Again, as in the previous case, the two unknown quantities $V_I^{m+1/2}$ and $T_I^{m+1/2}$ depend on four known quantities V_I^m , $V_I^{m-1/2}$, T_I^m and $T_I^{m-1/2}$. For the correct matrix representation, consider the following system of equations:

$$\begin{aligned} V_I^{m+1/2} &= V_I^{m-1/2} + \frac{1}{\rho_I} \frac{\Delta t}{h} T_I^m 2i \sin \frac{kh}{2} \\ V_I^m &= V_I^m \\ T_I^{m+1/2} &= T_I^{m-1/2} + C_I \frac{\Delta t}{h} V_I^m 2i \sin \frac{kh}{2} \\ T_I^m &= T_I^m. \end{aligned} \quad (56)$$

Now the system of equations (56) can be written in the matrix form

$$\mathbf{U}_I^{m+1/2} = \mathbf{G} \mathbf{U}_I^m \quad (57)$$

where

$$\mathbf{U}_I^{m+1/2} = \begin{bmatrix} V_I^{m+1/2} \\ V_I^m \\ T_I^{m+1/2} \\ T_I^m \end{bmatrix}, \quad \mathbf{G} = \begin{bmatrix} 0 & 1 & \frac{1}{\rho_I} \Delta 2i\hat{S} & 0 \\ 1 & 0 & 0 & 0 \\ C_I \Delta 2i\hat{S} & 0 & 0 & 1 \\ 0 & 0 & 1 & 0 \end{bmatrix}$$

and

$$\Delta = \frac{\Delta t}{h}, \quad \hat{S} = \sin \frac{kh}{2}.$$

The corresponding characteristic equation of matrix \mathbf{G} is

$$1 - 2\Lambda^2 + 4\Delta^2 \frac{C_I}{\rho_I} \hat{S}^2 \Lambda^2 + \Lambda^4 = 0 \quad (58)$$

We can see that this equation is the same as the characteristic equation (49) in the previous example. The only difference is in the value of \hat{S} . Therefore, we get the same stability condition (53) for the investigated scheme

$$\Delta t \leq \left(\frac{\rho_I}{C_I} \right)^{1/2} h.$$

This means that the analyzed velocity-stress staggered-grid FD scheme (54) is conditionally stable.

Material Grid Parameters

Material (or medium) grid parameters $\rho_I = \rho(Ih)$ and $C_I = C(Ih)$ used in the above equations can be understood as some appropriate discrete approximations to density and elastic modulus, respectively. If the medium is homogeneous, then, obviously, $\rho_I = \rho$ and $C_I = C$ for all grid points. If the medium is sufficiently smooth, local values of ρ and C will give good results. If the medium is not sufficiently smooth, then it is not trivial and intuitively obvious how to determine values of ρ_I and C_I . In the limit case we face a problem of having a material discontinuity in the medium

across which ρ and C (or at least one of them) change discontinuously. This problem is of the fundamental importance and will be addressed in a special section.

Staggered-grid FD Schemes – A Summary

The velocity-stress FD schemes analyzed in the previous sections correspond to the velocity-stress formulation of the equation of motion and Hooke's law. It can be anticipated that it is possible to find FD schemes for the other three mentioned formulations – displacement-stress, displacement-velocity-stress and displacement formulations. Here we show the best analyzed velocity-stress FD scheme given by equations (24) and (25) in the usual form with the updated variable on one side of the equation. Without analysis we also give the corresponding displacement-stress and displacement-velocity-stress FD schemes. A reader can realize some particular features of the different staggered-grid schemes by looking at them together. Note that in the 1D case there is no difference between the staggered grid and partly-staggered grid.

Displacement-stress FD scheme - solves equations (12)

$$\begin{aligned} T_{I+1/2}^m &= C_{I+1/2} \frac{1}{h} (D_{I+1}^m - D_I^m) \\ D_I^{m+1} &= 2D_I^m - D_I^{m-1} + \frac{1}{\rho_I} \frac{\Delta^2 t}{h} (T_{I+1/2}^m - T_{I-1/2}^m) + \frac{\Delta^2 t}{\rho_I} F_I^m \end{aligned} \quad (59)$$

Displacement-velocity-stress FD scheme- solves equations (13)

$$\begin{aligned} T_{I+1/2}^m &= C_{I+1/2} \frac{1}{h} (D_{I+1}^m - D_I^m) \\ V_I^{m+1/2} &= V_I^{m-1/2} + \frac{1}{\rho_I} \frac{\Delta t}{h} (T_{I+1/2}^m - T_{I-1/2}^m) + \frac{\Delta t}{\rho_I} F_I^m \\ D_I^{m+1} &= D_I^m + \Delta t V_I^{m+1/2} \end{aligned} \quad (60)$$

Velocity-stress FD scheme- solves equations (14)

$$\begin{aligned} T_{I+1/2}^m &= T_{I+1/2}^{m-1} + C_{I+1/2} \frac{\Delta t}{h} (V_{I+1}^{m-1/2} - V_I^{m-1/2}) \\ V_I^{m+1/2} &= V_I^{m-1/2} + \frac{1}{\rho_I} \frac{\Delta t}{h} (T_{I+1/2}^m - T_{I-1/2}^m) + \frac{\Delta t}{\rho_I} F_I^m \end{aligned} \quad (61)$$

All the above FD schemes are 2nd-order accurate both in time and space.

Displacement FD scheme - solves equation (15). Finding an appropriate FD scheme for the displacement formulation is a little bit more difficult simply because the equation of motion is the 2nd-order partial differential equation and we have to approximate the derivative

$$\left[C(x) d(x, t)_{,x} \right]_{,x} . \quad (62)$$

If we define an auxiliary function Φ ,

$$\Phi = C d_{,x} , \quad (63)$$

derivative (62) becomes $\Phi_{,x}$ and its 2nd-order approximation may be

$$\Phi_{,x}|_I \doteq \frac{1}{h} (\Phi_{I+1/2} - \Phi_{I-1/2}) . \quad (64)$$

Find now approximations to $\Phi_{I+1/2}$ and $\Phi_{I-1/2}$. From equation (63) we have

$$\frac{\Phi}{C} = d_{,x} . \quad (65)$$

Integrate equation (65) along the grid line between the points I and $I+1$:

$$\int_{x_I}^{x_{I+1}} \frac{\Phi(x)}{C(x)} dx = \int_{x_I}^{x_{I+1}} d_{,x}(x) dx .$$

Applying the mean-value theorem to the left-hand side integral and approximating the mean value by $\Phi_{I+1/2}$, we obtain

$$\Phi_{I+1/2} \int_{x_I}^{x_{I+1}} \frac{1}{C(x)} dx \doteq D_{I+1} - D_I . \quad (66)$$

Define an **effective material grid parameter** as an **integral harmonic average**

$$C_{I+1/2}^H = \left[\frac{1}{h} \int_{x_I}^{x_{I+1}} \frac{1}{C(x)} dx \right]^{-1} . \quad (67)$$

Then we can rewrite equation (66) in the form

$$\Phi_{I+1/2} \frac{h}{C_{I+1/2}^H} \doteq D_{I+1} - D_I .$$

Applying the equation at the time level m we get the approximation

$$\Phi_{I+1/2} \doteq \frac{1}{h} C_{I+1/2}^H (D_{I+1}^m - D_I^m) . \quad (68)$$

Now it is easy to obtain the displacement FD scheme solving equation (15):

$$\begin{aligned} D_I^{m+1} &= 2D_I^m - D_I^{m-1} \\ &+ \frac{1}{\rho_I} \frac{\Delta^2 t}{h^2} \left[C_{I+1/2}^H (D_{I+1}^m - D_I^m) - C_{I-1/2}^H (D_I^m - D_{I-1}^m) \right] + \frac{\Delta^2 t}{\rho_I} F_I^m . \end{aligned} \quad (69)$$

It is obvious that the two key points in obtaining the scheme were the integration of equation (65) and definition of the **harmonic average** (67) as the effective material grid parameter. Note that the integration leading to the integral harmonic averaging of the elastic modulus $C(x)$ was originally suggested by Tikhonov and Samarskii (see, e.g., Boore 1972; Mitchell 1969, p. 23) as a mathematical tool to avoid the derivative of the modulus $C(x)$ in approximating term (62) that appears in the displacement formulation of the equation of motion. The trick was used then by some authors in 2D and 3D modeling because they recognized good numerical results obtained with the

schemes obtained using the harmonic averaging. Obviously, the main problem is how to approximate the mixed-derivative term, for example,

$$\left[C(x,z) d(x,z,t)_{,x} \right]_{,z}$$

that appears in the 2D and 3D cases. Probably the most accurate displacement schemes based on the trick were developed by Zahradník (1995), and Zahradník and Priolo (1995) for the 2D case. Moczo et al. (1999) generalized Zahradník's approach in the 3D case. The schemes were shown to be sufficiently accurate in the heterogeneous media if the P-to-S wave velocity ratio was smaller than approximately 2.2 (Moczo et al. 1999).

An important aspect is that in the above papers still the fundamental and true reason for the harmonic averaging in heterogeneous media was not recognized. We will clarify this in the next section.

Contact of Two Media – A Material Discontinuity

Because we have to include material discontinuities in models of the Earth's interior as one of the principal features of the medium, the problem of incorporating the boundary conditions on material discontinuities is of fundamental importance as already noted in the section on the heterogeneous and homogeneous FD schemes. Before we analyze the problem, we give a brief historical overview of how the medium heterogeneity and material discontinuities were accounted for in the FD modeling of seismic wave propagation and seismic motion.

In their pioneering work, Alterman and Karal (1968) used the displacement FD scheme and homogeneous approach for models with simple geometry of the material discontinuities. They introduced a concept of fictitious grid points in order to approximate boundary conditions on material discontinuities.

Difficulties in application of the homogeneous approach to curved discontinuities led Boore (1972) to his explicit continuous stress method. Boore tried to explicitly include stress-continuity condition on discontinuities differently from the homogeneous and heterogeneous approaches. Due to poor numerical properties of the method Boore (1972) applied the heterogeneous approach in his SH modeling. In order to follow detailed variation of the torsion modulus and, at the same time, to avoid derivative of the modulus, he calculated effective grid moduli as integral harmonic averages along grid lines between two neighboring grid points as suggested by Tikhonov and Samarskii (see, e.g., Mitchell 1969, p.23).

Ilan et al. (1975), and Ilan and Loewenthal (1976) solved the P-SV problem on the horizontal and vertical planar discontinuities with the homogeneous approach. Instead of the fictitious grid points they used Taylor expansions of displacement to couple the equation of motion with the boundary conditions.

Kelly et al. (1976) presented their heterogeneous P-SV schemes with simple intuitive averaging of material parameters. They compared the heterogeneous and homogeneous formulations using numerical tests and showed unacceptable difference between the two approaches in the case of the corner-edge model.

Kummer and Behle (1982) followed the approach of Ilan et al. (1975) and derived the 2nd-order SH schemes for different types of grid points lying on the step-like polygonal discontinuity between two homogeneous blocks.

A major step forward in the FD modeling of seismic wave propagation in heterogeneous media was made by Virieux (1984, 1986) who used the idea of the staggered grid (Madariaga 1976). Although Virieux did not say explicitly how he determined material grid parameters in his heterogeneous 2nd-order SH and P-SV velocity-stress schemes, his numerical results, in general, were acceptable at that time. The accuracy of the staggered-grid schemes did not suffer from large values of Poisson's ratio, which was the case of all displacement schemes on conventional grids. Virieux also discussed the discrepancy between the homogeneous and heterogeneous formulations found by Kelly et al. (1976). He found it difficult to explain features of the homogeneous solution. We consider this a likely indication of a problem to find a proper FD approximation to the boundary conditions.

An attempt to incorporate boundary conditions into a displacement FD scheme was made by Sochacki et al. (1991). They *a priori* assumed validity of the equation of motion at the discontinuity, wrote the equation in divergence form, and integrated it across the discontinuity. Then they approximated the integrated equation of motion.

Schoenberg and Muir (1989) developed calculus allowing one to replace a stack of thin flat anisotropic layers by an equivalent (in the long-wavelength limit) homogeneous anisotropic medium. In other words, they found Hooke's law for an averaged medium. They did this to simplify modeling of wave propagation for seismic exploration and, at the same time, to account for anisotropy in sedimentary basins. Muir et al. (1992) applied the Schoenberg-Muir (1989) calculus to a grid cell that contains material discontinuity, i.e., in general, they treated contents of the cell as a stack of thin flat layers that can be averaged by the Schoenberg-Muir calculus.

Zahradník and Priolo (1995) published a methodologically important work. They explicitly addressed the fundamental question – whether the heterogeneous approach is justified, i.e., whether it is possible to find a heterogeneous formulation of the equation of motion. Assuming a discontinuity in material parameters they obtained from the equation of motion an expression whose dominant term is equivalent to the traction

continuity condition. This result was interpreted as justification of the FD schemes constructed purely from equations of motion (without explicit treatment of the traction continuity).

Graves (1996) suggested an intuitive method how to determine effective material grid parameters in the 3D 4th-order velocity-stress staggered-grid schemes and numerically demonstrated good level of accuracy. Graves' (1996) paper is important because, as far as we know, it was the first one on the staggered-grid modeling which explicitly and clearly explained how the heterogeneity is taken into account. Similarly clear explanation of the material grid parameterization was given by Ohminato and Chouet (1997) for their 3D 2nd-order displacement-stress scheme.

Takeuchi and Geller's (2000) scheme based on optimally accurate FD operators allows for material discontinuity which coincides with the grid lines (2D) or planes (3D). Following the approach of Geller and Takeuchi (1995), Mizutani (2002) developed a scheme for medium with a material discontinuity not coinciding with the grid line (2D problem).

Moczo et al. (2002) analyzed an 1D problem in a medium consisting of two halfspaces. They considered boundary conditions at a welded planar interface of two halfspaces. They showed simple physical models of the contact of two media and found an averaged medium representing the boundary conditions at the contact. They concluded the 1D case with a heterogeneous formulation of the equation of motion and Hooke's law, and the corresponding heterogeneous FD scheme. Moczo et al. (2002) then analyzed the 3D problem, suggested a 4th-order heterogeneous staggered-grid FD scheme, and demonstrated its superior accuracy compared to the standard staggered-grid FD schemes.

Here we closely follow the analysis of the 1D case given by Moczo et al. (2002).

Welded interface between two halfspaces. Consider two elastic halfspaces with a welded interface in the plane $x = 0$. The wave propagation in the halfspace is described by equations (12) with density ρ_1 and modulus C_1 in one halfspace and ρ_2 and C_2 in the other halfspace. At the welded interface the continuity of displacement and traction apply:

$$d_1(0) = d_2(0) \quad , \quad \tau_1(0) = \tau_2(0) \quad . \quad (70)$$

We look for a proper heterogeneous FD scheme. Because a FD scheme is nothing else than a discrete approximation to an original differential problem, first we have to find a heterogeneous formulation of the differential problem, that is, the same form of the

equation of motion and Hooke's law for points at the material discontinuity and point outside the material discontinuity.

Simple physical model. Behavior of a linear elastic body can be represented by behavior of a spring (Hooke element). The stress-strain relation for the spring is

$$\tau = C \varepsilon . \quad (71)$$

A welded contact of two elastic bodies can be represented by a system of two springs connected in series. The stresses acting on the springs are equal,

$$\tau = \tau_1 = \tau_2 \quad (72)$$

in agreement with the traction-continuity condition. The strains are additive:

$$\varepsilon = \varepsilon_1 + \varepsilon_2 . \quad (73)$$

In a heterogeneous FD scheme we may have a grid point located just at an interface. Such a grid point has to represent properly the welded contact. In terms of our simple model, the grid point has to represent some 'average spring' which would, at the same time,

- a. obey the same form of the stress-strain relation as is relation (71),
- b. satisfy equality of the stresses (72), that is, the boundary condition at the contact.

This is equivalent to finding an average elastic modulus \bar{C} and average strain $\bar{\varepsilon}$ such that the two connected identical springs with the same elastic moduli \bar{C} and the same strains $\bar{\varepsilon}$ is an equivalent system to the considered system of two springs with moduli C_1 and C_2 connected in series. Because the resultant strain ε of the system of two identical springs connected in series is $\varepsilon = 2\bar{\varepsilon}$, we get from equation (73)

$$2\bar{\varepsilon} = \frac{\tau}{C_1} + \frac{\tau}{C_2}$$

from which easily follows

$$\tau = \bar{C} \bar{\varepsilon} , \quad (74)$$

where

$$\bar{\varepsilon} = \frac{1}{2}(\varepsilon_1 + \varepsilon_2) \quad (75)$$

and

$$\bar{C} = \frac{2}{\frac{1}{C_1} + \frac{1}{C_2}} = \frac{2C_1C_2}{C_1 + C_2} . \quad (76)$$

Relations (74) – (76) show that it is possible to find an average spring which satisfies the two conditions a. and b. The fundamental finding is that the **elastic modulus of the average spring is the harmonic average of the elastic moduli of the two connected springs**.

In the elastodynamic problem we also have to include the acceleration. Consider a system of two connected particles with masses m_1 and m_2 . The particles move together, i.e., they have the same acceleration (which is in agreement with the displacement continuity at the welded contact of two media)

$$\vec{a} = \vec{a}_1 = \vec{a}_2 . \quad (77)$$

The forces acting on the particles are

$$\vec{F}_1 = m_1 \vec{a} , \quad \vec{F}_2 = m_2 \vec{a} . \quad (78)$$

The resultant force \vec{F} acting on the system is

$$\vec{F} = \vec{F}_1 + \vec{F}_2 . \quad (79)$$

We want to find such an average mass \bar{m} and average force $\vec{\bar{F}}$ that the system of two connected particles of the same mass \bar{m} and subject to the same forces $\vec{\bar{F}}$ is an equivalent system to the considered system of two particles of masses m_1 and m_2 .

Since the resultant force \vec{F} of the equivalent system is $\vec{F} = 2\vec{\bar{F}}$, we get from equations (78) and (79)

$$2\vec{\bar{F}} = m_1 \vec{a} + m_2 \vec{a} ,$$

from which it immediately follows

$$\vec{\bar{F}} = \bar{m} \vec{a} , \quad (80)$$

where

$$\vec{\bar{F}} = \frac{1}{2}(\vec{F}_1 + \vec{F}_2) \quad (81)$$

and

$$\bar{m} = \frac{1}{2}(m_1 + m_2) . \quad (82)$$

We see that it is possible to find an average particle which obeys the same law as any of the particles, equations (78), and, at the same time, satisfies the condition of equality of the accelerations (77). An important finding is that **the mass of the average particle is the arithmetic average of the masses of the two connected particles.**

Applying this result to unit volumes of a continuum with densities ρ_1 and ρ_2 we get

$$\vec{\bar{F}} = \bar{\rho} \vec{a} \quad (83)$$

and

$$\bar{\rho} = \frac{1}{2}(\rho_1 + \rho_2) . \quad (84)$$

Both above considerations on the simple physical models can be mathematically unified. Let $\varphi_i(x)$, $c_i(x)$ and $g_i(x)$; $i \in \{1, 2\}$, be real functions of a real argument x such that

$$\begin{aligned} \varphi_1(x) &= c_1(x) g_1(x) \\ \varphi_2(x) &= c_2(x) g_2(x) \end{aligned} \quad (85)$$

and

$$\varphi_1(0) = \varphi_2(0) . \quad (86)$$

Functions c_i and g_i may have discontinuities of the first order at $x = 0$. Define

$$\bar{g}(0) = \frac{1}{2}[g_1(0) + g_2(0)] . \quad (87)$$

Then it is easy to show that

$$\varphi_1(0) = \varphi_2(0) = \bar{c}(0) \bar{g}(0) , \quad (88)$$

where

$$\bar{c}(0) = \frac{2}{\frac{1}{c_1(0)} + \frac{1}{c_2(0)}} = \frac{2 c_1(0) c_2(0)}{c_1(0) + c_2(0)} . \quad (89)$$

If

$$c_1(x) = \frac{1}{r_1(x)} , \quad c_2(x) = \frac{1}{r_2(x)} \quad (90)$$

we have

$$\varphi_1(0) = \varphi_2(0) = \frac{1}{\bar{r}(0)} \bar{g}(0) , \quad (91)$$

where

$$\bar{r}(0) = \frac{1}{2} [r_1(0) + r_2(0)] . \quad (92)$$

Heterogeneous formulation of the equation of motion and Hooke's law. Recalling equations (12), that is, the displacement-stress formulation, we can write the entire set of differential equations for both halfspaces and boundary conditions for the material discontinuity, that is, for the interface between the two halfspaces at $x = 0$:

$$\begin{aligned} \ddot{d}_1 &= \frac{1}{\rho_1} (\tau_{1,x} + f_1) , & \tau_1 &= C_1 d_{1,x} \\ \ddot{d}_2 &= \frac{1}{\rho_2} (\tau_{2,x} + f_2) , & \tau_2 &= C_2 d_{2,x} \end{aligned} \quad (93)$$

$$\ddot{d}_1(0) = \ddot{d}_2(0) , \quad \tau_1(0) = \tau_2(0) . \quad (94)$$

Then, based on the previous analysis, we can replace the boundary conditions by the same form of the equation of motion and Hooke's law as we have for each of the halfspaces:

$$\ddot{d}(0) = \frac{1}{\bar{\rho}(0)} [\bar{\tau}_{,x}(0) + \bar{f}(0)] \quad (95)$$

$$\tau(0) = \bar{C}(0) \overline{d_{,x}}(0) , \quad (96)$$

where

$$\bar{\rho}(0) = \frac{1}{2}[\rho_1(0) + \rho_2(0)] \quad (97)$$

$$\bar{C}(0) = \frac{2}{\frac{1}{C_1(0)} + \frac{1}{C_2(0)}} \quad (98)$$

$$\overline{\tau_{,x}}(0) + \bar{f}(0) = \frac{1}{2}[\tau_{1,x}(0) + \tau_{2,x}(0) + f_1(0) + f_2(0)] \quad (99)$$

$$\overline{d_{,x}}(0) = \frac{1}{2}[d_{1,x}(0) + d_{2,x}(0)] . \quad (100)$$

Looking at equations (95) and (96) it is obvious that we have one and the same form of the equation of motion and Hooke's law for all spatial points – no matter what is their position with respect to the material discontinuity. In other words, we have the heterogeneous formulation of the differential problem, and thus the basis for finding its FD approximation (that is, a proper FD scheme).

Now it is more obvious that suggesting heterogeneous FD schemes over decades without having the heterogeneous formulation of the differential problem was just intuitive guessing even for the relatively simple 1D problem.

Heterogeneous FD schemes. Having the heterogeneous formulation of the differential problem still we can have different FD schemes to approximate it. Of course, the schemes may differ for example by the spatial grid and order of approximation in space and time. There are, however, two important aspects:

- the harmonic averaging of the elastic moduli and arithmetic averaging of densities at the material discontinuity,
- averaging of the spatial derivatives of the functions at the material discontinuity.

Only more detailed analysis or numerical tests can reveal, which of the two aspects is more important.

Without going into details (see Moczo et al. 2002), the following staggered-grid FD scheme gives sufficient accuracy in a sense that it is capable 'to see' a true position of the material discontinuity in the grid; the discontinuity may be located at any grid point or anywhere between two neighboring grid points:

Displacement-stress FD scheme

$$\begin{aligned} T_{I+1/2}^m &= C_{I+1/2}^H \frac{1}{h} (D_{I+1}^m - D_I^m) \\ D_I^{m+1} &= 2D_I^m - D_I^{m-1} + \frac{1}{\rho_I^A} \frac{\Delta^2 t}{h} (T_{I+1/2}^m - T_{I-1/2}^m) + \frac{\Delta^2 t}{\rho_I^A} F_I^m, \end{aligned} \quad (101)$$

where

$$\rho_I^A = \frac{1}{h} \int_{x_{I-1/2}}^{x_{I+1/2}} \rho(x) dx \quad (102)$$

and

$$C_{I+1/2}^H = \left[\frac{1}{h} \int_{x_I}^{x_{I+1}} \frac{1}{C(x)} dx \right]^{-1}. \quad (103)$$

In principle, the integral averaging allows both for smooth variation and discontinuous variation of the elastic modulus and density. Moczo et al. (2002) numerically tested accuracy of the scheme in media with material discontinuity and smoothly heterogeneous media. The FD scheme with arithmetic averaging of the density and harmonic averaging of the elastic modulus ‘can see’ the true position of the material discontinuity no matter whether the discontinuity goes through a grid point or not. Even for the smooth heterogeneity without material discontinuities it is much better to use scheme (101).

We see that, in fact, this FD scheme differs from scheme (59) only by the definition of the effective grid modulus and density.

Analogously to the displacement-stress FD scheme it is possible to obtain displacement-velocity-stress and velocity-stress FD schemes derived from the corresponding heterogeneous differential formulations. The schemes read

Displacement-velocity-stress FD scheme

$$\begin{aligned} T_{I+1/2}^m &= C_{I+1/2}^H \frac{1}{h} (D_{I+1}^m - D_I^m) \\ V_I^{m+1/2} &= V_I^{m-1/2} + \frac{1}{\rho_I^A} \frac{\Delta t}{h} (T_{I+1/2}^m - T_{I-1/2}^m) + \frac{\Delta t}{\rho_I^A} F_I^m \\ D_I^{m+1} &= D_I^m + \Delta t V_I^{m+1/2} \end{aligned} \quad (104)$$

Velocity-stress FD scheme

$$\begin{aligned}
 T_{I+1/2}^m &= T_{I+1/2}^{m-1} + C_{I+1/2}^H \frac{\Delta t}{h} (V_{I+1}^{m-1/2} - V_I^{m-1/2}) \\
 V_I^{m+1/2} &= V_I^{m-1/2} + \frac{1}{\rho_I^A} \frac{\Delta t}{h} (T_{I+1/2}^m - T_{I-1/2}^m) + \frac{\Delta t}{\rho_I^A} F_I^m
 \end{aligned} \tag{105}$$

Let us note that we numerically compared accuracy of the interior FD schemes (101) - (105) and found no differences.

While schemes (101) - (105) are the 2nd-order accurate in space, it is possible to have schemes of the higher-order in space and time. However, while, for example, the 4th-order in space reduces the memory requirements due to approximately twice smaller number of grid spacings required per wavelength (therefore – twice larger grid spacing compared to the 2nd-order), the 4th-order in time does not comparably reduce the time step but, obviously, increases the number of time levels which have to be kept in core memory for updating the next time level.

An example of the 4th-order velocity-stress scheme is

$$\begin{aligned}
 T_{I+1/2}^m &= T_{I+1/2}^{m-1} \\
 &+ C_{I+1/2}^H \frac{\Delta t}{h} \left[a (V_{I+2}^{m-1/2} - V_{I-1}^{m-1/2}) + b (V_{I+1}^{m-1/2} - V_I^{m-1/2}) \right] \\
 V_I^{m+1/2} &= V_I^{m-1/2} \\
 &+ \frac{1}{\rho_I^A} \frac{\Delta t}{h} \left[a (T_{I+3/2}^m - T_{I-3/2}^m) + b (T_{I+1/2}^m - T_{I-1/2}^m) \right] + \frac{\Delta t}{\rho_I^A} F_I^m
 \end{aligned} \tag{106}$$

$a = -1/24 \quad , \quad b = 9/8 \quad .$

In the case of the displacement scheme, it is the same as scheme (69) except the definition of the effective grid density.

Note that averaging is performed over one grid spacing. Consider first a material discontinuity between two homogeneous media. If the material discontinuity is exactly at a grid position of the displacement/particle velocity, the only averaged material grid parameter is the density assigned to the grid position. If the discontinuity is exactly at a grid position of the stress, the only averaged material grid parameter is the elastic modulus assigned to the grid position. If the discontinuity is anywhere between the grid position of the displacement/particle velocity and the grid position of the stress, then

there are two material parameters averaged – the density assigned to the nearest grid position of displacement/particle velocity, and the elastic modulus assigned to the nearest grid position of the stress. Obviously, if the medium is smoothly heterogeneous or it consists of smoothly heterogeneous blocks separated by material discontinuities, averaged densities and averaged elastic moduli are assigned to all grid positions. The values of averaged densities and elastic moduli are, in general, calculated by numerical integration performed over distance of one grid spacing and centered about the grid position to which the averaged parameter is to be assigned.

The accuracy of the described FD scheme as well as inaccuracy of schemes with other than arithmetic averaging of the density and harmonic averaging of the elastic modulus are demonstrated in the results presented in the chapter on numerical examples. The results were obtained using the 1DFD program package that is a part of this introduction.

Also note that while the reason for definition of the integral harmonic average of the elastic modulus (67) in the derivation of the displacement FD scheme was the Tikhonov-Samarski's trick to avoid spatial differentiating of the modulus, we obtained the harmonic averaging as a necessary condition for the traction continuity at the material discontinuity in the heterogeneous formulation of the differential problem. Similarly, we obtained arithmetic averaging of the density as the necessary condition for displacement continuity at the material discontinuity.

Free Surface

Consider a free surface at $x = 0$ and medium at $x \geq 0$. At the free surface, traction is zero. In our simple 1D case this means that stress $\tau = 0$. Recall, for example, the velocity-stress formulation of the equation of motion and Hooke's law:

$$\rho \dot{v} = \tau_{,x} + f \quad , \quad \dot{\tau} = C v_{,x} \quad .$$

Because we usually are interested in computing particle velocity at the free surface, locate the grid position for the particle velocity just at the free surface, grid index $I = 0$, and thus the nearest grid position for the stress is half grid spacing from the free surface inside the medium, grid index $I = 1/2$, see Figure 4.

It is obvious that if we want to use the FD scheme for the interior grid point, the scheme for updating the particle velocity, the second of equations (105), needs value $T_{-1/2}^m$, that is, half grid spacing beyond the free surface (outside the medium), see Figure 5.

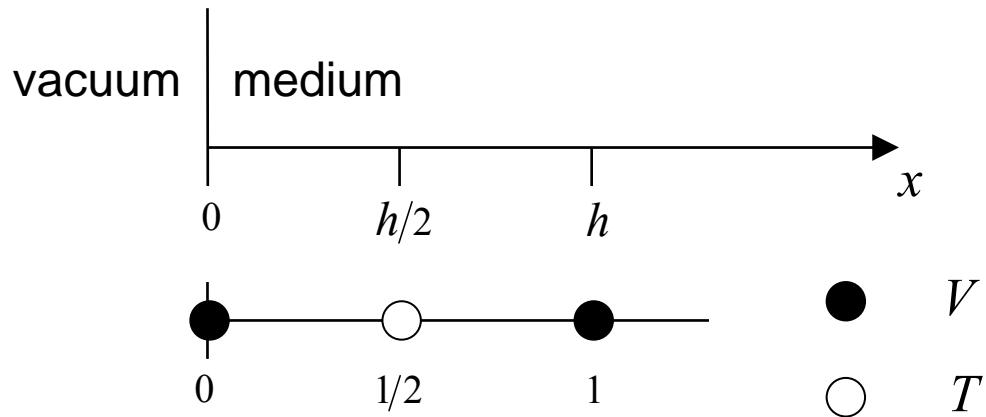


Figure 4. Position of the free surface in the staggered spatial grid for the velocity-stress FD scheme.

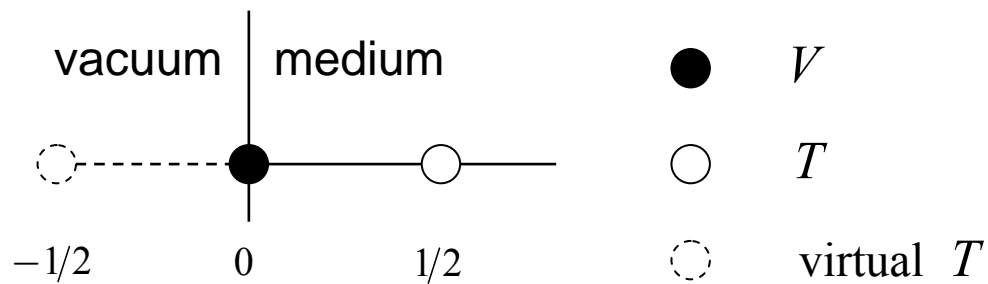


Figure 5. Free surface and the position of the virtual stress outside the medium.

Levander (1988) suggested a technique which can be called the (antisymmetric) **stress imaging**. The idea is: if we assume

$$\tau(-h/2) = -\tau(h/2) ,$$

that is,

$$T_{-1/2}^m = -T_{1/2}^m ,$$

we ensure that

$$\tau(0) = 0,$$

which is the traction-free boundary condition at the free surface.

Kristek et al. (2002) demonstrated that in the 3D case the stress-imaging technique in the 4th-order FD modeling needs at least twice more grid spacings per wavelength compared to what is enough inside the medium if the Rayleigh waves are to be propagated without significant grid dispersion even in the case of the simple homogeneous halfspace. Obviously, taking twice more grid spacings per wavelength degrades, in fact, the 4th-order scheme down to, approximately, the 2nd-order one.

Therefore, Rodrigues (1993) who had made the same (unpublished) conclusions on the stress-imaging technique, suggested applying the stress imaging to the grid vertically refined near the free surface. His approach is explained in the paper by Kristek et al. (2002) and numerically tested. The technique gives the 4th-order accuracy, however, requires three times smaller time step. The consequence is three times more time levels to be computed compared to the regular staggered-grid scheme. (The factor of 3 comes from the most natural refinement of the staggered-grid; see, for example Kristek et al., 2002. For the other possible refinement see Wang et al., 2001.)

In order to keep both the 4th-order accuracy and computational efficiency, Kristek et al. (2002) developed a technique based on the adjusted FD approximations, **the AFDA technique**. The principle of their technique is:

- directly prescribed zero values of the stress-tensor components at the free surface (in 2D or 3D, there is always at least one stress-tensor component located at the free surface),
- application of the 4th-order FD approximations which only use the values at the grid positions inside the medium.

Obviously, no stress imaging, that is, no virtual values above the free surface, are necessary.

For updating $V_0^{m+1/2}$ we can obtain the following 2nd-order scheme

$$V_0^{m+1/2} = V_0^{m-1/2} + \frac{1}{\rho_0^A} \frac{\Delta t}{h} \left(3T_{1/2}^m - \frac{1}{3}T_{3/2}^m \right),$$

where

$$\rho_0^A = \frac{2}{h} \int_0^{h/2} \rho(x) dx.$$

Note that the density is averaged only over the half grid spacing inside the medium.
 The 4th-order scheme is

$$V_0^{m+1/2} = V_0^{m-1/2} + \frac{1}{\rho_0^A} \frac{\Delta t}{h} \left(\frac{35}{8} T_{1/2}^m - \frac{35}{24} T_{3/2}^m + \frac{21}{40} T_{5/2}^m - \frac{5}{56} T_{7/2}^m \right).$$

In both above schemes we directly used the boundary condition $\tau(0) = 0$, that is, $T_0^m = 0$.

In the case of the 4th-order scheme also derivatives at other grid positions have to be approximated by the adjusted FD approximations – see Kristek et al. (2002) or Moczo et al. (2004) for the complete FD scheme.

Moczo et al. (2004) demonstrated very good accuracy of the AFDA technique even in the models with lateral material discontinuities reaching the free surface.

Simulation of the traction-free condition along a nonplanar 2D or 3D surface is much more difficult task. This is not surprising due to the definition of the FD method. In other words, it is an inherent problem of the method. Until now no really satisfactory technique has been found. For a review of different approaches until 1996 see Robertsson (1996), Moczo et al. (1997), Ohminato and Chouet (1997), and Robertsson and Holliger (1997). Recent development can be found, for example, in papers by Hestholm (1999), Mittet (2002), Laws and Kragh (2002), Hestholm and Ruud (2002).

Wave Excitation

It is obvious that the body-force term in the equation of motion can be used to simulate source. In principle, it is enough to prescribe a desired source-time function and apply it at the grid position of the displacement or particle velocity.

The wavefield excitation is more complicated in 3D. A detailed explanation, based on approaches by Alterman and Karal (1968), Fäh (1992), Frankel (1993), Zahradník (1995a), Zahradník and Moczo (1996), Graves (1996), and Moczo et al. (1997) can be found in the introductory text by Moczo (1998).

For the alternative approaches see Yomogida and Etgen (1993) and Coutant et al. (1995).

Here we do not refer to the dynamic source modeling which would deserve a special chapter.

Boundaries of the Grid

The spatial FD grid has to have a finite size. Therefore it is bounded by artificial boundaries – for example grid planes which do not have neighbor grid points from one side. The boundaries of the grid should be designed so that they would represent the interaction of the wavefield inside the computational domain, covered by the grid, with the medium outside. In principle, the boundary of the grid may be anything between two extreme possibilities – absolutely reflecting or absolutely transparent. One possibility might be, for example, the boundary coinciding with a material discontinuity. A special case is a plane of symmetry.

In most cases, however, the boundary is placed so that it should be transparent for waves impinging on the boundary from inside the medium. We can speak about **nonreflecting** or **absorbing boundaries** (or absorbing boundary conditions, **ABC**). In the FD method such a boundary can be only approximated.

A large number of approximations to the nonreflecting boundaries have been developed. There are based on several ideas but, basically, most of them fall into one of two groups:

- a finite boundary zone in which the wave is gradually attenuated,
- an approximation to one-way wave equation at the boundary grid point (or several points – depending on the order of the scheme).

Examples of the first approach are papers by Israeli and Orszag (1981), Korn and Stöckl (1982), Cerjan et al. (1985), Kosloff and Kosloff (1986), Sochacki et al. (1987), Béranger (1994), Chew and Liu (1996), Collino and Tsogka (1998, 2001), Chen et al. (2000), Komatitsch and Tromp (2003), Festa and Nielsen (2003). The papers by Béranger introduced the **Perfectly Matched Layers (PML)** that have recently become very popular because it is probably so far the best tool to prevent artificial reflections from the grid boundaries; see three latter papers.

Examples of the second approach are papers by Lysmer and Kuhlemeyer (1969), Lindman (1975), Engquist and Majda (1977), Clayton and Engquist (1977), Reynolds (1978), Emmerman and Stephen (1983), Higdon (1990, 1991, 1992, 1994), Randall (1988), Stacey (1988), Peng and Toksöz (1994, 1995), Renaut and Petersen (1989), Zhu (1999), Liu and Archuleta (2000), Givoli (2004).

The approach is to apply a paraxial (one-way) wave equation at the grid boundary since such an equation only permits energy propagation in a limited range of angles. An example of the 1st-order paraxial equation can be the equation for the SH-wave propagating in the x-direction,

$$\frac{1}{c} \dot{d} + d_{,x} = 0 .$$

Paraxial equations can be replaced by the FD schemes which are then applied at the boundary. For years the formulas obtained by Clayton and Engquist (1977), the A1 formulas, had been the most popular and used. Emerman and Stephen (1983) showed that the Clayton and Engquist's condition is unstable for $\beta/\alpha < 0.46$. Here, β and α are the S- and P-wave velocities. Stacey (1988) showed stability of his condition for $\alpha/\beta < 2.2$. Emerman and Stephen (1983) suggested a modification of the Clayton and Engquist (1977) condition which is stable for any $\beta/\alpha > 0$.

Another approach is based on minimizing the coefficient of reflection at the artificial boundary such as in Reynolds (1978) and Peng and Toksöz (1994, 1995).

Higdon (1991) developed an approximation of the absorbing boundary condition that is based on the composition of simple 1st-order differential operators. Each operator gives perfect absorption for a plane wave impinging on the boundary at certain velocity and angle of incidence.

Recently, Liu and Archuleta (2000) combined the Clayton-Engquist's A1 formulas with those by Higdon (1991) and obtained a well-working nonreflecting boundary. Their formulas are given in Moczo et al. (2002).

Here we show several nonreflecting boundaries in a unified representation. As in the previous sections, we only include the 1D case.

We finish with a unified representation of several boundary conditions. Consider a nonreflecting boundary at $x=0$, that is at the grid position with index 0. A displacement value D_0^{m+1} can be updated according to the formula

$$\begin{aligned} D_0^{m+1} = & A_{01}D_1^{m+1} + A_{02}D_2^{m+1} \\ & + A_{10}D_0^m + A_{11}D_1^m + A_{12}D_2^m \\ & + A_{20}D_0^{m-1} + A_{21}D_1^{m-1} + A_{22}D_2^{m-1}, \end{aligned} \quad (107)$$

where the coefficients A_{pq} ; $p, q \in \{0, 1, 2\}$ are given in Table 1. In the table, Δt is the time step, h is the grid spacing, c is the velocity, and

$$\begin{aligned}h_{1x} &= (\gamma - bG) / B \cdot G \\h_{1t} &= (1 - bG) / B \cdot G \\h_{xt} &= b / B \\c_{1t} &= 1 - \gamma \\c_{xt} &= \gamma \\G &= 1 + \gamma \\B &= 1 - b \\\gamma &= c \Delta t / h \\b &= 0.4.\end{aligned}\tag{108}$$

The formulas (108) are simplified for the 1D case. Non-simplified formulas are given in Moczo et al. (2002).

The formula (107) is applicable to the particle velocity if the velocity-stress FD scheme is used. If the displacement-velocity-stress FD scheme is used, it is possible to apply the formula to either the displacement or particle velocity.

Table 1.
 Coefficients of the absorbing boundary conditions (107)

	Clayton & Engquist (A1) 1977	Reynolds 1978	Emerman & Stephen 1983	Liu & Archuleta 2000
A_{00}	0	0	0	0
A_{01}	0	0	$\frac{\Delta t - h/c}{\Delta t + h/c}$	h_{1x}
A_{02}	0	0	0	0
A_{10}	$1 - \frac{c\Delta t}{h}$	$1 - \frac{c\Delta t}{h}$	$\frac{2h/c}{\Delta t + h/c}$	$c_{1t} + h_{1t}$
A_{11}	$\frac{c\Delta t}{h}$	$1 + \frac{c\Delta t}{h}$	$\frac{2h/c}{\Delta t + h/c}$	$c_{xt} + h_{xt} - h_{1x} c_{1t}$
A_{12}	0	0	0	$-h_{1x} c_{xt}$
A_{20}	0	0	$\frac{\Delta t - h/c}{\Delta t + h/c}$	$-h_{1t} c_{1t}$
A_{21}	0	$-1 - \frac{c\Delta t}{h}$	-1	$-h_{xt} c_{1t} - h_{1t} c_{xt}$
A_{22}	0	$\frac{c\Delta t}{h}$	0	$-h_{xt} c_{xt}$

Incorporation of the Realistic Attenuation

Stress-Strain Relation in Viscoelastic Medium

There are two key points which determine the incorporation of the attenuation into time-domain computations of seismic wave propagation and seismic motion:

1. Earth's materials remember their past, that is, the stress-strain relation also depends on time. This is due to the fact that the behavior of the material combines behaviors of both, elastic solids and viscous fluids. We can approximate such a behavior using **viscoelastic** models of medium.
2. The observations show that the internal friction (a measure of attenuation) in the Earth, Q^{-1} , is nearly constant over the seismic frequency range. This is due to the fact that the Earth's material is composed of different minerals and the attenuation in each of them is contributed by several physical processes.

For a linear isotropic viscoelastic material the stress-strain relation is given by **Boltzmann superposition and causality principle**. In a simple scalar notation it is

$$\sigma(t) = \int_{-\infty}^t \psi(t-\tau) \dot{\epsilon}(\tau) d\tau, \quad (109)$$

where $\sigma(t)$ is stress, $\dot{\epsilon}(t)$ time derivative of strain, and $\psi(t)$ **stress relaxation function** defined as a stress response to Heaviside unit step function in strain. According to equation (109), the stress at a given time t is determined by the entire history of the strain until time t . The upper integration limit ensures the causality. Mathematically, the integral in equation (109), also called the hereditary integral, represents a time convolution of the relaxation function and strain rate. We can use symbol $*$ for the convolution. Equation (109) becomes

$$\sigma(t) = \psi(t) * \dot{\epsilon}(t). \quad (110)$$

Due to properties of convolution,

$$\sigma(t) = \dot{\psi}(t) * \varepsilon(t) . \quad (111)$$

Since $\psi(t)$ is the stress response to a unit step function in strain, its time derivative,

$$M(t) = \dot{\psi}(t) \quad (112)$$

is the stress response to the Dirac δ -function in strain. Equation (111) can be written as

$$\sigma(t) = M(t) * \varepsilon(t) . \quad (113)$$

Hereafter we will use symbol \mathcal{F} for the direct and \mathcal{F}^{-1} for the inverse Fourier transforms

$$\mathcal{F}\{x(t)\} = \int_{-\infty}^{\infty} x(t) \exp(-i\omega t) dt , \quad \mathcal{F}^{-1}\{X(\omega)\} = \frac{1}{2\pi} \int_{-\infty}^{\infty} X(\omega) \exp(i\omega t) d\omega .$$

ω is the angular frequency. An application of the Fourier transform to equation (113) gives

$$\sigma(\omega) = M(\omega) \cdot \varepsilon(\omega) . \quad (114)$$

In general, $M(\omega)$ is a complex, frequency-dependent **viscoelastic modulus**. From equations (112) - (114) we get

$$\dot{\psi}(t) = \mathcal{F}^{-1} \{M(\omega)\} \quad (115)$$

and, due to properties of the Fourier transform,

$$\psi(t) = \mathcal{F}^{-1} \left\{ \frac{M(\omega)}{i\omega} \right\} . \quad (116)$$

Equation (114) indicates that the incorporation of the linear viscoelasticity and consequently attenuation into the frequency-domain computations is much easier than those in the time-domain computations – real frequency-independent moduli are simply replaced by complex, frequency-dependent quantities (**the correspondence principle in the linear theory of viscoelasticity**).

The time derivative of the stress is, see equation (111),

$$\dot{\sigma}(t) = \dot{\psi}(t) * \dot{\epsilon}(t) \quad (117)$$

or, due to equation (112),

$$\dot{\sigma}(t) = M(t) * \dot{\epsilon}(t) . \quad (118)$$

An instantaneous elastic response of the viscoelastic material is given by the so-called **unrelaxed modulus** M_U , a long-term equilibrium response is given by the **relaxed modulus** M_R

$$M_U = \lim_{t \rightarrow 0} \psi(t) \quad , \quad M_R = \lim_{t \rightarrow \infty} \psi(t) . \quad (119)$$

In the frequency domain

$$M_U = \lim_{\omega \rightarrow \infty} M(\omega) \quad , \quad M_R = \lim_{\omega \rightarrow 0} M(\omega) . \quad (120)$$

The **modulus defect** or **relaxation of modulus** is

$$\delta M = M_U - M_R . \quad (121)$$

Given the viscoelastic modulus, the **quality factor** $Q(\omega)$ is

$$Q(\omega) = \text{Re } M(\omega) / \text{Im } M(\omega) . \quad (122)$$

It is obvious that a numerical integration of the stress-strain relation (109) is practically intractable due to the large computer time and memory requirements. This led many modelers to incorporate only oversimplified $Q(\omega)$ laws in the time-domain computations. (In fact, some modelers still use the oversimplified $Q(\omega)$ laws despite the significant progress in incorporation of more realistic attenuation into the time-domain computations.)

On the other hand, the observations on attenuation of seismic waves led Liu et al. (1976) to use a superposition of several relaxation mechanisms to approximate the nearly constant $Q(\omega)$.

Conversion of the Convolutory Stress-Strain Relation into a Differential Form

Before we briefly review how different authors approached the problem characterized by the above two key aspects, consider $M(\omega)$ as a rational function

$$M(\omega) = \frac{P_m(i\omega)}{Q_n(i\omega)} \quad (123)$$

with

$$P_m(i\omega) = \sum_{l=1}^m p_l (i\omega)^l, \quad Q_n(i\omega) = \sum_{l=1}^n q_l (i\omega)^l. \quad (124)$$

The application of the inverse Fourier transform to equation (114) with $M(\omega)$ given by equation (123) leads to

$$\sum_{l=1}^n q_l \frac{d^l \sigma(t)}{dt^l} = \sum_{l=1}^m p_l \frac{d^l \varepsilon(t)}{dt^l}, \quad (125)$$

the n^{th} -order differential equation for $\sigma(t)$, which can be eventually numerically solved much more easily than the convolution integral. In other words, the convolution integral in equation (109) can be converted into a differential form if $M(\omega)$ is a rational function of $i\omega$.

Day and Minster (1984) assumed that, in general, the viscoelastic modulus is not a rational function. Therefore they suggested approximating a viscoelastic modulus by an n^{th} -order rational function and determining its coefficients by the Padé approximant method. They obtained n ordinary differential equations for n additional **internal variables**, which replace the convolution integral. The sum of the internal variables multiplied by the unrelaxed modulus gives an additional viscoelastic term to the elastic stress. The revolutionary work of Day and Minster not only developed one particular approach but, in fact, indirectly suggested the future evolution – a direct use of the rheological models whose $M(\omega)$ is a rational function of $i\omega$.

Emmerich and Korn (1987) realized that an acceptable relaxation function corresponds to rheology of what they defined as the **generalized Maxwell body** – n Maxwell bodies and one Hooke element (elastic spring) connected in parallel; see

Figure 6. Note that the generalized Maxwell body in the literature on rheology is defined without the additional single Hooke element. Therefore, we denote the model considered by Emmerich and Korn (1987) by **GMB-EK**.

Because, in fact, any model consisting of linear springs and dashpots (Stokes elements) connected in series or parallel has its viscoelastic modulus in form of a rational function of $i\omega$, the GMB-EK allowed replacing the convolution integral by a differential form. Emmerich and Korn (1987) obtained for the new variables similar differential equations as Day and Minster (1984). In order to fit an arbitrary $Q(\omega)$ law they chose the relaxation frequencies logarithmically equidistant over a desired frequency range and used the least-square method to determine weight factors of the relaxation mechanisms (classical Maxwell bodies). Emmerich and Korn (1987) demonstrated that their approach is better than the approach based on the Padé approximant method in both accuracy and computational efficiency.

Independently, Carcione et al. (1988a,b), in accordance with the approach of Liu et al. (1976), assumed the **generalized Zener body (GZB)** - n Zener bodies, that is, n standard linear bodies, connected in parallel; see Figure 7. Carcione et al. developed a theory for the GZB and introduced term memory variables for the obtained additional variables.

We will briefly review the GMB-EK and GZB presented in papers by Emmerich and Korn (1987) and Carcione et al. (1988a,b), respectively. It is, however, useful first to remind basics of the simple rheological models.

The GZB and GMB-EK Rheological Models

Models which quite well approximate rheological properties and behavior of the real Earth's material can be constructed by connecting the simplest rheological elements, Hooke and Stokes elements, in parallel or series. The properties of the models can be analyzed in the time and frequency domains. There are relatively simple rules in both domains that allow obtaining mathematical representations of the models. The **frequency-domain rules for linear rheological models** are given in Table 2.

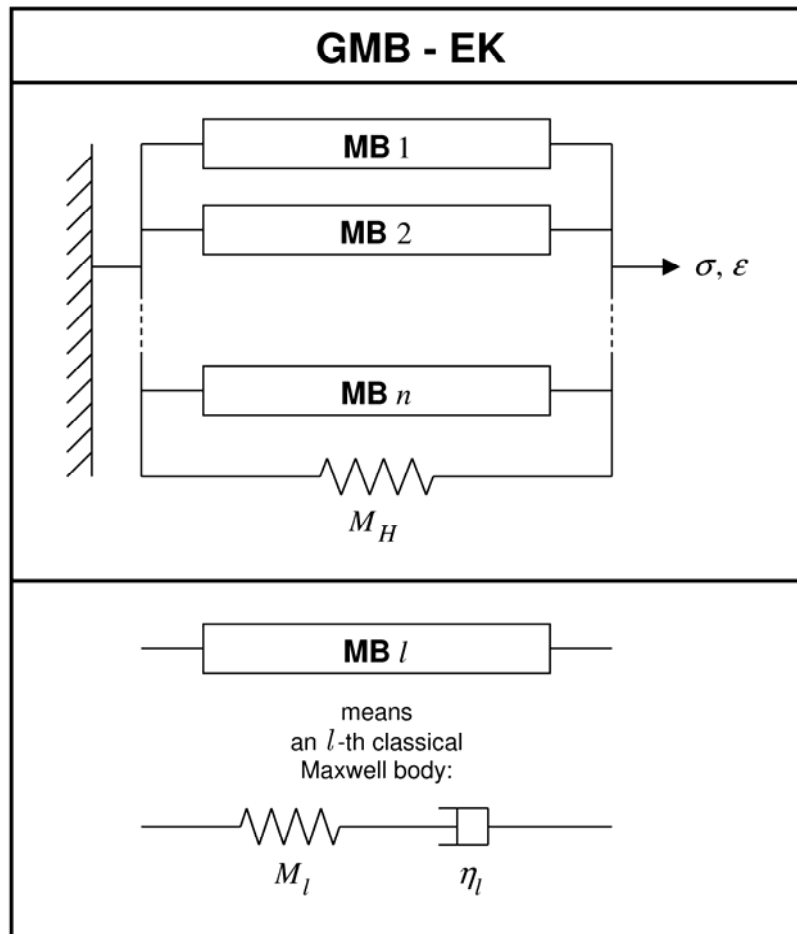


Figure 6. Rheological model of the Generalized Maxwell Body (GMB-EK) defined by Emmerich and Korn (1987). M_H and M_l denote elastic moduli, η_l viscosity.

Table 2.
 Frequency-domain rules for linear rheological models

element	stress-strain relation
Hooke (spring)	$\sigma(\omega) = M \cdot \varepsilon(\omega)$, M - elastic modulus
Stokes (dashpot)	$\sigma(\omega) = i\omega\eta \cdot \varepsilon(\omega)$, η - viscosity

connection	σ	ε
in series	equal	additive
in parallel	additive	equal

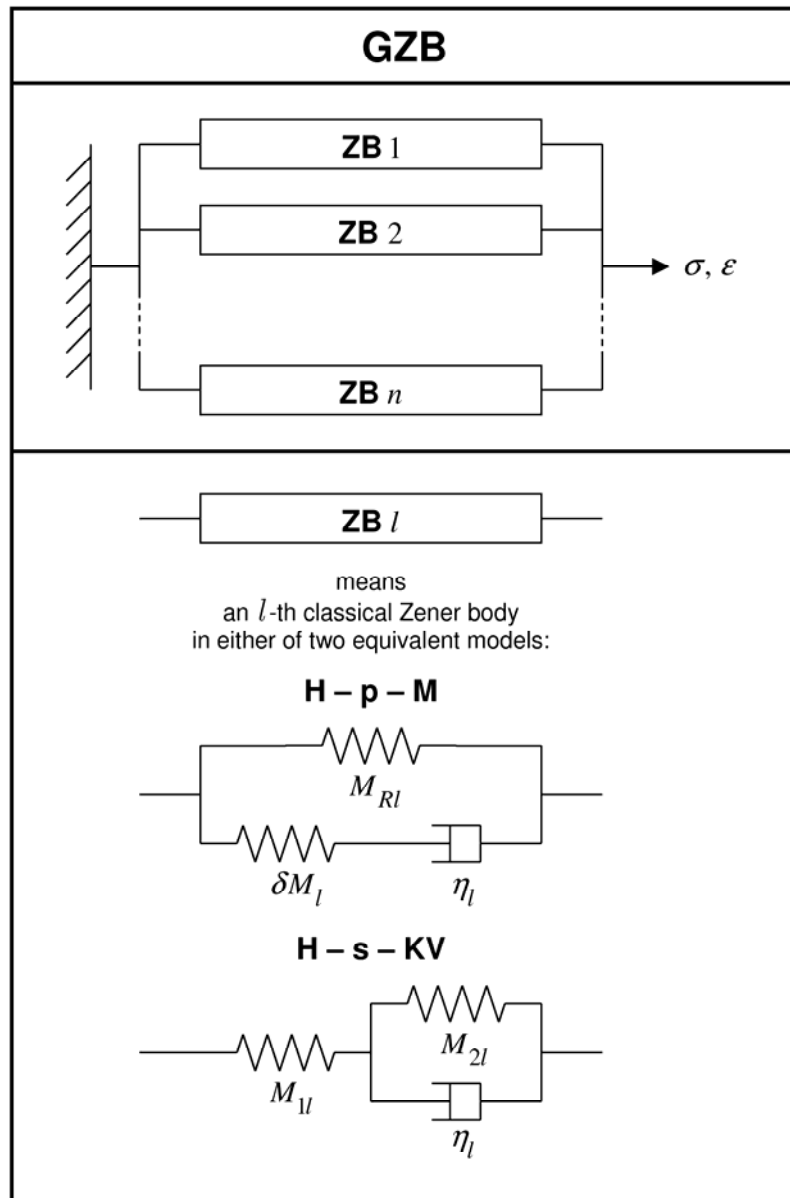


Figure 7. Rheological model of the Generalized Zener Body (GZB). For a classical Zener body (standard linear body) there are two equivalent models: H-p-M , that is, Hooke element connected in parallel with Maxwell body, and H-s-KV, that is, Hooke element connected in series with Kelvin-Voigt body. In the H-p-M model it is easier to recognize the relaxed modulus M_{Rl} and modulus defect δM_l . M_{1l} and M_{2l} in the H-s-KV model denote elastic moduli. In both models η_l stands for viscosity.

GMB-EK. For the GMB-EK we easily find

$$M(\omega) = M_H + \sum_{l=1}^n \frac{iM_l \omega}{\omega_l + i\omega} \quad (126)$$

with **relaxation frequencies**

$$\omega_l = \frac{M_l}{\eta_l}; \quad l = 1, \dots, n. \quad (127)$$

We find relaxed and unrelaxed moduli

$$M_R \equiv \lim_{\omega \rightarrow 0} M(\omega) = M_H, \quad M_U \equiv \lim_{\omega \rightarrow \infty} M(\omega) = M_R + \sum_{l=1}^n M_l. \quad (128)$$

Since $M_U = M_R + \delta M$,

$$M_l = \delta M_l. \quad (129)$$

Without any simplification we can consider

$$\delta M_l = a_l \delta M; \quad \sum_{l=1}^n a_l = 1. \quad (130)$$

Then

$$M(\omega) = M_R + \delta M \sum_{l=1}^n \frac{ia_l \omega}{\omega_l + i\omega}. \quad (131)$$

Using relation (116) we easily obtain the relaxation function

$$\psi(t) = \left[M_R + \delta M \sum_{l=1}^n a_l e^{-\omega_l t} \right] \cdot H(t), \quad (132)$$

where $H(t)$ is the Heaviside unit step function. The above formulas were presented by Emmerich and Korn (1987).

GZB. From the two equivalent models of the GZB (see Figure 7) we choose the one in which a single ZB is of the H-p-M type (Hooke element in parallel with Maxwell body). This is because we can immediately see the meaning ($M_{Rl}, \delta M_l$) of the elastic moduli of both Hooke elements in each ZB. For the GZB we easily obtain a well-known

$$M(\omega) = \sum_{l=1}^n M_{Rl} \frac{1 + i\tau_{\varepsilon l}\omega}{1 + i\tau_{\sigma l}\omega} \quad (133)$$

with **relaxation times**

$$\tau_{\varepsilon l} = \frac{\eta_l}{\delta M_l} \frac{M_{Ul}}{M_{Rl}}, \quad \tau_{\sigma l} = \frac{\eta_l}{\delta M_l}, \quad \frac{\tau_{\varepsilon l}}{\tau_{\sigma l}} = \frac{M_{Ul}}{M_{Rl}} \quad (134)$$

and

$$M_{Ul} = M_{Rl} + \delta M_l. \quad (135)$$

The unrelaxed and relaxed moduli are

$$\begin{aligned} M_R &\equiv \lim_{\omega \rightarrow 0} M(\omega) = \sum_{l=1}^n M_{Rl} \\ M_U &\equiv \lim_{\omega \rightarrow \infty} M(\omega) = \sum_{l=1}^n M_{Rl} \frac{\tau_{\varepsilon l}}{\tau_{\sigma l}} = M_R + \sum_{l=1}^n \delta M_l. \end{aligned} \quad (136)$$

Using relation (116) we easily obtain the relaxation function

$$\psi(t) = \left\{ \sum_{l=1}^n M_{Rl} \left[1 - \left(1 - \frac{\tau_{\varepsilon l}}{\tau_{\sigma l}} \right) \exp(-t/\tau_{\sigma l}) \right] \right\} \cdot H(t) \quad (137)$$

Assuming simplification (Carcione, 2001)

$$M_{Rl} = \frac{1}{n} M_R \quad (138)$$

we get

$$\begin{aligned} M(\omega) &= \frac{M_R}{n} \sum_{l=1}^n \frac{1 + i\tau_{\varepsilon l}\omega}{1 + i\tau_{\sigma l}\omega}, \\ \psi(t) &= M_R \left[1 - \frac{1}{n} \sum_{l=1}^n \left(1 - \frac{\tau_{\varepsilon l}}{\tau_{\sigma l}} \right) \exp(-t/\tau_{\sigma l}) \right] \cdot H(t) \end{aligned} \quad (139)$$

Formulas (138) and (139) were presented by Carcione (2001). As far as we know, papers dealing with the incorporation of the attenuation based on the GZB, starting from Liu et al. (1976), had the same error – the missing factor $\frac{1}{n}$ in the viscoelastic modulus and relaxation function ($\frac{1}{L}$ in most of the papers, L being the number of classical Zener bodies, that is, the number of relaxation mechanisms).

The Relation between the GZB and GMB-EK

After papers by Emmerich and Korn (1987) and Carcione et al. (1988a,b) different authors decided either for the GMB-EK or GZB.

The GMB-EK formulas were used by Emmerich (1992), Fäh 1992, Moczo and Bard (1993), and in many other papers. Moczo et al. (1997) applied the approach also in the finite-element method and hybrid finite-difference – finite-element method. An important aspect was that in the papers one memory variable was defined for one displacement component. Later Xu and McMechan (1995) introduced term composite memory variables which, however, did not differ from the variables used from the very beginning in the above papers.

Robertsson et al. (1994) implemented the memory variables based on the GZB rheology into the staggered-grid velocity-stress finite-difference scheme. Their numerical results do not suffer from the missing factor $1/n$ because they were performed for $n = 1$. Blanch et al. (1995) suggested an approximate single-parameter method, τ -method, to approximate constant $Q(\omega)$ law. Xu and McMechan (1998) used simulated annealing for determining a best combination of relaxation mechanisms to approximate a desired $Q(\omega)$ law. In the two latter papers the factor $1/n$ was missing in the relaxation functions.

As far as we know, in many following papers the authors using the GZB did not comment on the rheology of the GMB-EK and the corresponding time-domain algorithms, and the authors using the GMB-EK did not comment those for the GZB. Thus, two parallel sets of papers and algorithms had been developed during years.

Therefore, following Moczo and Kristek (2004), look at the relation between the GZB and GMB-EK rheologies. Consider again the ZB (H-p-M) model. The application of the frequency-domain rules (Table 2) to the l -th ZB, that is to (H-p-M), gives

$$\sigma_l(\omega) \cdot \left(\frac{1}{\delta M_l} + \frac{1}{i \eta_l \omega} \right) = \left(1 + \frac{M_{Rl}}{\delta M_l} + \frac{M_{Rl}}{i \eta_l \omega} \right) \cdot \varepsilon(\omega) . \quad (140)$$

Defining

$$\omega_l = \frac{\delta M_l}{\eta_l} \quad (141)$$

and rearranging equation (140) we get

$$\sigma_l(\omega) = M_l(\omega) \cdot \varepsilon(\omega) ; \quad M_l(\omega) = M_{Rl} + \frac{i \delta M_l \omega}{\omega_l + i \omega} . \quad (142)$$

For n ZB (H-p-M) connected in parallel, that is, for the GZB (Figure 7), the stress is

$$\sigma(\omega) = \sum_{l=1}^n \sigma_l(\omega) = \left[\sum_{l=1}^n M_l(\omega) \right] \cdot \varepsilon(\omega) \quad (143)$$

and thus

$$M(\omega) = \sum_{l=1}^n M_{Rl} + \sum_{l=1}^n \frac{i \delta M_l \omega}{\omega_l + i \omega} . \quad (144)$$

Since

$$M_R = \sum_{l=1}^n M_{Rl} , \quad M_U = M_R + \sum_{l=1}^n \delta M_l , \quad M_U = M_R + \delta M , \quad (145)$$

without loss of generality we can consider

$$\delta M_l = a_l \delta M ; \quad \sum_{l=1}^n a_l = 1 \quad (146)$$

and get

$$M(\omega) = M_R + \delta M \sum_{l=1}^n \frac{i a_l \omega}{\omega_l + i \omega} . \quad (147)$$

We see that for the GZB (H-p-M), Figure 7, we obtained exactly the same $M(\omega)$ as it has been obtained by Emmerich and Korn (1987) for their GMB-EK (Figure 6). It is also easy to get the same for the GZB (H-s-KV) or to rewrite non-simplified $\psi(t)$ for the GZB, equation (137), into the form of $\psi(t)$ for the GMB-EK, equation (132), without any simplification. In other words, the rheology of the GMB-EK and GZB is one and the same. As a consequence, we can continue with the GMB-EK and its

simpler-form relations compared to those developed in papers on the GZB with two relaxation times. Also note that there is no need for a simplification (138) in equations (139).

Introduction of the Anelastic Functions

We will use term anelastic functions instead of memory variables. It is easy to rewrite the viscoelastic modulus (147) and relaxation function (132) using the unrelaxed modulus,

$$M(\omega) = M_U - \delta M \sum_{l=1}^n \frac{a_l \omega_l}{\omega_l + i \omega} \quad (148)$$

and

$$\psi(t) = \left[M_U - \delta M \sum_{l=1}^n a_l (1 - e^{-\omega_l t}) \right] \cdot H(t) , \quad (149)$$

and obtain the time derivative of the relaxation function

$$\begin{aligned} M(t) &= \dot{\psi}(t) \\ &= -\delta M \sum_{l=1}^n a_l \omega_l e^{-\omega_l t} \cdot H(t) + \left[M_U - \delta M \sum_{l=1}^n a_l (1 - e^{-\omega_l t}) \right] \cdot \delta(t). \end{aligned} \quad (150)$$

Inserting equation (150) into equation (113) gives

$$\begin{aligned} \sigma(t) &= - \int_{-\infty}^t \delta M \sum_{l=1}^n a_l \omega_l e^{-\omega_l(t-\tau)} \cdot H(t-\tau) \cdot \varepsilon(\tau) d\tau \\ &\quad + \int_{-\infty}^t M_U \cdot \delta(t-\tau) \cdot \varepsilon(\tau) d\tau \\ &\quad - \int_{-\infty}^t \delta M \sum_{l=1}^n a_l (1 - e^{-\omega_l(t-\tau)}) \cdot \delta(t-\tau) \cdot \varepsilon(\tau) d\tau \end{aligned} \quad (151)$$

and

$$\sigma(t) = M_U \cdot \varepsilon(t) - \delta M \sum_{l=1}^n a_l \omega_l \int_{-\infty}^t \varepsilon(\tau) \cdot e^{-\omega_l(t-\tau)} d\tau . \quad (152)$$

Now it is possible to replace the convolution integral by additional functions (**anelastic functions, internal variables, new variables, memory variables**). While Day and Minster (1984), Emmerich and Korn (1987) and Carcione et al. (1988a,b) defined the additional functions as dependent also on the material properties, for an important reason that will be explained later, Kristek and Moczo (2003) defined their anelastic functions as independent of the material properties. Here we follow Kristek and Moczo (2003). Defining an anelastic function

$$\zeta_l(t) = \omega_l \int_{-\infty}^t \varepsilon(\tau) \cdot e^{-\omega_l(t-\tau)} d\tau, \quad l=1, \dots, n \quad (153)$$

we get the stress-strain relation in the form

$$\sigma(t) = M_U \cdot \varepsilon(t) - \sum_{l=1}^n \delta M a_l \zeta_l(t). \quad (154)$$

Applying time derivative to equation (153) we get

$$\begin{aligned} \dot{\zeta}_l(t) &= \omega_l \frac{d}{dt} \int_{-\infty}^t \varepsilon(\tau) \cdot e^{-\omega_l(t-\tau)} d\tau \\ &= \omega_l \left[-\omega_l \int_{-\infty}^t \varepsilon(\tau) \cdot e^{-\omega_l(t-\tau)} d\tau + \varepsilon(t) \right] \\ &= \omega_l \left[-\zeta_l(t) + \varepsilon(t) \right] \end{aligned} \quad (155)$$

and

$$\dot{\zeta}_l(t) + \omega_l \zeta_l(t) = \omega_l \varepsilon(t) \quad ; \quad l=1, \dots, n. \quad (156)$$

Equations (154) and (156) define the time-domain **stress-strain relation for the viscoelastic medium** whose rheology corresponds to rheology of the GMB-EK (and to its equivalent – the GZB).

If the staggered-grid velocity-stress finite-difference scheme is to be used, then the time derivative of the stress is needed. In such a case, $M(t)$ given by equation (150) is inserted into relation (118) and the above procedure of obtaining the anelastic functions and stress-strain relation can be followed with time derivatives of the stress and strain instead of the stress and strain themselves. An alternative procedure is to apply time

derivatives to equations (154) and (156), and define the anelastic function as the time derivative of the anelastic function (153). In either case we obtain

$$\dot{\sigma}(t) = M_U \cdot \dot{\varepsilon}(t) - \sum_{l=1}^n \delta M a_l \xi_l(t) \quad (157)$$

and

$$\dot{\xi}_l(t) + \omega_l \xi_l(t) = \omega_l \dot{\varepsilon}(t) \quad ; \quad l = 1, \dots, n \quad (158)$$

It is useful to define **anelastic coefficients**

$$Y_l = a_l \frac{\delta M}{M_U} \quad ; \quad l = 1, \dots, n \quad (159)$$

Then the stress-strain relations (154) and (157) become

$$\sigma(t) = M_U \cdot \varepsilon(t) - \sum_{l=1}^n M_U Y_l \zeta_l(t) \quad (160)$$

and

$$\dot{\sigma}(t) = M_U \cdot \dot{\varepsilon}(t) - \sum_{l=1}^n M_U Y_l \xi_l(t) \quad (161)$$

The related equations (156) and (158) are unchanged. It is clear that the stress or its time derivative can be calculated if the unrelaxed modulus and anelastic coefficients are known. The unrelaxed modulus is directly related to the elastic speed of wave propagation, the anelastic coefficients have to be determined from $Q(\omega)$ -law.

Using the anelastic coefficient, the elastic modulus and viscosity in the l -th MB are $M_U Y_l$ and $\frac{1}{\omega_l} M_U Y_l$, respectively, the relaxed modulus is

$$M_R = M_U \left(1 - \sum_{l=1}^n Y_l \right),$$

and viscoelastic modulus

$$M(\omega) = M_U \left[1 - \sum_{l=1}^n Y_l \frac{\omega_l}{\omega_l + i \omega} \right] \quad (162)$$

(Note that Emmerich and Korn 1987, used slightly less numerically accurate $y_l = a_l \delta M / M_R$; $l = 1, \dots, n$.) The quality factor (122) is then

$$\frac{1}{Q(\omega)} = \frac{\sum_{l=1}^n Y_l \frac{\omega_l \omega}{\omega_l^2 + \omega^2}}{1 - \sum_{l=1}^n Y_l \frac{\omega_l^2}{\omega_l^2 + \omega^2}} . \quad (163)$$

From equation (163) we can get

$$Q^{-1}(\omega) = \sum_{l=1}^n \frac{\omega_l \omega + \omega_l^2 Q^{-1}(\omega)}{\omega_l^2 + \omega^2} Y_l . \quad (164)$$

Equation (164) can be used to numerically fit any $Q(\omega)$ -law. Emmerich and Korn (1987) demonstrated that a sufficiently accurate approximation to nearly constant $Q(\omega)$ is obtained if the relaxation frequencies ω_l cover the frequency range under interest logarithmically equidistantly. If, for example, $Q(\omega)$ values are known at frequencies $\tilde{\omega}_k$; $k = 1, \dots, 2n-1$, with $\tilde{\omega}_1 = \omega_1$, $\tilde{\omega}_{2n-1} = \omega_n$, equation (164) can be solved for the anelastic coefficients using the least square method.

A more detailed discussion of the frequency range and its sampling by frequencies $\tilde{\omega}_k$ can be found in the paper by Graves and Day (2003; equations 13 and 14).

In practice, a phase velocity at certain reference frequency ω_r , instead of the elastic velocity corresponding to the unrelaxed modulus, is known from measurements. The phase velocity $c(\omega)$ is given by

$$\frac{1}{c(\omega)} = \text{Re} \left[\left(\frac{M(\omega)}{\rho} \right)^{-1/2} \right] . \quad (165)$$

From equations (162) and (165) we get (Moczo et al. 1997) for the phase velocity $c(\omega_r)$

$$M_U = \rho c^2(\omega_r) \frac{R + \Theta_1}{2R^2} , \quad (166)$$

where

$$R = \left(\Theta_1^2 + \Theta_2^2 \right)^{1/2},$$

$$\Theta_1 = 1 - \sum_{l=1}^n Y_l \frac{1}{1 + (\omega_r/\omega_l)^2}, \quad \Theta_2 = \sum_{l=1}^n Y_l \frac{\omega_r/\omega_l}{1 + (\omega_r/\omega_l)^2}. \quad (167)$$

Thus, using equations (166) and (167), the unrelaxed modulus can be determined from the anelastic coefficients Y_l ; $l = 1, \dots, n$, and phase velocity $c(\omega_r)$.

Equations for the 1D Case – A Summary

We can now generalize equations (12) - (15) for the **smoothly heterogeneous viscoelastic medium**. The considered formulations are:

displacement-stress formulation

$$\rho \ddot{d} = \sigma_{,x} + f, \quad \sigma = M_U \cdot \varepsilon - \sum_{l=1}^n M_U Y_l^M \zeta_l \quad (168)$$

$$\dot{\zeta}_l + \omega_l \zeta_l = \omega_l \varepsilon \quad ; \quad l = 1, \dots, n \quad (169)$$

displacement-velocity-stress formulation

$$\rho \dot{v} = \sigma_{,x} + f, \quad v = \dot{d}, \quad \sigma = M_U \cdot \varepsilon - \sum_{l=1}^n M_U Y_l^M \zeta_l \quad (170)$$

$$\dot{\zeta}_l + \omega_l \zeta_l = \omega_l \varepsilon \quad ; \quad l = 1, \dots, n \quad (171)$$

velocity-stress formulation

$$\rho \dot{v} = \sigma_{,x} + f, \quad \dot{\sigma} = M_U \cdot \dot{\varepsilon} - \sum_{l=1}^n M_U Y_l^M \xi_l \quad (172)$$

$$\dot{\xi}_l + \omega_l \xi_l = \omega_l \dot{\varepsilon} \quad ; \quad l = 1, \dots, n \quad (173)$$

displacement formulation

$$\rho \ddot{d} = (M_U \cdot \varepsilon)_{,x} - \sum_{l=1}^n (M_U Y_l^M \zeta_l)_{,x} + f \quad (174)$$

$$\dot{\zeta}_l + \omega_l \zeta_l = \omega_l \varepsilon \quad ; \quad l = 1, \dots, n \quad (175)$$

In equations (168) - (175), M and ε stand for

$\lambda + 2\mu$ and $d_{,x}$ in the case of the P wave

or

2μ and $\frac{1}{2}d_{,x}$ in the case of the S wave.

Note that in the above equations we used the upper index M for the anelastic functions to indicate that the anelastic function corresponds to modulus M .

An FD Scheme for the Anelastic Functions

With the 2nd-order accuracy, ζ_l and $\dot{\zeta}_l$ may be approximated by a simple arithmetic average in time and central difference formula,

$$\zeta_l(t_m) \doteq \frac{1}{2} (\zeta_l(t_{m+1/2}) + \zeta_l(t_{m-1/2})) \quad ; \quad l = 1, \dots, n \quad (176)$$

and

$$\dot{\zeta}_l(t_m) \doteq \frac{1}{\Delta t} (\zeta_l(t_{m+1/2}) - \zeta_l(t_{m-1/2})) \quad ; \quad l = 1, \dots, n \quad (177)$$

respectively, where t_m denotes the m -th time level. Then each of the equations for the anelastic functions can be solved by

$$\zeta_l(t_{m+1/2}) = \frac{2\omega_l \Delta t}{2 + \omega_l \Delta t} \varepsilon(t_m) + \frac{2 - \omega_l \Delta t}{2 + \omega_l \Delta t} \zeta_l(t_{m-1/2}) . \quad (178)$$

In the stress-strain relation related to the time level t_m ,

$$\sigma(t_m) = M_U \cdot \varepsilon(t_m) - \sum_{l=1}^n M_U Y_l^M \zeta_l(t_m) , \quad (179)$$

the value of $\zeta_l(t_m)$ is needed. It is obtained from $\zeta_l(t_{m-1/2})$ and $\zeta_l(t_{m+1/2})$ using equation (176). This means that both values, $\zeta_l(t_{m-1/2})$ and $\zeta_l(t_{m+1/2})$, have to be kept in memory for a spatial position at one time.

It is, however, possible (Kristek and Moczo, 2003) to avoid the necessity to keep in memory both values. Insert equation (178) into (176) and obtain

$$\zeta_l(t_m) = -\frac{\omega_l \Delta t}{2 - \omega_l \Delta t} \varepsilon(t_m) + \frac{2}{2 - \omega_l \Delta t} \zeta_l(t_{m+1/2}) . \quad (180)$$

Insertion of equation (180) into the stress-strain relation (179) and rearrangement gives

$$\sigma(t_m) = \tilde{M} \varepsilon(t_m) - \sum_{l=1}^n \tilde{Y}_l^M \zeta_l(t_{m+1/2}) \quad (181)$$

where

$$\begin{aligned} \tilde{M} &= M_U \left(1 + \sum_{l=1}^n G_{1l} Y_l^M \right) , \quad \tilde{Y}_l^M = G_{2l} M_U Y_l^M \\ G_{1l} &= \frac{\omega_l \Delta t}{2 - \omega_l \Delta t} , \quad G_{2l} = \frac{2}{2 - \omega_l \Delta t} . \end{aligned} \quad (182)$$

Using scheme (178) and a proper scheme for equation (181) it is enough to have only one variable for one anelastic function at one grid position at one time.

Note that equation (181) gives an apparent dependence of $\sigma(t_m)$ on the anelastic function only at the time level $t_{m+1/2}$. This is just due to approximation (176).

In the case of the staggered-grid velocity-stress finite-difference scheme, the form of equations is the same; only ζ_l and ε have to be replaced by ξ_l and $\dot{\varepsilon}$, respectively.

In principle, we could now write FD schemes for solving equations (168) - (175) for the smoothly heterogeneous viscoelastic medium. Instead, we continue with considerations on the presence of a material discontinuity and consequently finish with FD schemes for the viscoelastic medium with both the smooth heterogeneity and material discontinuities.

Contact of Two Viscoelastic Media – A Material Discontinuity

It is not a trivial task to find a heterogeneous formulation of the differential problem if the stress is given in the form of equation (160). In this situation it is, however, possible to try an approximation based on experience with very good accuracy of the FD scheme for the elastic medium with material discontinuities (Moczo et al. 2002). We will follow the approach suggested by Kristek and Moczo (2003) which has been shown sufficiently accurate using numerical tests against the discrete wavenumber method (Bouchon 1981, Coutant 1989).

Consider a contact of two viscoelastic media. Each of the two media is described by a real density and complex frequency dependent modulus given, in the case of the GMB-EK (or, equivalently, GZB) rheology, by equation (162). The question is how to determine density, elastic (unrelaxed) modulus \bar{M}_U , and anelastic coefficients $Y_l^{\bar{M}}$; $l = 1, \dots, n$ for an averaged medium that should represent the contact of two media (that is the boundary conditions at the interface between the two media) if a material discontinuity goes through a grid cell.

We do not have any reason to consider other than volume arithmetic averaging for the density using formula (102).

If we numerically average the viscoelastic modulus in the frequency domain (we can, for example, determine a volume harmonic average over the grid cell), we obtain an average viscoelastic modulus \bar{M} in the frequency domain. Having the averaged viscoelastic modulus, we can determine a quality factor corresponding to this modulus, equation (122), at frequencies $\tilde{\omega}_k$; $k = 1, \dots, 2n-1$:

$$Q_{\bar{M}}(\tilde{\omega}_k) = \text{Re } \bar{M}(\tilde{\omega}_k) / \text{Im } \bar{M}(\tilde{\omega}_k) ; k = 1, 2, \dots, 2n-1 . \quad (183)$$

Having the values $Q_{\bar{M}}(\tilde{\omega}_k)$, $k = 1, 2, \dots, 2n-1$, we can apply a proper curve-fitting procedure in order to approximate a desired/observed $Q(\omega)$ -law. If we assume that the rheology of the averaged medium can be approximated by the GMB-EK rheology, we can apply the least-square method to equation (164) to determine anelastic coefficients $Y_l^{\bar{M}}$; $l = 1, \dots, n$ for the averaged medium from $Q_{\bar{M}}(\tilde{\omega}_k)$, $k = 1, 2, \dots, 2n-1$.

What remains to determine is the average unrelaxed (elastic) modulus \bar{M}_U . It follows from equation (120) that $\bar{M}_U = \lim_{\omega \rightarrow \infty} \bar{M}(\omega)$. An implication is that, in the limit, the harmonic averaging of the viscoelastic modulus gives the harmonic averaging of the unrelaxed modulus. This means that the unrelaxed (elastic) modulus \bar{M}_U for the

averaged viscoelastic medium can be obtained in the same way as in the perfectly elastic medium, for example, using formula (103).

FD Schemes for the 1D Case – A Summary

Now we can summarize the possible FD schemes for the 1D problem in a viscoelastic medium with a smooth variation of material parameters and/or material discontinuities. In addition to already defined discrete variables, let $Z_{I,l}^m$ and E_I^m , be the discrete approximations to $\zeta_{I,l}^m = \zeta(Ih, m\Delta t, \omega_l)$ and $\varepsilon_I^m = \varepsilon(Ih, m\Delta t)$, respectively. Let T_I^m be the discrete approximation now to $\sigma_I^m = \sigma(Ih, m\Delta t)$.

Displacement-stress FD scheme

$$\begin{aligned}
 E_{I+1/2}^m &= \frac{1}{h} \left[a(D_{I+2}^m - D_{I-1}^m) + b(D_{I+1}^m - D_I^m) \right] \quad \text{for the P wave} \\
 E_{I+1/2}^m &= \frac{1}{2h} \left[a(D_{I+2}^m - D_{I-1}^m) + b(D_{I+1}^m - D_I^m) \right] \quad \text{for the S wave} \\
 Z_{I+1/2,l}^{m+1/2} &= \frac{2\omega_l \Delta t}{2 + \omega_l \Delta t} E_{I+1/2}^m + \frac{2 - \omega_l \Delta t}{2 + \omega_l \Delta t} Z_{I+1/2,l}^{m-1/2} \\
 T_{I+1/2}^m &= \tilde{M}_{I+1/2} E_{I+1/2}^m - \sum_{l=1}^n \tilde{Y}_{I+1/2,l}^{\bar{M}} Z_{I+1/2,l}^{m+1/2} \\
 D_I^{m+1} &= 2D_I^m - D_I^{m-1} + \frac{1}{\rho_I^A} \frac{\Delta^2 t}{h} \left[a(T_{I+3/2}^m - T_{I-3/2}^m) + b(T_{I+1/2}^m - T_{I-1/2}^m) \right] \\
 &\quad + \frac{\Delta^2 t}{\rho_I^A} F_I^m
 \end{aligned} \tag{184}$$

where

$$a = -\frac{1}{24} \quad , \quad b = \frac{9}{8} \quad \text{in the 4th-order scheme} \tag{185}$$

$$a = 0 \quad , \quad b = 1 \quad \text{in the 2nd-order scheme} \tag{186}$$

$$\begin{aligned}
 \tilde{\bar{M}}_{I+1/2} &= \bar{M}_{U,I+1/2} \left(1 + \sum_{l=1}^n G_{1l} Y_{I+1/2,l}^{\bar{M}} \right) \\
 \tilde{Y}_{I+1/2,l}^{\bar{M}} &= G_{2l} \bar{M}_{U,I+1/2} Y_{I+1/2,l}^{\bar{M}} \\
 \rho_I^A &= \frac{1}{h} \int_{x_{I-1/2}}^{x_{I+1/2}} \rho(x) dx \\
 \bar{M}_{U,I+1/2} &= \left[\frac{1}{h} \int_{x_I}^{x_{I+1}} \frac{1}{\lambda(x) + 2\mu(x)} dx \right]^{-1} \quad \text{for the P wave} \\
 \bar{M}_{U,I+1/2} &= \left[\frac{1}{h} \int_{x_I}^{x_{I+1}} \frac{1}{2\mu(x)} dx \right]^{-1} \quad \text{for the S wave} \\
 G_{1l} &= \frac{\omega_l \Delta t}{2 - \omega_l \Delta t}, \quad G_{2l} = \frac{2}{2 - \omega_l \Delta t}
 \end{aligned} \tag{187}$$

Displacement-velocity-stress FD scheme

$$\begin{aligned}
 E_{I+1/2}^m &= \frac{1}{h} \left[a(D_{I+2}^m - D_{I-1}^m) + b(D_{I+1}^m - D_I^m) \right] \quad \text{for the P wave} \\
 E_{I+1/2}^m &= \frac{1}{2h} \left[a(D_{I+2}^m - D_{I-1}^m) + b(D_{I+1}^m - D_I^m) \right] \quad \text{for the S wave} \\
 Z_{I+1/2,l}^{m+1/2} &= \frac{2\omega_l \Delta t}{2 + \omega_l \Delta t} E_{I+1/2}^m + \frac{2 - \omega_l \Delta t}{2 + \omega_l \Delta t} Z_{I+1/2,l}^{m-1/2} \\
 T_{I+1/2}^m &= \tilde{\bar{M}}_{I+1/2} E_{I+1/2}^m - \sum_{l=1}^n \tilde{Y}_{I+1/2,l}^{\bar{M}} Z_{I+1/2,l}^{m+1/2} \\
 V_I^{m+1/2} &= V_I^{m-1/2} + \frac{1}{\rho_I^A} \frac{\Delta t}{h} \left[a(T_{I+3/2}^m - T_{I-3/2}^m) + b(T_{I+1/2}^m - T_{I-1/2}^m) \right] \\
 &\quad + \frac{\Delta t}{\rho_I^A} F_I^m \\
 D_I^{m+1} &= D_I^m + \Delta t V_I^{m+1/2}
 \end{aligned} \tag{188}$$

and relations (185) - (187) apply.

Velocity-stress FD scheme

$$\begin{aligned}
 H_{I+1/2}^m &= \frac{1}{h} \left[a(V_{I+2}^m - V_{I-1}^m) + b(V_{I+1}^m - V_I^m) \right] \quad \text{for the } P \text{ wave} \\
 H_{I+1/2}^m &= \frac{1}{2h} \left[a(V_{I+2}^m - V_{I-1}^m) + b(V_{I+1}^m - V_I^m) \right] \quad \text{for the } S \text{ wave} \\
 X_{I+1/2,l}^{m+1/2} &= \frac{2\omega_l \Delta t}{2 + \omega_l \Delta t} H_{I+1/2}^m + \frac{2 - \omega_l \Delta t}{2 + \omega_l \Delta t} X_{I+1/2,l}^{m-1/2} \\
 T_{I+1/2}^m &= T_{I+1/2}^{m-1} + \Delta t \left[\tilde{M}_{I+1/2} H_{I+1/2}^m - \sum_{l=1}^n \tilde{Y}_{I+1/2,l}^{\bar{M}} X_{I+1/2,l}^{m+1/2} \right] \\
 V_I^{m+1/2} &= V_I^{m-1/2} + \frac{1}{\rho_I^A} \frac{\Delta t}{h} \left[a(T_{I+3/2}^m - T_{I-3/2}^m) + b(T_{I+1/2}^m - T_{I-1/2}^m) \right] \\
 &\quad + \frac{\Delta t}{\rho_I^A} F_I^m
 \end{aligned} \tag{189}$$

where $H_{I+1/2}^m$ and $X_{I+1/2,l}^{m\pm 1/2}$ replaced $E_{I+1/2}^m$ and $Z_{I+1/2,l}^{m\pm 1/2}$ as their time derivatives.

Relations (185) - (187) apply.

We do not show here the **displacement FD scheme**. We do not know the 4th-order scheme. A 2nd-order scheme can be obtained easily. The displacement schemes have not been used lately by FD modelers.

Equations and Considerations for the 3D Case

In the 3D case it is assumed that the rheology of the medium is described by one GMB-EK (or, equivalently, GZB) for the complex frequency-dependent bulk modulus and one GMB-EK for the complex frequency-dependent shear modulus. The stress-strain relation is (Kristek and Moczo, 2003)

$$\begin{aligned}
 \sigma_{ij} &= \kappa \varepsilon_{kk} \delta_{ij} + 2\mu \left(\varepsilon_{ij} - \frac{1}{3} \varepsilon_{kk} \delta_{ij} \right) \\
 &\quad - \sum_l^n \left[\kappa Y_l^\kappa \zeta_l^{kk} \delta_{ij} + 2\mu Y_l^\mu \left(\zeta_l^{ij} - \frac{1}{3} \zeta_l^{kk} \delta_{ij} \right) \right]
 \end{aligned} \tag{190}$$

where $i, j, k \in \{1, 2, 3\}$, the equal-index summation convention does not apply to l , $\kappa(x_i)$ and $\mu(x_i)$ are unrelaxed (elastic) bulk and shear moduli, and Y_l^κ and Y_l^μ are the corresponding anelastic coefficients. The latter are obtained from

$$Y_l^\kappa = \left(\alpha^2 Y_l^\alpha - \frac{4}{3} \beta^2 Y_l^\beta \right) / \left(\alpha^2 - \frac{4}{3} \beta^2 \right) , \quad Y_l^\mu = Y_l^\beta ; l = 1, \dots, n , \quad (191)$$

where $\alpha = \left[(\kappa + \frac{4}{3} \mu) / \rho \right]^{1/2}$ and $\beta = (\mu / \rho)^{1/2}$ are elastic (corresponding to unrelaxed moduli) P and S wave velocities, and anelastic coefficients Y_l^α and Y_l^β are obtained from the desired or measured Q_α and Q_β values using the system of equations

$$Q_\nu^{-1}(\tilde{\omega}_k) = \sum_{l=1}^n \frac{\omega_l \tilde{\omega}_k + \omega_l^2 Q_\nu^{-1}(\tilde{\omega}_k)}{\omega_l^2 + \tilde{\omega}_k^2} Y_l^\nu ; k = 1, \dots, 2n-1, \quad \nu \in \{\alpha, \beta\} . \quad (192)$$

For the anelastic functions we have the system of $6n$ independent equations

$$\dot{\zeta}_l^{ij} + \omega_l \zeta_l^{ij} = \omega_l \varepsilon_{ij} ; \quad l = 1, \dots, n , \quad (193)$$

where the equal-index summation convention does not apply to any index.

While equations (190) and (193) are usable for the conventional displacement, or staggered-grid displacement-stress and displacement-velocity-stress finite-difference schemes, equations

$$\begin{aligned} \dot{\sigma}_{ij} = & \kappa \dot{\varepsilon}_{kk} \delta_{ij} + 2\mu \left(\dot{\varepsilon}_{ij} - \frac{1}{3} \dot{\varepsilon}_{kk} \delta_{ij} \right) \\ & - \sum_l^n \left[\kappa Y_l^\kappa \zeta_l^{kk} \delta_{ij} + 2\mu Y_l^\mu \left(\zeta_l^{ij} - \frac{1}{3} \zeta_l^{kk} \delta_{ij} \right) \right] \end{aligned} \quad (194)$$

and

$$\dot{\xi}_l^{ij} + \omega_l \xi_l^{ij} = \omega_l \dot{\varepsilon}_{ij} ; \quad l = 1, \dots, n \quad (195)$$

are needed for the staggered-grid velocity-stress finite-difference schemes. Again, the equal-index summation convention does not apply to index l in equation (194) and to any index in equation (195).

In analogy to the 1D case, we can obtain for the stress-strain relation

$$\zeta_l^{ij}(t_{m+1/2}) = \frac{2\omega_l \Delta t}{2 + \omega_l \Delta t} \varepsilon_{ij}(t_m) + \frac{2 - \omega_l \Delta t}{2 + \omega_l \Delta t} \zeta_l^{ij}(t_{m-1/2}) \quad (196)$$

and

$$\sigma_{ij}(t_m) = \tilde{\kappa} \varepsilon_{kk}(t_m) \delta_{ij} + 2\tilde{\mu} \left(\varepsilon_{ij}(t_m) - \frac{1}{3} \varepsilon_{kk}(t_m) \delta_{ij} \right) - \sum_{l=1}^n \left[\tilde{Y}_l^\kappa \zeta_l^{kk}(t_{m+1/2}) \delta_{ij} + 2\tilde{Y}_l^\mu \left(\zeta_l^{ij}(t_{m+1/2}) - \frac{1}{3} \zeta_l^{kk}(t_{m+1/2}) \delta_{ij} \right) \right], \quad (197)$$

where

$$\begin{aligned} \tilde{\kappa} &= \kappa \left(1 + \sum_{l=1}^n G_{1l} Y_l^\kappa \right), & \tilde{\mu} &= \mu \left(1 + \sum_{l=1}^n G_{1l} Y_l^\mu \right) \\ \tilde{Y}_l^\kappa &= G_{2l} \kappa Y_l^\kappa, & \tilde{Y}_l^\mu &= G_{2l} \mu Y_l^\mu \\ G_{1l} &= \frac{\omega_l \Delta t}{2 - \omega_l \Delta t}, & G_{2l} &= \frac{2}{2 - \omega_l \Delta t}. \end{aligned} \quad (198)$$

Using scheme (196) and a proper scheme for equation (197) it is enough to have only one variable for one anelastic function at one grid position at one time.

In the case of the staggered-grid velocity-stress finite-difference scheme, the form of equations is the same; only ζ_l^{ij} and ε_{ij} have to be replaced by $\dot{\zeta}_l^{ij}$ and $\dot{\varepsilon}_{ij}$.

The FD schemes for the 3D problem can be easily obtained based on the above equations in analogy with the FD schemes (184) - (189).

Notes on the accuracy and computational efficiency. It is obvious that the incorporation of the realistic attenuation considerably increases the number of variables and parameters that have to be kept in computer (core) memory and number of operations. In order to reduce the increased memory requirements and also computational time, Zeng (1996), and, independently, Day (1998), and Day and Bradley (2001) developed approaches that allow spatial sampling of the anelastic functions and coefficients in a grid coarser than the grid for elastic quantities. Graves and Day (2003) analyzed stability and accuracy of the scheme with the coarse spatial sampling and defined effective modulus and quality factor necessary to achieve sufficient accuracy.

A problem with the coarse spatial sampling (coarse graining in Day's terminology) as it is shown in Figure 1 in the papers by Day (1998), and Day and Bradley (2001) is that it may easily happen that the medium from one side of some thought surface or real material discontinuity is characterized over, say, one half of the whole considered frequency range while the medium from the other side of the thought surface or discontinuity is characterized over the other half of the whole frequency range. In other words, the behavior of the two parts of the smoothly heterogeneous medium or two media in contact is characterized in two disjunctive (not overlapping) frequency sub-

intervals. It is then obvious that the two media cannot physically interact. Consequently, the two media cannot be averaged.

In principle, the geometry of the coarse spatial sampling shown in both papers is not the only possible. Keeping the same spatial periodicity of the relaxation frequencies, anelastic coefficients and functions, that is $2h$, it is possible to distribute them in such a way that no surface or material discontinuity can divide the volume of a grid cell into two parts characterized in two disjunctive frequency sub-intervals. Still the alternative spatial distribution does not provide a satisfactory solution because it may happen that one part of the medium (or one medium in contact) will be characterized using, for example, relaxation frequencies $\omega_1, \omega_3, \omega_5, \omega_7$ while the other part of the medium (or the other medium in contact) will be characterized using $\omega_2, \omega_4, \omega_6, \omega_8$, which certainly is not a good solution.

At a given spatial grid point, one can think about accounting for the relaxation frequencies, anelastic coefficients and functions not located at the grid point by a properly weighted values of the anelastic coefficients and functions located around the considered grid point. Such averaging, however, poses a problem: Because the anelastic functions (that is, internal variables or memory variables) originally introduced by Day and Minster (1984), Emmerich and Korn (1987) and Carcione et al. (1988a, b) are material-dependent (as already mentioned), any such spatial averaging (accounting for the functions missing at the considered grid point) would introduce an additional artificial averaging of the material parameters. This, obviously, is not good.

There would be no problem with the coarse spatial sampling and at the same time with weighted spatial averaging of the anelastic functions at a grid point with only one of the all anelastic functions if the anelastic functions were material-independent. Therefore, Kristek and Moczo (2003) introduced material-independent anelastic functions and therefore we followed the approach in this text.

Despite the increasing computer power numerical modelers of seismic wave propagation and earthquake motion have to include at least some of the computer memory and time optimization procedures if they want to address the present-time challenging seismological problems. Irregular spatial grids, grids with varying time steps, characterization of heterogeneity using distribution of material-cell types, core and disk memory optimizations, and parallelization are examples of procedures which can make the FD modeling significantly more efficient. A reader can find more details, for example, in papers by Graves (1996), Moczo et al. (1999), Tessmer (2000), Moczo et al. (2001), Caserta et al. (2002), Kang and Baag (2004).

Program Package 1DFD

The Fortran95 Computer Program Package for Finite-Difference Numerical Generation and Simulation of a 1D Seismic Wavefield in a 1D Heterogeneous Viscoelastic Medium

Introduction

The program package consists of five Fortran95 programs. Three of them,

- program 1DFD_DS,
- program 1DFD_DVS,
- program 1DFD_VS,

perform FD computations according to the

- displacement-stress (DS) staggered-grid FD scheme,
- displacement-velocity-stress (DVS) staggered-grid FD scheme,
- velocity-stress (VS) staggered-grid FD scheme

for a 1D wavefield in a 1D heterogeneous viscoelastic medium. Two other programs,

- program MODEL_PREP_1D,
- program SOURTF,

perform the model and source-time function preparation as input data for the computational programs 1DFD_DS, 1DFD_DVS, 1DFD_VS.

The medium can be bounded from one side (in the programs it is the upper horizontal plane $z = 0$) by either of the following boundaries:

- free surface (traction-free condition),
- plane of symmetry,
- rigid boundary,
- nonreflecting boundary (several types).

The medium can be bounded from the other side (the bottom horizontal plane $z = z_{MAX} > 0$) by a nonreflecting boundary (several types).

The medium can be either

- perfectly elastic or
- viscoelastic with rheology given by the GMB-EK model.

The medium can be

- homogeneous,
- smoothly heterogeneous,
- piece-wise homogeneous (material discontinuities between neighboring homogeneous blocks),
- piece-wise smoothly heterogeneous (material discontinuities between neighboring smoothly heterogeneous blocks).

The material discontinuities can be placed anywhere within the spatial grid, that is, the position of the material discontinuity can be directly at the grid point or anywhere between two neighboring grid points.

The wavefield can be generated by a body-force term whose source-time function represents displacement. (Note that the application of the source-time function corresponding to the particle velocity would give the particle velocity instead of the displacement in the DS and DVS FD schemes. The application of the source-time function corresponding to the particle velocity would give the acceleration instead of the particle velocity in the DVS and VS FD schemes.)

Program 1DFD_DS

Input files

Program 1DFD_DS requires five input files:

- an auxiliary file containing just the name of the current computation,
- an input file with controlling parameters for the computation,
- a file containing the elastic material parameters of the model,
- a file containing the anelastic material parameters of the model,
- a file containing the source-time function.

Auxiliary file '**HF_1DFD_DS**'

The file type is ASCII and contains the following variable:

<i>Name of Variable</i>	<i>Type</i>	<i>Description</i>
JOBNAME	A17	The name of the current computation. This name is taken as a base for constructing the names of other input and output files.

Input data file '**JOBNAME.IN**'

The file type is ASCII and contains several controlling variables associated in the nine namelists. The file also contains positions of receivers.

NAMelist /NAMES/ MO_FILE_NAME, Q_FILE_NAME

<i>Name of Variable</i>	<i>Type</i>	<i>Description</i>
MO_FILE_NAME	A20	The name of the file containing elastic parameters and densities describing material cells. The elastic parameters have to be computed according to equation (103) and densities according to equation (102).
Q_FILE_NAME	A20	The name of the file containing anelastic coefficients describing material cells. The anelastic coefficients have to be computed according to equation (183).

NAMelist /KEYS/ KEY_TLD, KEY_SND

<i>Name of Variable</i>	<i>Type</i>	<i>Description</i>
KEY_TLD	logical	.TRUE.: An output file in ASCII format is generated. It contains time levels of the displacements at specified receivers. .FALSE.: The output file is not generated.
KEY_SND	logical	.TRUE.: An output file in SismoVi format is generated It contains time levels of the displacements at specified receivers. .FALSE.: The output file is not generated.

NAMelist /CONTROLDATA/ MT1 , MT2 , DT , IPAS1 , MZ , H

<i>Name of Variable</i>	<i>Type</i>	<i>Description</i>
MT1, MT2	integer	The computation is performed from the time level MT1 until the time level MT2. MT1 has to be always equal to 1. MT2 has to be an odd number.
DT	real	The time step Δt in seconds. It has to satisfy the stability condition for the 4 th -order staggered grid DS FD scheme, i.e. $\Delta t \leq \frac{6}{7} \frac{h}{v_{\max}}$, where v_{\max} is the maximum P-wave or S-wave velocity and h is a grid spacing.
IPAS1	integer	If IPAS1 = 1, then the displacement values at each time level are stored. If IPAS1 = 2 (3,...), then the displacement values at each second (third,...) time level are stored.
MZ	integer	The total number of the grid points in the grid minus 1. One grid point represents, in fact, one physical horizontal plane.
H	real	The grid spacing in meters. The total size of the grid in meters is (MZ+1)*H.

NAMelist /ATTEN/ FRJMAX, FRANGE, NRFREQ

This namelist refers to inclusion of the realistic model of attenuation based on rheology of the model GMB-EK.

<i>Name of Variable</i>	<i>Type</i>	<i>Description</i>
FRJMAX	real	<p>The upper limit of the frequency range in which the anelastic coefficients Y_l fits the desired Futterman $Q(\omega)$ law by solving equation (164). It should be larger than maximum frequency f_{AC} up to which the computation should be sufficiently accurate. For the 4th-order DS FD scheme $f_{AC} \approx \frac{v_{\min}}{6h}$, where v_{\min} is the minimum velocity in the model and h is a grid spacing. In fact, the effect of the grid dispersion is cumulative with increasing travel distance.</p> <p>If $FRJMAX = 0$, the attenuation is not included.</p>
FRANGE	real	<p>This variable determines the frequency range for the attenuation in which the anelastic coefficients Y_l fit the desired Futterman $Q(\omega)$ law by solving equation (164). $FRANGE = 3$, e.g., means frequency range $\langle FRJMAX * 10^{-3}, FRJMAX \rangle$.</p>
NRFREQ	integer	The number of relaxation frequencies describing the rheology of the GMB-EK.

NAMelist /NONREF/ OMG, WB, KTTO, KTBO

This namelist refers to the nonreflecting boundaries of the grid. Several types of the nonreflecting boundaries are included.

<i>Name of Variable</i>	<i>Type</i>	<i>Description</i>
OMG	real	The dominant frequency in <i>Hz</i> at which artificial reflections should be suppressed more than at other frequencies.
WB	real	The weight coefficient b for the Liu-Archuleta type of nonreflecting boundary (108). It has to satisfy condition $0 \leq b \leq 0.4$.

<i>Name of Variable</i>	<i>Type</i>	<i>Description</i>
KTTO	integer	The key determining type of the top boundary of the grid: < 0: free surface = 0: plane of symmetry = 1: rigid boundary = 2: Reynolds = 3: Peng & Toksöz = 4: Emmerman & Stephen = 5: Clayton & Engquist A1 = 6: Liu-Archuleta
KTBO	integer	The key determining type of the bottom boundary of the grid: = 1: rigid boundary = 2: Reynolds = 3: Peng & Toksöz = 4: Emmerman & Stephen = 5: Clayton & Engquist A1 = 6: Liu-Archuleta

NAMelist /TXT/ TEXT

<i>Name of Variable</i>	<i>Type</i>	<i>Description</i>
TEXT	A20	An arbitrary alphanumeric text (e.g., describing the computation)

NAMelist /SNAP/ IPAS2
 Included only if KEY_SND = .TRUE.

<i>Name of Variable</i>	<i>Type</i>	<i>Description</i>
IPAS2	integer	If IPAS2 = 1, then the displacement values at each time level are stored. If IPAS2 = 2 (3,...), then the displacement values at each second (third,...) time level are stored.

NAMelist /SOURCE/ LS

<i>Name of Variable</i>	<i>Type</i>	<i>Description</i>
LS	integer	The index (position) of the grid point at which the body force will be applied.

NAMelist /REC/ MR

<i>Name of Variable</i>	<i>Type</i>	<i>Description</i>
MR	integer	The number of receivers.

At the end of the file, MR integer numbers in the free form specify grid indices of the receivers. Index 0 means the top boundary of the computational model.

Input data file *MO_FILE_NAME*

The file type is binary and contains the arithmetic averages of density and harmonic averages of modulus in all grid cells. Data is read by

```
READ ( 14 ) ( DEN(L), M (L ), L = 0, MZ )
```

<i>Name of Variable</i>	<i>Type</i>	<i>Description</i>
DEN (L)	real	The arithmetic average of the density in $kg \cdot m^{-3}$. The average is taken over a distance of H centered at the grid point which is the position of the displacement in the grid cell L, see equation (102).
M (L)	real	The harmonic average of the unrelaxed torsion modulus μ (S wave) or $\lambda + 2\mu$ (P wave); both in Pa. The average is taken over a distance of H centered at the grid point which is the position of the displacement in the grid cell L, see equation (103).

Input data file **Q_FILE_NAME**

The file type is binary and contains **NRFREQ** anelastic coefficients for each grid cell. Data is read by

```
READ ( 15 ) ( YM (L,1:NRFREQ), L = 0, MZ)
```

<i>Name of Variable</i>	<i>Type</i>	<i>Description</i>
YM (L, IFREQ)	real	The anelastic material coefficient at the IFREQ-th relaxation frequency corresponding to viscoelastic modulus M determined using equation (183).

Input data file '**STF.DAT**'

The file type is ASCII and contains the source-time function of the body force. Data is read by

```
J = 1
DO
  READ (10,*,IOSTAT = IOS) SOURTF (J)
  IF (IOS == -1) EXIT
  J = J + 1
END DO
```

<i>Name of Variable</i>	<i>Type</i>	<i>Description</i>
SOURTF (J)	real	The source-time function at time level J.

Output files

Program 1DFD_DS generates several output files depending on the input parameters:

- a log file containing the input parameters (as read by the program) and error messages,
- a file containing displacement values at specified receivers in ASCII format if **KEY_TLD = .TRUE.**,

- a file containing displacement values at specified receivers in the SismoVi format if `KEY_SND = .TRUE.` (SismoVi is a Python code for visualization of multiple traces developed by Geza Seriani).

Log file '**JOBNAME.LOG**'

The file type is ASCII and contains the input parameters read from file '**JOBNAME.IN**'. If there is an error, then the file also contains the error message.

Output data file '**JOBNAME_D.DAT**'

The file is generated only if `KEY_TLD = .TRUE.`

The file type is ASCII and contains values of the displacement at the specified receivers at each IPAS1 time level in the column form, e.g.

<i>Time</i>	<i>Displacement values at receiver 1</i>	<i>Displacement values at receiver 2</i>	<i>...</i>	<i>Displacement values at receiver MR</i>
-------------	--	--	------------	---

Output data file '**JOBNAME_SD.DAT**'

The file is generated only if `KEY_SND = .TRUE.`

The file type is ASCII and contains values of the displacement at the specified receivers at each IPAS2 time level in the SismoVi format.

Program 1DFD_DVS

Input files

Program 1DFD_DVS requires five input files:

- an auxiliary file containing just the name of the current computation,
- an input file with controlling parameters for the computation,
- a file containing the elastic material parameters of the model,
- a file containing the anelastic material parameters of the model,
- a file containing the source-time function.

Auxiliary file '**HF_1DFD_DVS**'

The file type is ASCII and contains the following variable:

<i>Name of Variable</i>	<i>Type</i>	<i>Description</i>
JOBNAME	A17	The name of the current computation. This name is taken as a base for constructing the names of other input and output files.

Input data file '**JOBNAME.IN**'

The file type is ASCII and contains several controlling variables associated in the nine namelists. The file also contains positions of receivers.

NAMelist /NAMES/ MO_FILE_NAME, Q_FILE_NAME

<i>Name of Variable</i>	<i>Type</i>	<i>Description</i>
MO_FILE_NAME	A20	The name of the file containing elastic parameters and densities describing material cells. The elastic parameters have to be computed according to equation (103) and densities according to equation (102).
Q_FILE_NAME	A20	The name of the file containing anelastic coefficients describing material cells. The anelastic coefficients have to be computed according to equation (183).

NAMelist /KEYS/ KEY_TLD, KEY_SND, KEY_TLV, KEY_SNV

<i>Name of Variable</i>	<i>Type</i>	<i>Description</i>
KEY_TLD	logical	.TRUE.: An output file in ASCII format is generated. It contains time levels of the displacements at specified receivers. .FALSE.: The output file is not generated.
KEY_SND	logical	.TRUE.: An output file in SismoVi format is generated. It contains time levels of the displacements at specified receivers. .FALSE.: The output file is not generated.
KEY_TLV	logical	.TRUE.: An output file in ASCII format is generated. It contains time levels of the particle velocities at specified receivers. .FALSE.: The output file is not generated.
KEY_SNV	logical	.TRUE.: An output file in SismoVi format is generated. It contains time levels of the particle velocities at specified receivers. .FALSE.: The output file is not generated.

NAMelist /CONTROLDATA/ MT1 , MT2 , DT , IPAS1 , MZ , H

<i>Name of Variable</i>	<i>Type</i>	<i>Description</i>
MT1, MT2	integer	The computation is performed from the time level MT1 until the time level MT2. MT1 has to be always equal to 1.
DT	real	The time step Δt in seconds. It has to satisfy the stability condition for the 4 th -order staggered grid DVS FD scheme, i.e. $\Delta t \leq \frac{6}{7} \frac{h}{v_{\max}}$, where v_{\max} is the maximum P-wave or S-wave velocity and h is a grid spacing.
IPAS1	integer	If IPAS1 = 1, then the displacement and/or particle-velocity values at each time level are stored. If IPAS1 = 2 (3,...), then the displacement and/or particle-velocity values at each second (third,...) time level are stored.

<i>Name of Variable</i>	<i>Type</i>	<i>Description</i>
MZ	integer	The total number of the grid points in the grid minus 1. One grid point represents, in fact, one physical horizontal plane.
H	real	The grid spacing in meters. The total size of the grid in meters is (MZ+1)*H.

NAMelist /ATTEN/ FRJMAX, FRANGE, NRFREQ

This namelist refers to inclusion of the realistic model of attenuation based on rheology of the model GMB-EK.

<i>Name of Variable</i>	<i>Type</i>	<i>Description</i>
FRJMAX	real	<p>The upper limit of the frequency range in which the anelastic coefficients Y_l fits the desired Futterman $Q(\omega)$ law by solving equation (164). It should be larger than maximum frequency f_{AC} up to which the computation should be sufficiently accurate. For the 4th-order DS FD scheme $f_{AC} \approx \frac{v_{\min}}{6h}$, where v_{\min} is the minimum velocity in the model and h is a grid spacing. In fact, the effect of the grid dispersion is cumulative with increasing travel distance.</p> <p>If FRJMAX = 0, the attenuation is not included.</p>
FRANGE	real	<p>This variable determines the frequency range for the attenuation in which the anelastic coefficients Y_l fit the desired Futterman $Q(\omega)$ law by solving equation (164).</p> <p>FRANGE = 3, e.g., means frequency range $\langle \text{FRJMAX} * 10^{-3}, \text{FRJMAX} \rangle$.</p>
NRFREQ	integer	The number of relaxation frequencies describing the rheology of the GMB-EK.

NAMelist /NONREF/ OMG, WB, KTTO, KTBO

This namelist refers to the nonreflecting boundaries of the grid. Several types of the nonreflecting boundaries are included.

<i>Name of Variable</i>	<i>Type</i>	<i>Description</i>
OMG	real	The dominant frequency in <i>Hz</i> at which artificial reflections should be suppressed more than at other frequencies.
WB	real	The weight coefficient <i>b</i> for the Liu-Archuleta type of nonreflecting boundary (108). It has to satisfy condition $0 \leq b \leq 0.4$.
KTTO	integer	The key determining type of the top boundary of the grid: <div style="margin-left: 40px;"> < 0: free surface $= 0$: plane of symmetry $= 1$: rigid boundary $= 2$: Reynolds $= 3$: Peng & Toksöz $= 4$: Emmerman & Stephen $= 5$: Clayton & Engquist A1 $= 6$: Liu-Archuleta </div>
KTBO	integer	The key determining type of the bottom boundary of the grid: <div style="margin-left: 40px;"> $= 1$: rigid boundary $= 2$: Reynolds $= 3$: Peng & Toksöz $= 4$: Emmerman & Stephen $= 5$: Clayton & Engquist A1 $= 6$: Liu-Archuleta </div>

NAMelist /TXT/ TEXT

<i>Name of Variable</i>	<i>Type</i>	<i>Description</i>
TEXT	A20	An arbitrary alphanumeric text (e.g. describing the computation)

NAMelist /SNAP/ IPAS2

Included only if **KEY_SND** = .TRUE. or **KEY_SNV** = .TRUE.

<i>Name of Variable</i>	<i>Type</i>	<i>Description</i>
IPAS2	integer	If IPAS2 = 1, then the displacement and/or particle-velocity values at each time level are stored. If IPAS2 = 2 (3,...), then the displacement and/or particle-velocity values at each second (third,...) time level are stored.

NAMelist /SOURCE/ LS

<i>Name of Variable</i>	<i>Type</i>	<i>Description</i>
LS	integer	The index (position) of the grid point at which the body force will be applied.

NAMelist /REC/ MR

<i>Name of Variable</i>	<i>Type</i>	<i>Description</i>
MR	integer	The number of receivers.

At the end of the file **MR** integer numbers in the free form specify grid indices of the receivers. Index 0 means the top boundary of the computational model.

Input data file **MO_FILE_NAME**

The file type is binary and contains the arithmetic averages of density and harmonic averages of modulus in all grid cells. Data is read by

```
READ ( 14 ) ( DEN(L), M (L ), L = 0, MZ)
```

<i>Name of Variable</i>	<i>Type</i>	<i>Description</i>
DEN (L)	real	The arithmetic average of the density in $kg \cdot m^{-3}$. The average is taken over a distance of H centered at the grid point which is the position of the displacement in the grid cell L, see equation (102).
M (L)	real	The harmonic average of the unrelaxed torsion modulus μ (S wave) or $\lambda + 2\mu$ (P wave); both in Pa. The average is taken over a distance of H centered at the grid point which is the position of the displacement in the grid cell L, see equation (103).

Input data file **Q_FILE_NAME**

The file type is binary and contains NRFREQ anelastic coefficients for each grid cell. Data is read by

```
READ ( 15 ) ( YM (L,1:NRFREQ), L = 0, MZ)
```

<i>Name of Variable</i>	<i>Type</i>	<i>Description</i>
YM (L, IFREQ)	real	The value of the anelastic material coefficient at the IFREQ-th relaxation frequency corresponding to viscoelastic modulus M determined using equation (183).

Input data file **'STF.DAT'**

The file type is ASCII and contains the source-time function of the body force. Data is read by

```

J = 1
DO
  READ (10,*,IOSTAT = IOS) SOURTF (J)
  IF (IOS == -1) EXIT
  J = J + 1
END DO
    
```

<i>Name of Variable</i>	<i>Type</i>	<i>Description</i>
SOURTF (J)	real	The source-time function at time level J.

Output files

Program 1DFD_DVS generates several output files depending on the input parameters:

- a log file containing the input parameters (as read by the program) and error messages,
- a file containing displacement values at specified receivers in ASCII format if KEY_TLD = .TRUE.,
- a file containing displacement values at specified receivers in the SismoVi format if KEY_SND = .TRUE.,
- a file containing particle-velocity values at specified receivers in ASCII format if KEY_TLV = .TRUE.,
- a file containing particle-velocity values at specified receivers in the SismoVi format if KEY_SNV = .TRUE..

Log file '**JOBNAME.LOG**'

The file type is ASCII and contains the input parameters read from file '**JOBNAME.IN**'. If there is some error the file also contains the error message.

Output data file '**JOBNAME_D.DAT**'

The file is generated only if KEY_TLD = .TRUE.

The file type is ASCII and contains values of the displacement at the specified receivers at each IPAS1 time level in the column form, e.g.

<i>Time</i>	<i>Displacement values at receiver 1</i>	<i>Displacement values at receiver 2</i>	<i>...</i>	<i>Displacement values at receiver MR</i>
-------------	--	--	------------	---

Output data file '**JOBNAME_SD.DAT**'

The file is generated only if KEY_SND = .TRUE.

The file type is ASCII and contains values of the displacement at the specified receivers at each IPAS2 time level in the SismoVi format.

Output data file '**JOBNAME_V.DAT**'

The file is generated only if KEY_TLV = .TRUE.

The file type is ASCII and contains values of the particle velocity at the specified receivers at each IPAS1 time level in the column form, e.g.

<i>Time</i>	<i>Particle-velocity values at receiver 1</i>	<i>Particle-velocity values at receiver 2</i>	<i>...</i>	<i>Particle-velocity values at receiver MR</i>
-------------	---	---	------------	--

Output data file '**JOBNAME_SV.DAT**'

The file is generated only if KEY_SNV = .TRUE.

The file type is ASCII and contains values of the particle velocity at the specified receivers at each IPAS2 time level in the SismoVi format.

Program 1DFD_VS

Input files

Program 1DFD_VS requires five input files:

- an auxiliary file containing just the name of the current computation,
- an input file with controlling parameters for the computation,
- a file containing the elastic material parameters of the model,
- a file containing the anelastic material parameters of the model,
- a file containing the source-time function.

Auxiliary file 'HF_1DFD_VS'

The file type is ASCII and contains the following variable:

<i>Name of Variable</i>	<i>Type</i>	<i>Description</i>
JOBNAME	A17	The name of the current computation. This name is taken as a base for constructing the names of other input and output files.

Input data file '*JOBNAME*.IN'

The file type is ASCII and contains several controlling variables associated in the nine namelists. The file also contains positions of receivers.

NAMelist /NAMES/ MO_FILE_NAME, Q_FILE_NAME

<i>Name of Variable</i>	<i>Type</i>	<i>Description</i>
MO_FILE_NAME	A20	The name of the file containing elastic parameters and densities describing material cells. The elastic parameters have to be computed according to equation (103) and densities according to equation (102).
Q_FILE_NAME	A20	The name of the file containing anelastic coefficients describing material cells. The anelastic coefficients have to be computed according to equation (183).

NAMelist /KEYS/ KEY_TLV, KEY_SNV

<i>Name of Variable</i>	<i>Type</i>	<i>Description</i>
KEY_TLV	logical	.TRUE.: An output file in ASCII format is generated. It contains time levels of the particle velocities at specified receivers. .FALSE.: The output file is not generated.
KEY_SNV	logical	.TRUE.: An output file in SismoVi format is generated. It contains time levels of the particle velocities at specified receivers. .FALSE.: The output file is not generated.

NAMelist /CONTROLData/ MT1 , MT2 , DT , IPAS1 , MZ , H

<i>Name of Variable</i>	<i>Type</i>	<i>Description</i>
MT1, MT2	integer	The computation is performed from the time level MT1 until the time level MT2. MT1 has to be always equal to 1.
DT	real	The time step Δt in seconds. It has to satisfy the stability condition for the 4 th -order staggered grid VS FD scheme, i.e. $\Delta t \leq \frac{6}{7} \frac{h}{v_{\max}}$, where v_{\max} is the maximum P-wave or S-wave velocity and h is a grid spacing.
IPAS1	integer	If IPAS1 = 1, then the particle-velocity values at each time level are stored. If IPAS1 = 2 (3,...), then the particle-velocity values at each second (third,...) time level are stored.
MZ	integer	The total number of the grid points in the grid minus 1. One grid point represents, in fact, one physical horizontal plane.
H	real	The grid spacing in meters. The total size of the grid in meters is (MZ+1)*H.

NAMelist /ATTEN/ FRJMAX, FRANGE, NRFREQ

This namelist refers to inclusion of the realistic model of attenuation based on rheology of the model GMB-EK.

<i>Name of Variable</i>	<i>Type</i>	<i>Description</i>
FRJMAX	real	<p>The upper limit of the frequency range in which the anelastic coefficients Y_l fits the desired Futterman $Q(\omega)$ law by solving equation (164). It should be larger than maximum frequency f_{AC} up to which the computation should be sufficiently accurate. For the 4th-order VS FD scheme $f_{AC} \approx \frac{v_{\min}}{6h}$, where v_{\min} is the minimum velocity in the model and h is a grid spacing. In fact, the effect of the grid dispersion is cumulative with increasing travel distance.</p> <p>If FRJMAX = 0, the attenuation is not included.</p>
FRANGE	real	<p>This variable determines the frequency range for the attenuation in which the anelastic coefficients Y_l fit the desired Futterman $Q(\omega)$ law by solving (164). FRANGE = 3, e.g., means frequency range $\langle \text{FRJMAX} * 10^{-3}, \text{FRJMAX} \rangle$.</p>
NRFREQ	integer	The number of relaxation frequencies describing the rheology of the GMB-EK.

NAMelist /NONREF/ OMG, WB, KTTO, KTBO

This namelist refers to the nonreflecting boundaries of the grid. Several types of the nonreflecting boundaries are included.

<i>Name of Variable</i>	<i>Type</i>	<i>Description</i>
OMG	real	The dominant frequency in <i>Hz</i> at which artificial reflections should be suppressed more than at other frequencies.
WB	real	The weight coefficient b for the Liu-Archuleta type of nonreflecting boundary (108). It has to satisfy condition $0 \leq b \leq 0.4$.

<i>Name of Variable</i>	<i>Type</i>	<i>Description</i>
KTTO	integer	<p>The key determining type of the top boundary of the grid:</p> <ul style="list-style-type: none"> < 0: free surface = 0: plane of symmetry = 1: rigid boundary = 2: Reynolds = 3: Peng & Toksöz = 4: Emmerman & Stephen = 5: Clayton & Engquist A1 = 6: Liu-Archuleta
KTBO	integer	<p>The key determining type of the bottom boundary of the grid:</p> <ul style="list-style-type: none"> = 1: rigid boundary = 2: Reynolds = 3: Peng & Toksöz = 4: Emmerman & Stephen = 5: Clayton & Engquist A1 = 6: Liu-Archuleta

NAMelist /TXT/ TEXT

<i>Name of Variable</i>	<i>Type</i>	<i>Description</i>
TEXT	A20	An arbitrary alphanumeric text (e.g. describing the computation)

NAMelist /SNAP/ IPAS2

Included only if KEY_SNV = .TRUE.

<i>Name of Variable</i>	<i>Type</i>	<i>Description</i>
IPAS2	integer	<p>If IPAS2 = 1, then the particle-velocity values at each time level are stored.</p> <p>If IPAS2 = 2 (3,...), then the particle-velocity values at each second (third,...) time level are stored.</p>

NAMelist /SOURCE/ LS

<i>Name of Variable</i>	<i>Type</i>	<i>Description</i>
LS	integer	The index (position) of the grid point at which the body force will be applied.

NAMelist /REC/ MR

<i>Name of Variable</i>	<i>Type</i>	<i>Description</i>
MR	integer	The number of receivers.

At the end of the file MR integer numbers in free form specify grid indices of the receivers. Index 0 means the top boundary of the computational model.

Input data file *MO_FILE_NAME*

The file type is binary and contains the arithmetic averages of density and harmonic averages of modulus in all grid cells. Data is read

```
READ ( 14 ) ( DEN(L), M (L ), L = 0, MZ )
```

<i>Name of Variable</i>	<i>Type</i>	<i>Description</i>
DEN (L)	real	The arithmetic average of the density in $kg \cdot m^{-3}$. The average is taken over a distance of H centered at the grid point which is the position of the displacement in the grid cell L, see equation (102).
M (L)	real	The harmonic average of the unrelaxed torsion modulus μ (S wave) or $\lambda + 2\mu$ (P wave); both in Pa. The average is taken over a distance of H centered at the grid point which is the position of the displacement in the grid cell L, see equation (103).

Input data file **Q_FILE_NAME**

The file type is binary and contains **NRFREQ** anelastic coefficients for each grid cell. Data is read by

```
READ ( 15 ) ( YM (L,1:NRFREQ), L = 0, MZ)
```

<i>Name of Variable</i>	<i>Type</i>	<i>Description</i>
YM (L, IFREQ)	real	The anelastic material coefficient at the IFREQ-th relaxation frequency corresponding to viscoelastic modulus M determined using equation (183).

Input data file '**STF.DAT**'

The file type is ASCII and contains the source-time function of the body force. Data is read by

```
J = 1
DO
  READ (10,*,Iostat = IOS) SOURTF (J)
  IF (IOS == -1) EXIT
  J = J + 1
END DO
```

<i>Name of Variable</i>	<i>Type</i>	<i>Description</i>
SOURTF (J)	real	The source-time function at time level J.

Output files

Program 1DFD_VS generates several output files depending on the input parameters:

- a log file containing the input parameters (as read by the program) and error messages,
- a file containing particle-velocity values at specified receivers in ASCII format if **KEY_TLV = .TRUE.**,

- a file containing particle-velocity values at specified receivers in the SismoVi format if `KEY_SNV = .TRUE.`.

Log file '**JOBNAME.LOG**'

The file type is ASCII and contains the input parameters read from file '**JOBNAME.IN**'. If there is some error the file also contains the error message.

Output data file '**JOBNAME_V.DAT**'

The file is generated only if `KEY_TLV = .TRUE.`

The file type is ASCII and contains values of the particle velocity at the specified receivers at each IPAS1 time level in the column form, e.g.

<i>Time</i>	<i>Particle-velocity values at receiver 1</i>	<i>Particle-velocity values at receiver 2</i>	<i>...</i>	<i>Particle-velocity values at receiver MR</i>
-------------	---	---	------------	--

Output data file '**JOBNAME_SV.DAT**'

The file is generated only if `KEY_SNV = .TRUE.`

The file type is ASCII and contains values of the particle velocity at the specified receivers at each IPAS2 time level in the SismoVi format.

Program MODEL_PREP_1D

Input files

Program MODEL_PREP_1D requires one input file containing control parameters for the model preparation. The physical parameters of the model, i.e., the depth dependence of the velocity, density and quality factor should be described in the Fortran module 'mod_func.f90' using functions. The example is given below.

Input data file 'MODEL.IN'

The file type is ASCII and contains several controlling variables associated in the three namelists.

NAMELIST /CONTROL/ H, ZMAX, PTS, KEY_Q

<i>Name of Variable</i>	<i>Type</i>	<i>Description</i>
H	real	The grid spacing in meters.
ZMAX	real	The size of the model in meters. The top boundary of the model is at $z=0$, the bottom boundary is at $z=ZMAX$.
PTS	integer	The number of points for numerical integration in determination of the arithmetic (102) and harmonic (103) averages. The larger PTS the more precise numerical integration. PTS has to be even.
KEY_Q	logical	.TRUE.: The anelastic coefficients are computed from Q values. .FALSE.: The anelastic coefficients are equal to zero, i.e., the medium is elastic.

NAMelist /OUT_FILES/ MO_FILE_NAME, Q_FILE_NAME

<i>Name of Variable</i>	<i>Type</i>	<i>Description</i>
MO_FILE_NAME	A20	The name of the file containing elastic parameters and densities describing material cells. The elastic parameters are computed according to equation (103) and densities according to equation (102). The generated file is an input file for the FD computation.
Q_FILE_NAME	A20	The name of the file containing anelastic coefficients describing material cells. The anelastic coefficients are computed according to equation (183). The generated file is an input file for the FD computation.

NAMelist /PARAMS/ FRJMAX, FRANGE, NRFREQ, FREF

This namelist refers to inclusion of a realistic model of attenuation based on rheology of the GMB-EK.

<i>Name of Variable</i>	<i>Type</i>	<i>Description</i>
FRJMAX	real	The upper limit of the frequency range in which the anelastic coefficients Y_l fit the desired Futterman $Q(\omega)$ law by solving equation (164). It should be larger than maximum frequency f_{AC} up to which the computation should be sufficiently accurate. For the 4 th -order DS FD scheme $f_{AC} \approx \frac{v_{\min}}{6h}$, where v_{\min} is the minimum velocity in the model and h is a grid spacing. In fact, the effect of the grid dispersion is cumulative with increasing travel distance.
FRANGE	real	This variable determines the frequency range for the attenuation in which the anelastic coefficients Y_l fit the desired Futterman $Q(\omega)$ law. For example, FRANGE = 3 means frequency range $\langle \text{FRJMAX} * 10^{-3}, \text{FRJMAX} \rangle$.
NRFREQ	integer	The number of relaxation frequencies, i.e., the number of classical Maxwell bodies in the GMB-EK.

<i>Name of Variable</i>	<i>Type</i>	<i>Description</i>
FREF	real	The reference frequency at which the velocity and the factor quality are prescribed in the Fortran functions in the module 'mod_func.f90'.

Fortran module 'mod_func.f90'

The file type is ASCII and is a part of program MODEL_PREP_1D. It contains Fortran functions describing the velocity (function FUNCV (Z)), density (function FUNCRHO (Z)), and quality factor (function FUNCQ (Z)) as functions of the depth (i.e., variable z ; $z \in \langle 0, ZMAX \rangle$).

An example for the model of a single layer over halfspace is given below. The depth of a layer is 200 m with wave velocity 625 m/s , density 1600 kg/m^3 , and quality factor 50. The wave velocity in the halfspace is 3126 m/s , density 1800 kg/m^3 , and quality factor 1000 (i.e., the halfspace is elastic).

```

MODULE MOD_FUNC

IMPLICIT NONE

CONTAINS

!----- P or S-wave velocity
FUNCTION FUNCV (Z)

    REAL, INTENT(IN) :: Z
    REAL              :: FUNCV

    IF ( Z < 200.0 ) THEN
        !LAYER
        FUNCV = 625.
    ELSE
        !HALFSPACE
        FUNCV = 3126.
    END IF

END FUNCTION FUNCV

!----- Density
FUNCTION FUNCRHO (Z)

    REAL, INTENT(IN) :: Z
    REAL              :: FUNCRHO

    IF ( Z < 200.0 ) THEN
        !LAYER
        FUNCRHO = 1600.
    ELSE
        !HALFSPACE
        FUNCRHO = 1800.
    END IF

END FUNCTION FUNCRHO

!----- P or S-wave quality factor
FUNCTION FUNCQ (Z)

    REAL, INTENT(IN) :: Z
    REAL              :: FUNCQ

    IF ( Z < 200.0 ) THEN
        !LAYER
        FUNCQ = 50.
    ELSE
        !HALFSPACE
        FUNCQ = 10000.
    END IF

END FUNCTION FUNCQ

END MODULE

```


Output files

Program MODEL_PREP_1D generates three output files:

- a log file containing parameters of the generated grid,
- a file containing the elastic material parameters of the model,
- a file containing the anelastic material parameters of the model.

Log file 'MODEL.LOG'

The file type is ASCII and contains information on the generated grid, specifically:

- the grid spacing in meters,
- the number of grid cells,
- the value of parameter MZ.

Output data file *MO_FILE_NAME*

The file type is binary and contains the arithmetic averages of density and harmonic averages of modulus in all grid cells. The file serves as the input file for the FD computation. Data is written by

```
WRITE ( 14 ) ( DEN(L), M (L ), L = 0, MZ )
```

<i>Name of Variable</i>	<i>Type</i>	<i>Description</i>
DEN (L)	real	The arithmetic average of the density in $kg \cdot m^{-3}$. The average is taken over a distance of H centered at the grid point which is the position of the displacement in the grid cell L, see equation (102).
M (L)	real	The harmonic average of the unrelaxed torsion modulus μ (S wave) or $\lambda + 2\mu$ (P wave); both in Pa. The average is taken over a distance of H centered at the grid point which is the position of the displacement in the grid cell L, see equation (103).

Output data file **Q_***FILE_NAME*

The file type is binary and contains the **NRFREQ** anelastic coefficients for each grid cell. The file serves as the input file for the FD computation. Data is written by

```
WRITE ( 15 ) ( YM (L,1:NRFREQ), L = 0, MZ)
```

<i>Name of Variable</i>	<i>Type</i>	<i>Description</i>
YM (L, IFREQ)	real	The value of the anelastic material coefficient at the IFREQ-th relaxation frequency corresponding to the viscoelastic modulus M determined using equation (183)

Program SOURTF

Input files

Program **SOURTF** requires one input file containing the controlling parameters for the source-time function preparation.

Input file 'SOURTF.IN'

The file type is ASCII and contains several controlling variables associated in the two namelists.

NAMELIST /INPUT/ NSIG, DT

<i>Name of Variable</i>	<i>Type</i>	<i>Description</i>
NSIG	integer	The key determining the type of the generated signal: = 1: Kupper = 2: Ricker = 3: Gabor = 4: Berlage
DT	real	The time step Δt in seconds. It has to be the same as in the FD computation.

The next namelist is one of the following namelists - depending on the chosen type of the input signal.

Kupper signal (NSIG = 1)

The signal is defined by

$$s(t) = \sin\left(2\pi \frac{t}{T}\right) - \frac{1}{2} \sin\left(4\pi \frac{t}{T}\right),$$

where T is approximately the dominant period and the signal is defined in the interval $\langle 0, T \rangle$.

NAMelist /SIGNAL_1/ TP

<i>Name of Variable</i>	<i>Type</i>	<i>Description</i>
TP	real	The dominant period T .

Ricker signal (NSIG = 2)

The signal is defined by

$$s(t) = \frac{\sqrt{\pi}}{2} \left(a - \frac{1}{2} \right) e^{-a}; \quad a = \left(\pi \frac{t - t_S}{t_P} \right)^2,$$

where t_P is the dominant period, $t_S = 1.1t_P$, and the signal is defined in the interval $\langle 0, 2t_S \rangle$.

NAMelist /SIGNAL_2/ TP, TS

<i>Name of Variable</i>	<i>Type</i>	<i>Description</i>
TP	real	The dominant period t_P in seconds.
TS	real	The time shift t_S in seconds. If TS = 0, then TS is determined using $t_S = 1.1t_P$.

Gabor signal (NSIG = 3)

The signal is defined by

$$s(t) = e^{-\left(\frac{2\pi f_P (t - t_S)}{\gamma} \right)^2} \cos(2\pi f_P (t - t_S) + \Psi),$$

where f_P is (for certain values of γ and Ψ) the dominant frequency, γ controls the width of the signal envelope, $t_S = 0.45 \frac{\gamma}{f_P}$, and the signal is defined in the interval $\langle 0, 2t_S \rangle$.

NAMelist /SIGNAL_3/ GAMA, FP, PSI, TS

<i>Name of Variable</i>	<i>Type</i>	<i>Description</i>
GAMA	real	Parameter γ controlling the width of the signal envelope.
FP	real	The dominant frequency f_P in Hz.
PSI	real	Phase Ψ in radians.
TS	real	The time shift t_S in seconds. If TS = 0, then TS is determined using $t_S = 0.45 \frac{\gamma}{f_P}$.

***Berlage signal* (NSIG = 4)**

The signal is defined by

$$s(t) = (t - t_S)^\zeta e^{-\frac{2\pi f_P(t-t_S)}{\gamma}} \sin(2\pi f_P(t - t_S)),$$

where f_P is the dominant frequency, γ controls the width of the signal envelope, and the signal is defined in the interval $\langle 0, t_S \rangle$.

NAMelist /SIGNAL_4/ GAMA, FP, ZETA, TS

<i>Name of Variable</i>	<i>Type</i>	<i>Description</i>
GAMA	real	Parameter γ controlling the width of the signal envelope.
FP	real	The dominant frequency f_P in Hz.
ZETA	real	Parameter ζ .
TS	real	The time shift t_S in seconds.

Output files

Program SOURTF generates three output files:

- a file containing the source-time function which can be read by the FD code,
- a file containing the source-time function and its envelope,
- a file containing the power, amplitude and phase Fourier spectrum of the source-time function.

Output data file 'STF.DAT'

The file type is ASCII and contains the source-time function of the body force. Data is written by

```
DO J = 1, NT
  WRITE (10,*) SOURTF (J)
END DO
```

<i>Name of Variable</i>	<i>Type</i>	<i>Description</i>
SOURTF (J)	real	The source-time function at time level J.

Output data file 'SOURTF.DAT'

The file type is ASCII and contains the source-time function and its envelope in the three-column form, i.e.

<i>Time</i>	<i>Source-time function</i>	<i>Envelope of the source-time function</i>
-------------	---------------------------------	---

Output data file 'SPECTR.DAT'

The file type is ASCII and contains the power, amplitude and phase Fourier spectrum of the source-time function in the four-column form, i.e.

<i>Frequency</i>	<i>Power Fourier spectrum of the source-time function</i>	<i>Amplitude Fourier spectrum of the source-time function</i>	<i>Phase Fourier spectrum of the source-time function</i>
------------------	---	---	---

Numerical Examples

We present three simple numerical examples. They should help reader to use the program package 1DFD. The first example is the model of unbounded homogeneous elastic medium. A user can observe (un)stable behavior of the generated wave depending on the choice of the time step and the source-time function. Moreover, the user can observe performance of different types of nonreflecting boundaries.

The second example is the model of a single elastic layer over a elastic halfspace. The model allows observing the capability of the FD schemes to see a true position of a material discontinuity in the grid, investigate the effect of the layer on the surface motion, particularly, possible resonant phenomena in the layer.

The third example illustrates the incorporation of attenuation in the time-domain FD computations using the GMB-EK rheological model. A model of the unbounded viscoelastic homogeneous medium is used. The user can observe effects of the attenuation on the wave propagation.

All examples are supplemented by several exercises.

The examples together with the program package 1DFD can be found in the attached CD or at <http://www.spice-rtn.org/>.

Unbounded Homogeneous Elastic Medium *Example 1*

Description of the example

Physical model:

The unbounded homogeneous elastic medium with parameters:

P-wave velocity $V_P = 1125 \text{ m/s}$

S-wave velocity $V_S = 625 \text{ m/s}$

Density $\rho = 1600 \text{ kg/m}^3$

Source:

The plane S wave with the source-time function defined by Gabor signal

$$s(t) = e^{-\left(\frac{2\pi f_p(t-t_s)}{\gamma}\right)^2} \cos(2\pi f_p(t-t_s) + \Psi),$$

with parameters $\gamma = 1.0$, $f_P = 0.45 \text{ Hz}$, $\Psi = \frac{\pi}{2}$, $t_S = 1.0 \text{ s}$.

Computational model:

The size of the computational model:	31000 m
The grid spacing:	$h = 50 \text{ m}$
The time step:	$\Delta t \leq \frac{6}{7} \frac{h}{V_S} = 0.0685 \text{ s}$
The top boundary of the computational model:	nonreflecting boundary according to Emerman & Stephen (1983)
The bottom boundary of the computational model:	nonreflecting boundary according to Emerman & Stephen (1983)
The grid position of the body-force:	LS = 12

The chosen grid spacing implies the maximum frequency f_{AC} up to which the computation is sufficiently accurate:

$$f_{AC} = \frac{V_S}{6h} \doteq 2 \text{ Hz}$$

Output:

The receivers are placed at the first 51 grid points from the top boundary of the model. Depending on the applied FD scheme either the displacement (DS scheme) or particle velocity (VS scheme) or both (DVS scheme) will be stored.

Computational procedure

The computational procedure consists of

- the compilation of the computer codes,
- the generation of the computational model,
- the generation of the source-time function,
- the FD computation,
- the drawing of the results.

Compilation of the computer codes:

The program package 1DFD is written in standard Fortran90. Each program has its own Makefile written for the Linux operating systems with Intel® Fortran Compiler

8.0. They have to be edited and changed according to the used Fortran90 compiler. After that the user can compile the program package (using Linux statement 'make' in each directory).

Generation of the computational model:

Program MODEL_PREP_1D can be used to generate the computational model. The physical parameters of the model have to be prescribed in the Fortran module mod_func.f90 which contains three Fortran functions (FUNCV, FUNCRHO and FUNCQ). The listing of the module is below.

The module is in the directory with input files for Exercise 1 and has to be copied into the directory with the source file of program MODEL_PREP_1D. The program has to be recompiled. Then the executable file should be copied back into directory with the input files for Exercise 1. The computation should be run in the directory.

The controlling parameters are read in from file MODEL.IN (see below).

Program MODEL_PREP_1D generates the ASCII log file MODEL.LOG and two binary files, E_01.MO and E_01.Q, which serve as the input files for the FD computation.

mod_func.f90

```

MODULE MOD_FUNC

IMPLICIT NONE

CONTAINS

!----- P or S-wave velocity
FUNCTION FUNCV (Z)

    REAL, INTENT(IN) :: Z
    REAL              :: FUNCV

    FUNCV = 625.

END FUNCTION FUNCV

!----- Density
FUNCTION FUNCRHO (Z)

    REAL, INTENT(IN) :: Z
    REAL              :: FUNCRHO

    FUNCRHO = 1600.

END FUNCTION FUNCRHO

!----- P or S-wave quality factor
FUNCTION FUNCQ (Z)

    FUNCQ = 10000.

END FUNCTION FUNCQ

END MODULE
    
```

MODEL.IN

```

&CONTROL      H = 50, ZMAX = 31000, PTS = 10, KEY_Q = F /
&OUT_FILES    MO_FILE_NAME = 'E_01.MO', Q_FILE_NAME = 'E_01.Q'/
&PARAMS       FRJMAX = 5, FRANGE = 2, FREF = 0.5, NRFREQ = 1/
    
```

Generation of the source-time function:

The source-time function described by Gabor signal can be generated using program **SOURTF**. The executable file should be copied into directory with the input files for Exercise 1 and run there. Program reads the input data from file **SOURTF.IN** (see below) and generates three output files:

- **STF.DAT** containing the source-time function which can be read by the FD code,
- **SOURTF.DAT** containing the source-time function and its envelope,
- **SPECTR.DAT** containing the power, amplitude and phase Fourier spectra of the source-time function.

SOURTF.IN

```
&INPUT          NSIG = 3, DT = 0.0685/

&SIGNAL_3       GAMA = 1.0, FP = 0.45, PSI = 1.570796, TS = 1.0 /
```

The generated source-time function (file **SOURTF.DAT**) can be visualized using program **Gnuplot 4.0** and by running the script **Show_STF.gnuplot**. Similarly, the power Fourier spectrum of the source-time function can be visualized (file **SPECTR.DAT**) by running the script **Show_STF_spec.gnuplot** in **Gnuplot 4.0**.

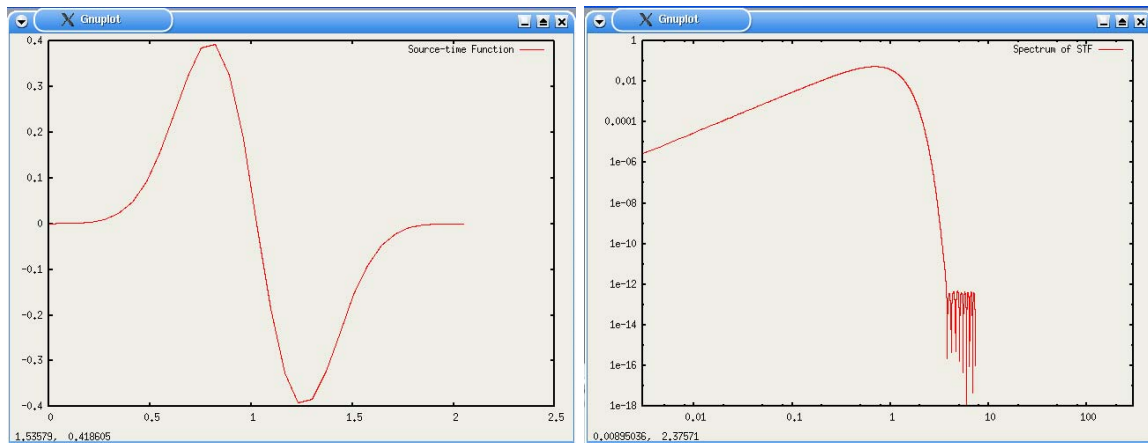


Figure 8. The source-time function, Gabor signal, (left), and its power Fourier spectrum (right) plotted using the Gnuplot scripts **Show_STF.gnuplot** and **Show_STF_spec.gnuplot**

The FD computation:

The next step is the FD computation. There is one input file containing the controlling parameters for each FD code in the directory with the input files for Exercise 1. The name of the input file is read in from the auxiliary file HF_1DFD_DS (or HF_1DFD_DVS or HF_1DFD_VS). The executable files should be copied into this directory and they should be run there.

The FD programs read the input data from file E_DS_01.IN (program 1DFD_DS), or E_DVS_01.IN (program 1DFD_DVS), or E_VS_01.IN (program 1DFD_VS). An example of E_DVS_01.IN is given below.

E_DVS_01.IN	
&NAMES	MO_FILE_NAME = 'E_01.MO', Q_FILE_NAME = 'E_01.Q' /
&KEYS	KEY_TLV = T, KEY_TLD = T, KEY_SNV = T, KEY_SND = T /
&CONTROLDATA	MT1 = 1, MT2 = 300, IPAS1 = 1, MZ = 620, H = 50, DT = 0.0685 /
&ATTEN	FRJMAX = 5., FRANGE = 2., NRFREQ = 1 /
&NONREF	OMG = 3.14, WB = 0.4, KTTO = 4, KTBO = 4 /
&TXT	TEXT = 'EXAMPLE 01' /
&SNAP	IPAS2 = 1 /
&SOURCE	LS = 12 /
&REC	MR = 51 /
50	49 48 47 46 45 44 43 42 41
40	39 38 37 36 35 34 33 32 31
30	29 28 27 26 25 24 23 22 21
20	19 18 17 16 15 14 13 12 11
10	9 8 7 6 5 4 3 2 1
0	

Program 1DFD_DVS produces one log file, E_DVS_01.LOG, and four files containing results:

- E_DVS_01_D.DAT - displacement values in the chosen receivers in the form of columns,
- E_DVS_01_V.DAT - particle velocity values in the chosen receivers in the form of columns,

- E_DVS_01_SD.DAT - displacement values in the chosen receivers in the SismoVi form,
- E_DVS_01_SV.DAT - particle velocity values in the chosen receivers in the SismoVi form.

A quick look at the one of the first two files on the screen can help indicate whether the computation is stable or unstable.

Drawing results:

Results can be drawn using the supplemented program **SismoVi 1.05** with the following settings (see red ellipses in the Fig. 9):

- Overlap: 98%
- Space length: 80

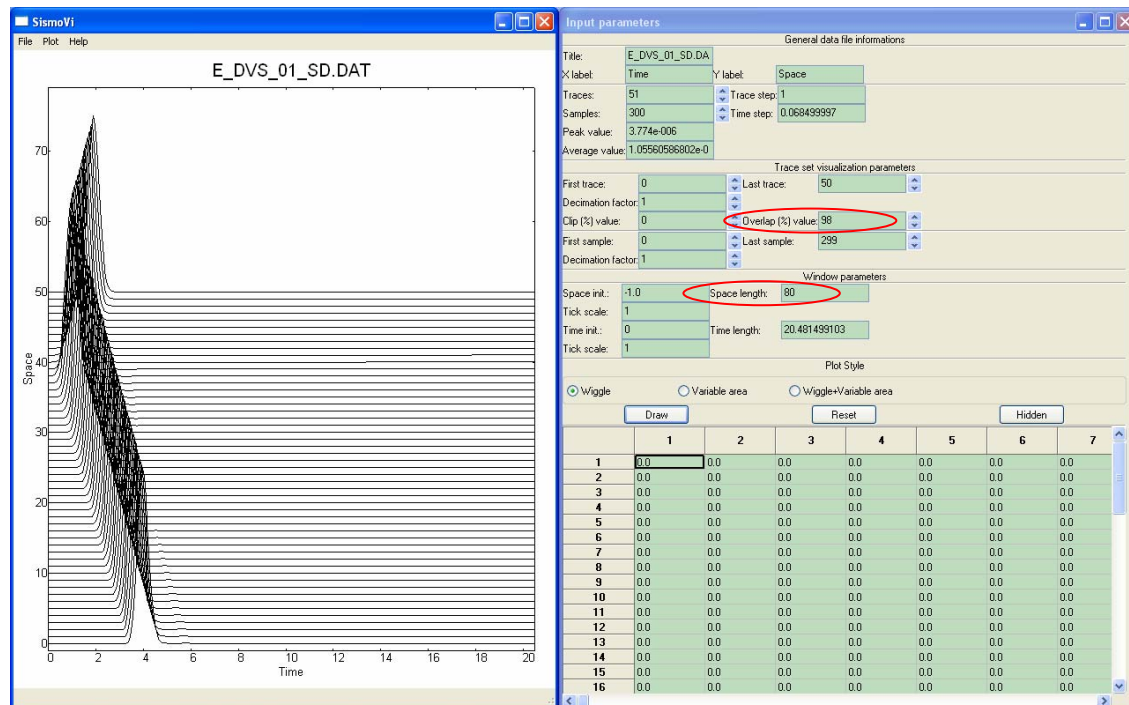


Figure 9. Results of Example 1 plotted using program SismoVi 1.05. Left –Traces of the displacement values stored at 51 receivers starting from the top boundary of the computational model. It is clearly seen that the wavefield is excited from the 13th grid position and there are two waves propagating in the opposite directions. Right – the controlling parameters. The red ellipses indicate the values which have to be changed. Setting up the space-length

parameter to 2 allows seeing spurious reflections from the top boundary of the computational region.

Exercises

- Use either 1D_FD_DS for the displacement-stress FD scheme or 1D_FD_DVS for the displacement-velocity-stress FD scheme or 1D_FD_VS for the velocity-stress scheme and compare results.
- Change the time step DT and observe the effect on stability. See the results when the stability condition is violated.
- Use different types of the nonreflecting boundary and see the amplitude of the spurious reflections. Compare performance of different types of the nonreflecting boundaries.
- Use the source-time functions with various frequency ranges and see the effect of the grid dispersion. The frequency range of Gabor signal is controlled by parameter γ - the lower γ the broader is the frequency range.
- Excite P wave instead of S wave.

Single Layer over Halfspace *Example 2*

Description of the example

Four models of the layer over halfspace are presented. They differ from each other by the layer thickness which is:

- A** 200.0 m
- B** 207.5 m
- C** 237.5 m
- D** 225.0 m

The purpose of computing four modifications is to demonstrate the capability of the scheme to see the true position of the layer-halfspace interface in the spatial grid. In the case of models **B** and **C**, the interface does not coincide with any grid position. For each model theoretical solution obtained by the analytical matrix method (file MICRO.DAT) is provided. (Program MICRO by V.Červený.)

Physical model:

A homogeneous elastic layer over halfspace. Four different layer thicknesses are considered: $\{200.0\text{ m}, 207.5\text{ m}, 237.5\text{ m}, 225.0\text{ m}\}$.

	Layer	Halfspace
P-wave velocity	$V_P = 1125\text{ m/s}$	$V_P = 5468\text{ m/s}$
S-wave velocity	$V_S = 625\text{ m/s}$	$V_S = 3126\text{ m/s}$
Density	$\rho = 1600\text{ kg/m}^3$	$\rho = 1800\text{ kg/m}^3$

Source:

Plane S wave with the source-time function defined by Gabor signal

$$s(t) = e^{-\left(\frac{2\pi f_p(t-t_s)}{\gamma}\right)^2} \cos(2\pi f_p(t-t_s) + \Psi),$$

with parameters: $\gamma = 1.0$, $f_p = 0.45\text{ Hz}$, $\Psi = \frac{\pi}{2}$, $t_s = 1.0\text{ s}$.

The plane wave is excited at the depth of 600 *m*.

Computational model:

The size of the computational model:	31000 <i>m</i>
The grid spacing:	$h = 50 \text{ m}$
The time step:	$\Delta t \leq \frac{6}{7} \frac{h}{\max(V_S)} = 0.0135 \text{ s}$
The top boundary of the computational model:	free-surface (zero-traction) condition
The bottom boundary of the computational model:	nonreflecting boundary according to Emerman & Stephen (1983)
The grid position of the body-force:	LS = 12

The chosen grid spacing implies the maximum frequency f_{AC} up to which the computation is sufficiently accurate:

$$f_{AC} = \frac{\min(V_S)}{6h} \doteq 2 \text{ Hz}$$

Output:

One receiver located at the free surface. Depending on the used FD scheme, either displacement (DS scheme) or particle velocity (VS scheme) or both (DVS scheme) will be stored.

Computational procedure

The computational procedure consists of

- the compilation of the computer codes,
- the generation of the computational model,
- the generation of the source-time function,
- the FD computation,
- the drawing of the results.

Compilation of the computer codes:

The program package 1DFD is written in standard Fortran90. Each program has its own Makefile written for the Linux operating systems with Intel® Fortran Compiler

8.0. They have to be edited and changed according to the used Fortran90 compiler. After that the user can compile the program package (using Linux statement 'make' in each directory).

Generation of the computational model:

Program MODEL_PREP_1D can be used to generate the computational model. The physical parameters of the model have to be prescribed in the Fortran module mod_func.f90 which contains three Fortran functions (FUNCV, FUNC_rho and FUNCQ). The listing of the module is below.

The module is in each subdirectory A, B, C or D of the directory with input files for Exercise 2 and has to be copied into the directory with the source file of program MODEL_PREP_1D. The program has to be recompiled. Then the executable file should be copied back into directory with the input files for Exercise 2. The computation should be run in the directory.

The controlling parameters are read in from file MODEL.IN (see below).

Program MODEL_PREP_1D generates the ASCII log file MODEL.LOG and two binary files, E_02.MO and E_02.Q, which serve as the input files for the FD computation.

MODEL.IN	
&CONTROL	H = 50, ZMAX = 31000, PTS = 100, KEY_Q = F /
&OUT_FILES	MO_FILE_NAME = 'E_02.MO', Q_FILE_NAME = 'E_02.Q' /
&PARAMS	FRJMAX = 5, FRANGE = 2, FREF = 0.5, NRFREQ = 1 /

mod_func.f90 for model A (thickness of a layer 200.0 m)

```
MODULE MOD_FUNC

IMPLICIT NONE

CONTAINS

!----- P or S-wave velocity
FUNCTION FUNCV (Z)

  REAL, INTENT(IN) :: Z
  REAL              :: FUNCV

  IF (Z<200.0) THEN
    !LAYER
    FUNCV = 625.
  ELSE
    !HALFSPACE
    FUNCV = 3126.
  END IF

END FUNCTION FUNCV

!----- Density
FUNCTION FUNCRHO (Z)

  REAL, INTENT(IN) :: Z
  REAL              :: FUNCRHO

  IF (Z<200.0) THEN
    !LAYER
    FUNCRHO = 1600.
  ELSE
    !HALFSPACE
    FUNCRHO = 1800.
  END IF

END FUNCTION FUNCRHO

!----- P or S-wave quality factor
FUNCTION FUNCQ (Z)

  FUNCQ = 10000.

END FUNCTION FUNCQ

END MODULE
```

Generation of the source-time function:

The source-time function described by Gabor signal can be generated using program **SOURTF**. The executable file should be copied into directory with the input files for Exercise 2 and run there. Program reads the input data from file **SOURTF.IN** (see below) and generates three output files:

- **STF.DAT** containing the source-time function which can be read by the FD code,
- **SOURTF.DAT** containing the source-time function and its envelope,
- **SPECTR.DAT** containing the power, amplitude and phase Fourier spectra of the source-time function.

SOURTF.IN

```
&INPUT          NSIG = 3, DT = 0.0135 /
&SIGNAL_3       GAMA = 1.0, FP = 0.45, PSI = 1.570796, TS = 1.0 /
```

The generated source-time function (file **SOURTF.DAT**) can be visualized using program **Gnuplot 4.0** and by running the script **Show_STF.gnuplot**. Similarly, the power Fourier spectrum of the source-time function can be visualized (file **SPECTR.DAT**) by running the script **Show_STF_spec.gnuplot** in **Gnuplot 4.0**.

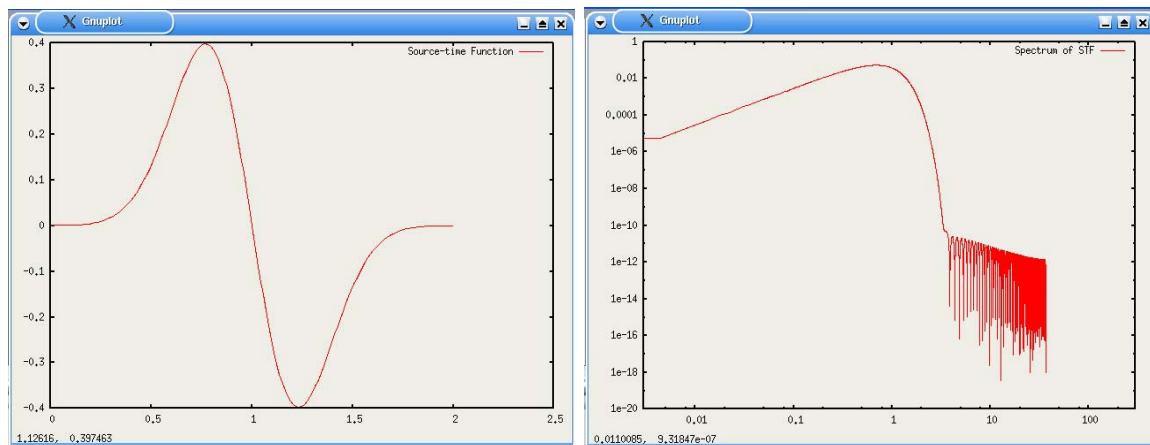


Figure 10. Source-time function described by Gabor signal (left) and its power Fourier spectrum (right) plotted using Gnuplot scripts **Show_STF.gnuplot** and **Show_STF_spec.gnuplot**

The FD computation:

The next step is the FD computation. There is one input file containing the controlling parameters for each FD code in the directory with the input files for Exercise 2. The name of the input file is read in from the auxiliary file HF_1DFD_DS (or HF_1DFD_DVS or HF_1DFD_VS). The executable files should be copied into this directory and they should be run there.

The FD programs read the input data from file E_DS_02.IN (program 1DFD_DS), or E_DVS_02.IN (program 1DFD_DVS), or E_VS_02.IN (program 1DFD_VS). An example of E_DVS_02.IN is given below.

E_DVS_02.IN

```

&NAMES      MO_FILE_NAME = 'E_02.MO', Q_FILE_NAME = 'E_02.Q' /
&KEYS       KEY_TLV = T, KEY_TLD = T, KEY_SNV = T, KEY_SND = T /
&CONTROLDATA MT1 = 1, MT2 = 3000, IPAS1 = 1, MZ = 620, H = 50,
            DT = 0.0137 /
&ATTEN      FRJMAX = 0., FRANGE = 2., NRFREQ = 1 /
&NONREF      OMG = 3.14, WB = 0.4, KTTO = -1, KTBO = 4 /
&TXT        TEXT = 'EXAMPLE 02' /
&SNAP       IPAS2 = 1 /
&SOURCE      LS = 12 /
&REC        MR = 1 /
0
    
```

Program 1DFD_DVS produces one log file, E_DVS_02.LOG, and four files containing results:

- E_DVS_02_D.DAT - displacement values in the chosen receivers in the form of columns,
- E_DVS_02_V.DAT - particle velocity values in the chosen receivers in the form of columns,
- E_DVS_02_SD.DAT - displacement values in the chosen receivers in the SismoVi form,
- E_DVS_02_SV.DAT - particle velocity values in the chosen receivers in the SismoVi form.

A quick look at the one of the first two files on the screen can help indicate whether the computation is stable or unstable.

Drawing results:

Results can be drawn using program **Gnuplot 4.0** and by running script **CompE02.gnuplot** (Fig. 11). Comparison of two particle-velocity traces will be displayed – one by the FD computation (green line) and one obtained by the analytical matrix method using program **MICRO** (red line).

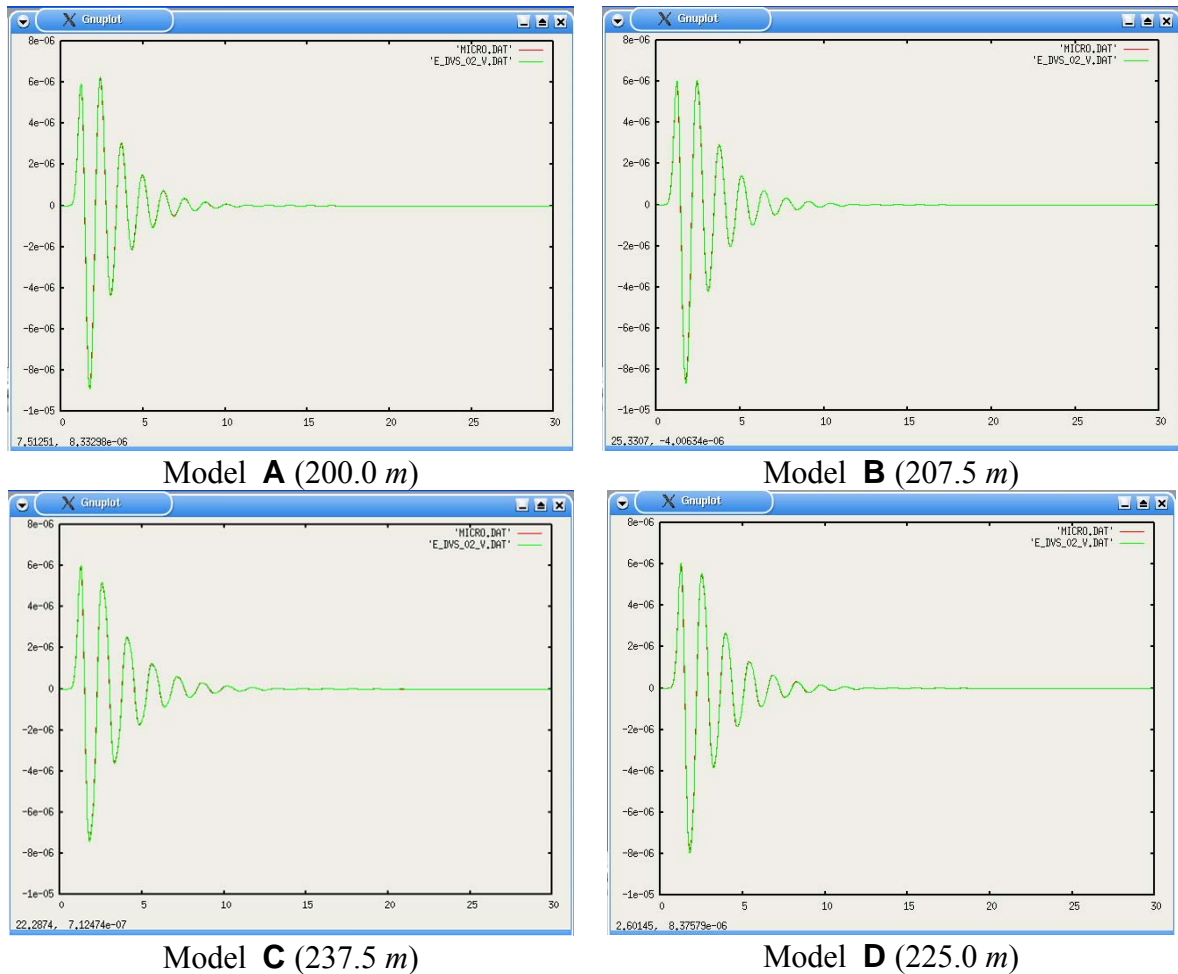


Figure 11. Results of Example 2 plotted using program Gnuplot 4.0. Two traces of the particle velocity recorded at the receiver on the free surface are compared together – the FD solution (green line) and the analytical matrix solution obtained using program MICRO (red line).

Exercises

- Vary the thickness of the layer within one grid spacing and observe differences in the seismic motion.
- Reduce the value of **PTS** in the input file **MODEL.IN** and observe the effect of accuracy of the numerical integration in computation of the effective material parameters on the capability of the FD scheme to see a true position of the material discontinuity.

Unbounded Homogenous Viscoelastic Medium

Example 3

Description of the example

The example illustrates the incorporation of attenuation in the time-domain FD computations using the GMB-EK rheological model. A plane wave is propagated through the viscoelastic medium. Seismograms at two receivers will be used to calculate the frequency-dependent apparent phase velocity $v_{app}(f)$ and apparent quality factor $Q_{app}(f)$.

Let Δx be the distance and $|v(x, f)|$ the Fourier amplitude spectrum of the particle-velocity time history at location x . Then the apparent Q is given by relation

$$Q_{app}^{-1}(f) = -\frac{v_{app}(f)}{\pi f \Delta x} [\ln |v(x + \Delta x, f)| - \ln |v(x, f)|]. \quad (199)$$

The frequency-dependent apparent phase velocity $v_{app}(f)$ is given by

$$v_{app}(f) = 2\pi f \frac{\Delta x}{\Phi(f)}, \quad (200)$$

where $\Phi(f)$ is the difference between the phase Fourier spectra of the particle-velocity time histories at locations $x + \Delta x$ and x . This calculation is performed using the supplemented program APPQ.

Finally, the apparent quality factor $Q_{app}(f)$ will be compared with the quality factor approximated using the GMB-EK, equation (163), where coefficients Y_l are determined by fitting desired $Q(\omega)$ using equation (164). The apparent phase velocity $v_{app}(f)$ will be compared with the phase velocity determined using equation (166).

Physical model:

A homogeneous viscoelastic unbounded medium with parameters:

The reference frequency	$f_{ref} = 0.5 \text{ Hz}$
P-wave velocity at frequency f_{ref}	$V_P(f_{ref}) = 1125 \text{ m/s}$
S-wave velocity at frequency f_{ref}	$V_S(f_{ref}) = 625 \text{ m/s}$

Density	$\rho = 1600 \text{ kg} / \text{m}^3$
Quality factor for P-waves at frequency f_{ref}	$Q_P(f_{ref}) = 50$
Quality factor for S-waves at frequency f_{ref}	$Q_S(f_{ref}) = 50$

Source:

The plane S wave with the source-time function defined by Gabor signal

$$s(t) = e^{-\left(\frac{2\pi f_P(t-t_S)}{\gamma}\right)^2} \cos(2\pi f_P(t-t_S) + \Psi),$$

with parameters: $\gamma = 0.5$, $f_P = 0.45 \text{ Hz}$, $\Psi = \frac{\pi}{2}$, $t_S = 0.5 \text{ s}$.

Computational model:

The size of the computational model:	31000 m
The grid spacing:	$h = 50 \text{ m}$
The time step:	$\Delta t \leq \frac{6}{7} \frac{h}{V_{S_unrelaxed}} = 0.0672 \text{ s}$ but $\Delta t = 0.02 \text{ s}$ will be used for a better estimate of $v_{app}(f)$ and $Q_{app}(f)$.
The top boundary of the computational model:	nonreflecting boundary according to Emerman & Stephen (1983)
The bottom boundary of the computational model:	nonreflecting boundary according to Emerman & Stephen (1983)
The grid position of the body-force:	LS = 112
The number of relaxation frequencies:	4

The frequency range in which the anelastic coefficients Y_l fit the desired Futterman $Q(\omega)$ law, equation (164): $\langle 5 \cdot 10^{-3}, 0.5 \rangle \text{ Hz}$

The chosen grid spacing implies the maximum frequency f_{AC} up to which the computation is sufficiently accurate:

$$f_{AC} = \frac{V_S}{6h} \doteq 2 \text{ Hz}$$

Output:

2 receivers separated by distance of 22 grid points, i.e. 1100 *m*. Depending on the used FD scheme, we will store either displacement (DS scheme) or particle velocity (VS scheme), or both (DVS scheme).

Computational procedure

The computational procedure consists of

- the compilation of the computer codes,
- the generation of the computational model,
- the generation of the source-time function,
- the FD computation,
- the computation of the apparent phase velocity and apparent quality factor,
- the computation of the phase velocity and quality factor in medium with the GMB-EK rheology,
- the comparison of the results.

Compilation of the computer codes:

The program package 1DFD is written in standard Fortran90. Each program has its own Makefile written for the Linux operating systems with Intel® Fortran Compiler 8.0. They have to be edited and changed according to the used Fortran90 compiler. After that the user can compile the program package (using Linux statement ‘make’ in each directory).

Generation of the computational model:

Program MODEL_PREP_1D can be used to generate the computational model. The physical parameters of the model have to be prescribed in the Fortran module mod_func.f90 which contains three Fortran functions (FUNCV, FUNCRHO and FUNCQ). The listing of the module is below.

The module is in the directory with input files for Exercise 3 and has to be copied into the directory with the source file of program MODEL_PREP_1D. The program has to be recompiled. Then the executable file should be copied back into directory with the input files for Exercise 3. The computation should be run in the directory.

The controlling parameters are read in from file MODEL.IN (see below).

mod_func.f90

```
MODULE MOD_FUNC

IMPLICIT NONE

CONTAINS

!----- P or S-wave velocity
  FUNCTION FUNCV (Z)

    REAL, INTENT(IN) :: Z
    REAL              :: FUNCV

    FUNCV = 625.

  END FUNCTION FUNCV

!----- Density
  FUNCTION FUNCRHO (Z)

    REAL, INTENT(IN) :: Z
    REAL              :: FUNCRHO

    FUNCRHO = 1600.

  END FUNCTION FUNCRHO

!----- P or S-wave quality factor
  FUNCTION FUNCQ (Z)

    FUNCQ = 50.

  END FUNCTION FUNCQ

END MODULE
```

MODEL.IN

```
&CONTROL      H = 50, ZMAX = 31000, PTS = 10, KEY_Q = T /  
&OUT_FILES    MO_FILE_NAME = 'E_03.MO',  Q_FILE_NAME = 'E_03.Q' /  
&PARAMS       FRJMAX = 5, FRANGE = 2, FREF = 0.5, NRFREQ = 4 /
```

Program **MODEL_PREP_1D** generates the ASCII log file **MODEL.LOG** and two binary files, **E_03.MO** and **E_03.Q**, which serve as the input files for the FD computation.

Generation of the source-time function:

The source-time function described by Gabor signal can be generated using program **SOURTF**. The executable file should be copied into directory with the input files for Exercise 3 and run there. Program reads the input data from file **SOURTF.IN** (see below) and generates three output files:

- **STF.DAT** containing the source-time function which can be read by the FD code,
- **SOURTF.DAT** containing the source-time function and its envelope,
- **SPECTR.DAT** containing the power, amplitude and phase Fourier spectra of the source-time function.

SOURTF.IN

```
&INPUT         NSIG = 3, DT = 0.02 /  
&SIGNAL_3      GAMA = 0.5, FP = 0.45, PSI = 1.570796, TS = 0.5 /
```

The generated source-time function (file **SOURTF.DAT**) can be visualized using program **Gnuplot 4.0** and by running the script **Show_STF.gnuplot**. Similarly, the power Fourier spectrum of the source-time function can be visualized (file **SPECTR.DAT**) by running the script **Show_STF_spec.gnuplot** in **Gnuplot 4.0**.

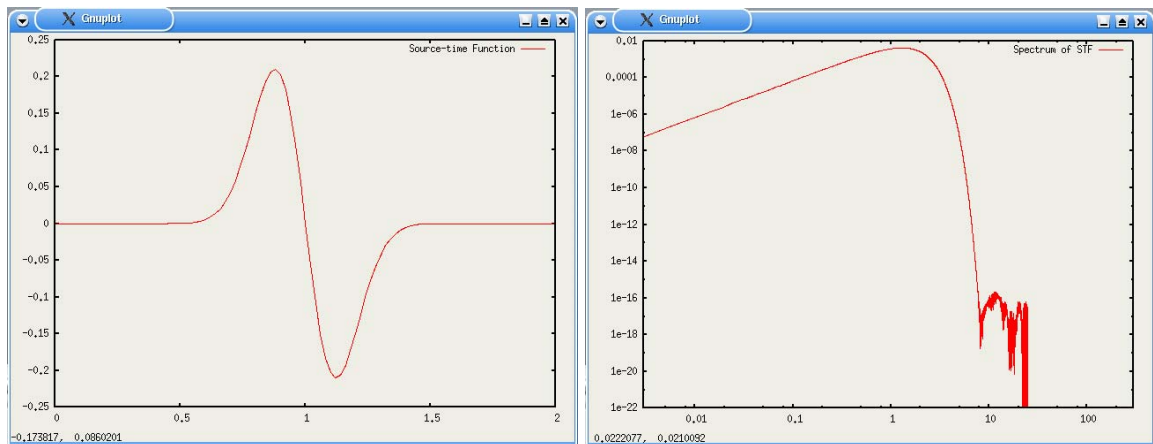


Figure 12. The source-time function, Gabor signal, (left), and its power Fourier spectrum (right) plotted using the Gnuplot scripts `Show_STF.gnuplot` and `Show_STF_spec.gnuplot`

The FD computation:

The next step is the FD computation. There is one input file containing the controlling parameters for each FD code in the directory with the input files for Exercise 1. The name of the input file is read in from the auxiliary file `HF_1DFD_DS` (or `HF_1DFD_DVS` or `HF_1DFD_VS`). The executable files should be copied into this directory and they should be run there.

The FD programs read the input data from file `E_DS_03.IN` (program `1DFD_DS`), or `E_DVS_03.IN` (program `1DFD_DVS`), or `E_VS_03.IN` (program `1DFD_VS`). An example of `E_DVS_03.IN` is given below.

Program `1DFD_DVS` produces one log file, `E_DVS_03.LOG`, and four files containing results:

- `E_DVS_03_D.DAT` - displacement values in the chosen receivers in the form of columns,
- `E_DVS_03_V.DAT` - particle velocity values in the chosen receivers in the form of columns,
- `E_DVS_03_SD.DAT` - displacement values in the chosen receivers in the SismoVi form,
- `E_DVS_03_SV.DAT` - particle velocity values in the chosen receivers in the SismoVi form.

E_DVS_03.IN

```

&NAMES      MO_FILE_NAME = 'E_03.MO', Q_FILE_NAME = 'E_03.Q' /
&KEYS       KEY_TLV = T, KEY_TLD = T, KEY_SNV = T, KEY_SND = T /
&CONTROLDATA MT1 = 1, MT2 = 800, IPAS1 = 1, MZ = 620, H = 50,
            DT = 0.02 /
&ATTEN      FRJMAX = 5., FRANGE = 2., NRFREQ = 4 /
&NONREF     OMG = 3.14, WB = 0.4, KTTO = 4, KTBO = 4 /
&TXT        TEXT = 'EXAMPLE 03' /
&SNAP       IPAS2 = 1 /
&SOURCE     LS = 112 /
&REC        MR = 2 /
88 110
    
```

A quick look at the one of the first two files on the screen can help indicate whether the computation is stable or unstable.

The computation of the apparent phase velocity and apparent quality factor:

Program APPQ can be used to calculate the apparent phase velocity and apparent quality factor according to equations (200) and (199).

The input parameters for program APPQ are read from file 'APPQ.IN' in the following structure:

NAMelist /INPUT/ MT, DT, DX, INPUT_FILE_NAME

<i>Name of Variable</i>	<i>Type</i>	<i>Description</i>
MT	integer	The number of samples in the input file containing the particle-velocity values at two receivers, i.e., the number of stored time levels in the output files of the FD computation.
DT	real	The time step Δt in seconds.

<i>Name of Variable</i>	<i>Type</i>	<i>Description</i>
DX	real	The distance between two receivers (in meters).
INPUT_FILE_NAME	character*20	The name of the input file containing the particle-velocity values at two receivers.

The input file INPUT_FILE_NAME containing the particle-velocity values at two receivers has to be ASCII with following column form:

<i>Time</i>	<i>Particle-velocity values at receiver 1</i>	<i>Particle-velocity values at receiver 2</i>
-------------	---	---

Note, that the plane wave has to propagate from receiver 1 to receiver 2 !

An example of the file 'APPQ.IN':

APPQ.IN	
&INPUT	MT=800, DT=0.02, DX = 1100., INPUT_FILE_NAME = 'E_DVS_03_V.DAT' /

The program will generate file 'APPQ.DAT' containing values of the apparent phase velocity and apparent quality factor in the column form:

<i>Frequency</i>	<i>Apparent quality factor</i>	<i>Apparent phase velocity</i>
------------------	------------------------------------	------------------------------------

The computation of the phase velocity and quality factor in medium with the GMB-EK rheology:

It is possible to numerically fit any $Q(\omega)$ -law using equation (164) and find the corresponding anelastic coefficients Y_l . Then the quality factor $Q(\omega)$ is calculated according to equation (163) and the unrelaxed modulus M_U using equation (166). The phase velocity $c(\omega)$ is calculated using equations (162) and (165).

The procedure to fit specifically Futterman $Q(\omega)$ -law is encoded in program FUTTER. The program generates a file with $Q(\omega)$ and $c(\omega)$ for both the theoretical Futterman $Q(\omega)$ -law and the GMB-EK approximation to the Futterman $Q(\omega)$ -law.

The program works in an interactive regime. The user is supposed to input the following variables: (values in Example 3)

- The reference frequency in Hz (0.5)
- Velocity at the reference frequency in m/s (625.)
- Quality factor at the reference frequency (50.)
- The frequency range (the same value and meaning as variable FRANGE in the input data for the FD computation or model preparation) (2.)
- The maximum frequency (the same value and meaning as variable FRJMAX in the input data for FD computation or model preparation) (5.)
- The number of the relaxation frequencies (the same value and meaning as variable NRFREQ in the input data for the FD computation or model preparation) (4)

The program then calculates and outputs on screen the unrelaxed velocity in m/s and generates the ASCII file 'FUTTER.DAT' with the following column form:

<i>Frequency</i>	<i>Approximated quality factor</i>	<i>Theoretical quality factor</i>	<i>Approximated phase velocity</i>	<i>Theoretical phase velocity</i>
------------------	--	---------------------------------------	--	---------------------------------------

Comparing results:

Results can be compared using program **Gnuplot 4.0** and by running script Show_Q.gnuplot and Show_v.gnuplot, Fig. 13. It is clear from the figure that in the frequency range (0.1, 2.0) Hz the FD computation gives the same apparent $Q_{app}(f)$ as $Q(f)$ approximated by the GMB-EK rheology. The similar comparison is true for the apparent phase velocity $v_{app}(f)$ and the phase velocity $c(f)$ determined by the GMB-EK rheology. Due to the frequency content of the source-time function and due to the grid dispersion a growing discrepancy above 2 Hz can be observed. On the other hand, the discrepancy below 0.1 Hz is due to the short time window of the computed seismic motion.

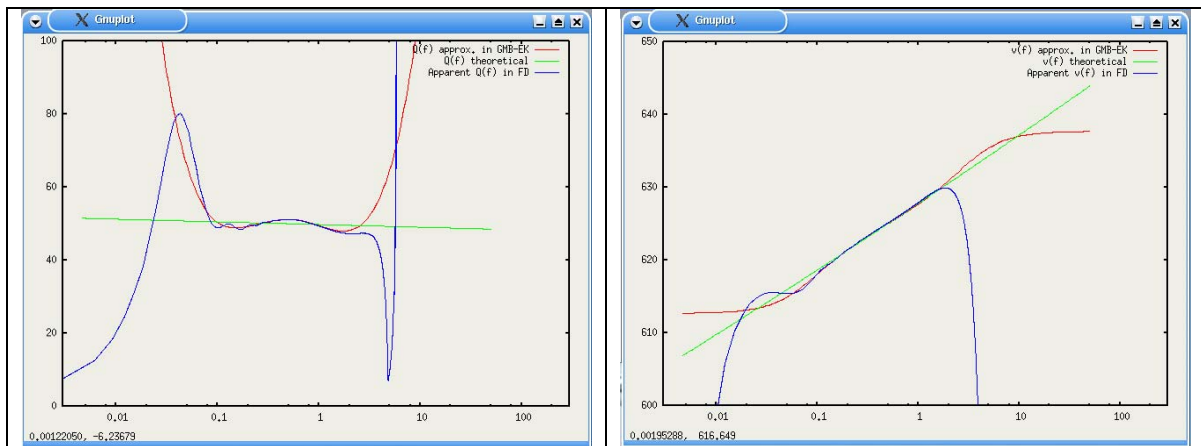


Figure 13. Comparison of the apparent $Q_{app}(f)$ and $v_{app}(f)$ in FD computation (blue), $Q(f)$ and $c(f)$ approximated by the GMB-EK rheology (red) and theoretical Futterman $Q(f)$ -law and $c(f)$ (green).

Exercise

- Change the number of relaxation frequencies, frequency range and maximum frequency and see the variations of seismic motion.

References

- Aki, K. and P. G. Richards, 1980.** Quantitative Seismology. Theory and Methods, Vol. II. *W.H. Freeman & Co.*, San Francisco.
- Alterman, Z. and F. C. Karal, 1968.** Propagation of elastic waves in layered media by finite-difference methods. *Bull. Seism. Soc. Am.* 58, 367-398.
- Andrews, D. J., 1973.** A numerical study of tectonic stress release by underground explosions. *Bull. Seism. Soc. Am.* 63, 1375 – 1391.
- Aoi, S. and H. Fujiwara, 1999.** 3D finite-difference method using discontinuous grids. *Bull. Seism. Soc. Am.* 89, 918-930.
- Bayliss, A., K. E. Jordan, B. J. LeMesurier, and E. Turkel, 1986.** A fourth-order accurate finite-difference scheme for the computation of elastic waves. *Bull. Seism. Soc. Am.* 76, 1115-1132.
- Bérenger, J.-P., 1994.** A perfectly matched layer for the absorption of electromagnetic waves. *J. Comp. Phys.* 114, 185-200.
- Blanch, J. O., J. O. A. Robertsson, and W. W. Symes, 1995.** Modeling of a constant Q: Methodology and algorithm for an efficient and optimally inexpensive viscoelastic technique. *Geophysics* 60, 176-184.
- Boore, D. M., 1970.** Love waves in nonuniform waveguides: finite difference calculations. *J. Geophys. Res.* 75, 1512-1527.
- Boore, D., 1972.** Finite-difference methods for seismic wave propagation in heterogeneous materials. *Methods in Computational Physics*, Vol. 11, B. A. Bolt, ed., *Academic Press*, New York.
- Bouchon, M., 1981.** A simple method to calculate Green's functions for elastic layered media. *Bull. Seism. Soc. Am.* 71, 959-971.
- Carcione, J. M., 2001.** Wave fields in real media: wave propagation in anisotropic, anelastic and porous media. *Pergamon*.

- Carcione, J. M., D. Kosloff, and R. Kosloff, 1988a.** Wave propagation simulation in a linear viscoacoustic medium. *Geophys. J.* 93, 393-407.
- Carcione, J. M., D. Kosloff, and R. Kosloff, 1988b.** Wave propagation simulation in a linear viscoelastic medium. *Geophys. J.* 95, 597-611.
- Caserta, A., V. Ruggiero, and P. Lanucara, 2002.** Numerical modelling of dynamical interaction between seismic radiation and near-surface geological structures: a parallel approach. *Computers & Geosciences* 28, 1069-1077.
- Cerjan, C., D. Kosloff, R. Kosloff and M. Reshef, 1985.** A nonreflecting boundary condition for discrete acoustic and elastic wave equations. *Geophysics* 50, 705-708.
- Chen, Y. H., R. T. Coates, and J. O. A. Robertsson, 2000.** Extension of PML ABC to Elastic Wave Problems in General Anisotropic and Viscoelastic Media: *Schlumberger OFSR research note*.
- Chew, W. C. and Q. H. Liu, 1996.** Perfectly matched layers for elastodynamics: a new absorbing boundary condition. *J. Comp. Acoustics* 4, 341-359.
- Clayton, R. and B. Engquist, 1977.** Absorbing boundary conditions for acoustic and elastic wave equations. *Bull. Seism. Soc. Am.* 67, 1529-1540.
- Collino, F. and C. Tsogka, 1998.** Application of the PML absorbing layer model to the linear elastodynamic problem in anisotropic heterogeneous media. *INRIA*, Rapport de recherche, n. 3471.
- Collino F. and C. Tsogka, 2001.** Applications of the PML absorbing layer model to the linear elastodynamic problem in anisotropic heterogeneous media. *Geophysics* 66, 294-305.
- Coutant, O., 1989.** Program of numerical simulation AXITRA. Res. Rep. LGIT (in French), *Universite Joseph Fourier*, Grenoble.
- Coutant, O., J. Virieux, and A. Zollo, 1995.** Numerical source implementation in a 2D finite difference scheme for wave propagation. *Bull. Seism. Soc. Am.* 85, 1507-1512.

- Crase, E., Ch. Wideman, M. Noble, and A. Tarantola, 1992.** Nonlinear elastic waveform inversion of land seismic reflection data, *J. Geophys. Res.* 97, 4685-4703.
- Cruz-Atienza, V. M. and J. Virieux, 2004.** Dynamic rupture simulation of non-planar faults with a finite-difference approach. *Geophys. J. Int.* 158, 939-954.
- Dablain, M. A., 1986.** The application of high-order differencing to the scalar wave equation. *Geophysics* 51, 54-66.
- Day, S. M., 1998.** Efficient simulation of constant Q using coarse-grained memory variables. *Bull. Seism. Soc. Am.* 88, 1051-1062.
- Day, S. M. and C. R. Bradley, 2001.** Memory-efficient simulation of anelastic wave propagation. *Bull. Seism. Soc. Am.* 91, 520-531.
- Day, S. M. and J. B. Minster, 1984.** Numerical simulation of wavefields using a Padé approximant method. *Geophys. J. Roy. astr. Soc.* 78, 105-118.
- Durran, D. R., 1999.** Numerical methods for wave equations in geophysical fluid dynamics. *Springer*.
- Emerman, S. H. and R. A. Stephen, 1983.** Comment on “Absorbing boundary conditions for acoustic and elastic wave equations,” by R. Clayton and B. Engquist. *Bull. Seism. Soc. Am.* 73, 661-665.
- Emmerich, H., 1992.** PSV-wave propagation in a medium with local heterogeneities: a hybrid formulation and its application. *Geophys. J. Int.* 109, 54-64.
- Emmerich, H. and M. Korn, 1987.** Incorporation of attenuation into time-domain computations of seismic wave fields. *Geophysics* 52, 1252-1264.
- Engquist, B. and A. Majda, 1977.** Absorbing boundary conditions for the numerical simulation of waves. *Math. Comput.* 31, 629–651.
- Falk, J., E. Tessmer, and D. Gajewski, 1996.** Tube wave modelling by the finite-differences method with varying grid spacing. *Pageoph*, 148, 77-93.

- Falk, J., E. Tessmer, and D. Gajewski, 1996.** Efficient finite-difference modelling of seismic waves using locally adjustable time steps. *Geophys. Prosp.*, 46, 603-616.
- Fäh, D., 1992.** A hybrid technique for the estimation of strong ground motion in sedimentary basins. Diss. ETH Nr. 9767, *Swiss Federal Institute of Technology*, Zurich.
- Festa, G. and S. Nielsen, 2003.** PML absorbing boundaries. *Bull. Seism. Soc. Am.*, 93, 891-903.
- Fornberg, B., 1988.** Generation of finite difference formulas on arbitrary spaced grids. *Math. Computation* 51, 699-706.
- Forsythe, G. E. and W. R. Wasow, 1960.** Finite Difference Methods for Partial Differential Equations. *J. Wiley & Sons*, New York.
- Frankel, A., 1993.** Three-dimensional simulations of ground motions in the San Bernardino Valley, California, for hypothetical earthquakes on the San Andreas fault. *Bull. Seism. Soc. Am.* 83, 1020-1041.
- Geller, R. J. and N. Takeuchi, 1995.** A new method for computing highly accurate DSM synthetic seismograms. *Geophys. J. Int.* 123, 449-470.
- Geller, R. J. and N. Takeuchi, 1998.** Optimally accurate second-order time-domain finite difference scheme for the elastic equation of motion: one-dimensional case. *Geophys. J. Int.* 135, 48-62.
- Givoli, D., 2004.** High-order local non-reflecting boundary conditions: a review. *Wave Motion* 39, 319-326.
- Graves, R. W., 1993.** Modeling three-dimensional site response effects in the Marina district basin, San Francisco, California. *Bull. Seism. Soc. Am.* 83, 1042-1063.
- Graves, R. W., 1996.** Simulating seismic wave propagation in 3D elastic media using staggered-grid finite differences. *Bull. Seism. Soc. Am.* 86, 1091-1106.
- Graves, R. W. and S. M. Day, 2003.** Stability and accuracy analysis of coarse-grain viscoelastic simulations. *Bull. Seism. Soc. Am.* 93, 283-300.

- Hayashi, K., D. R. Burns, and M. N. Toksöz, 2001.** Discontinuous-grid finite-difference seismic modeling including surface topography. *Bull. Seism. Soc. Am.* 91, 1750-1764.
- Hestholm, S., 1999.** Three-dimensional finite difference viscoelastic wave modelling including surface topography. *Geophys. J. Int.* 139, 852-878.
- Hestholm, S. and B. Ruud, 2002.** 3D free-boundary conditions for coordinate-transform finite-difference seismic modeling. *Geophys. Prosp.* 50, 463-474.
- Higdon, R. L., 1990.** Radiation boundary conditions for elastic wave propagation. *SIAM J. Num. Analysis* 27, 831-869.
- Higdon, R. L., 1991.** Absorbing boundary conditions for elastic waves. *Geophysics* 56, 231-241.
- Higdon, R. L., 1992.** Absorbing boundary conditions for acoustic and elastic waves in stratified media. *J. Comput. Phys.* 101, 386- 418.
- Higdon, R. L., 1994.** Radiation boundary conditions for dispersive waves. *SIAM J. Num. Analysis* 31, 64-100.
- Igel, H., P. Mora, and B. Riollet, 1995.** Anisotropic wave propagation through finite-difference grids. *Geophysics* 60, 1203-1216.
- Ilan, A. and D. Loewenthal, 1976.** Instability of finite-difference schemes due to boundary conditions in elastic media. *Geophys. Prosp.* 24, 431-453.
- Ilan, A., A. Ungar, and Z. S. Alterman, 1975.** An improved representation of boundary conditions in finite difference schemes for seismological problems. *Geophys. J. R. Astr. Soc.* 43, 727-745.
- Isaacson, E. and H. B. Keller, 1966.** Analysis of Numerical Methods. *J. Wiley & Sons*, New York.
- Israeli, M. and S. A. Orszag, 1981.** Approximation of Radiation Boundary Conditions. *J. Comput. Phys.* 41, 115-135.

- Jastram, C. and A. Behle, 1992.** Acoustic modeling on a grid of vertically varying spacing. *Geophys. Prosp.* 40, 157-169.
- Jastram, C. and E. Tessmer, 1994.** Elastic modelling on a grid with vertically varying spacing. *Geophys. Prosp.* 42, 357-370.
- Kang, T.-S. and Ch.-E. Baag, 2004.** Finite-difference seismic simulation combining discontinuous grids with locally variable timesteps. *Bull. Seism. Soc. Am.*, 94, 207-219.
- Kang, T.-S. and Ch.-E. Baag, 2004.** An efficient finite-difference method for simulating 3D seismic response of localized basin structures. *Bull. Seism. Soc. Am.*, 94, 1690-1705.
- Kelly, K. R., R. W. Ward, S. Treitel, and R. M. Alford, 1976.** Synthetic seismograms: a finite-difference approach. *Geophysics* 41, 2-27.
- Komatitsch, D. and J. Tromp, 2003.** A Perfectly Matched Layer (PML) absorbing condition for the second-order elastic wave equation. *Geophys. J. Int.* 154, 146-153.
- Korn, M. and H. Stöckl, 1982.** Reflection and transmission of Love channel waves at coal seam discontinuities computed with a finite difference method. *J. Geophys.* 50, 171-176.
- Kosloff, R. and D. Kosloff, 1986.** Absorbing boundaries for wave propagation problems. *J. Comp. Phys.* 63, 363-376.
- Kristek, J. and P. Moczo, 2003.** Seismic wave propagation in viscoelastic media with material discontinuities – a 3D 4th-order staggered-grid finite-difference modeling. *Bull. Seism. Soc. Am.* 93, 2273-2280.
- Kristek, J., P. Moczo, and R. J. Archuleta, 2002.** Efficient methods to simulate planar free surface in the 3D 4th-order staggered-grid finite-difference schemes. *Studia Geophys. Geod.* 46, 355-381.
- Kristek, J., P. Moczo, I. Irikura, T. Iwata, and H. Sekiguchi, 1999.** The 1995 Kobe mainshock simulated by the 3D finite differences. *The Effects of Surface Geology on Seismic Motion*, Vol. 3, K. Irikura, K. Kudo, H. Okada, and T. Sasatani, eds., 1361-1368, *Balkema*, Rotterdam.

- Kummer, B. and A. Behle, 1982.** Second-order finite-difference modeling of SH-wave propagation in laterally inhomogeneous media. *Bull. Seism. Soc. Am.* 72, 793-808.
- Laws, R. and E. Kragh, 2002.** Rough seas and time-lapse seismic. *Geophys. Prosp.* 50, 195-208.
- Levander, A. R., 1988.** Fourth-order finite-difference P-SV seismograms. *Geophysics* 53, 1425-1436.
- Lindman, E. L., 1975.** Free space boundary conditions for the time dependent wave equation. *J. Comp. Phys.* 18, 66-78.
- Liu, H.-P., D. L. Anderson, and H. Kanamori, 1976.** Velocity dispersion due to anelasticity; implications for seismology and mantle composition. *Geophys. J. R. astr. Soc.* 47, 41-58.
- Liu, P.-C. and R. J. Archuleta, 2000.** Personal communication.
- Lysmer, J. and R. L. Kuhlemeyer, 1969.** Finite Dynamic Model for Infinite Media. *J. Engng. Mech. Div. ASCE* 95, 859-877.
- Luo, Y. and G. Schuster, 1990.** Parsimonious staggered grid finite-differencing of the wave equation. *Geophys. Res. Let.* 17, 155-158.
- Madariaga, R., 1976.** Dynamics of an expanding circular fault. *Bull. Seism. Soc. Am.* 67, 163-182.
- Magnier, S.-A., P. Mora and A. Tarantola, 1994.** Finite differences on minimal grids. *Geophysics* 59, 1435-1443.
- Mikumo, T. and T. Miyatake, 1987.** Numerical modeling of realistic fault rupture processes. In: *Seismic Strong Motion Synthetics*, B.A. Bolt, ed., *Academic Press*, 91-151.
- Mitchell, A. R., 1969.** Computational Methods in Partial Differential Equations. *J. Wiley & Sons*, London.

- Mitchell, A. R. and D. F. Griffiths, 1994.** The Finite Difference Method in Partial Differential Equations. *J. Wiley & Sons*, New York.
- Mittet, R., 2002.** Free-surface boundary conditions for elastic staggered-grid modeling schemes. *Geophysics* 67, 1616-1623.
- Mizutani, H., 2002.** Accurate and efficient methods for calculating synthetic seismograms when elastic discontinuities do not coincide with the numerical grid. PhD. Thesis. *The University of Tokyo*.
- Moczo, P., 1989.** Finite-difference technique for SH-waves in 2-D media using irregular grids - application to the seismic response problem. *Geophys. J. Int.* 99, 321-329.
- Moczo, P., 1998.** Introduction to Modeling Seismic Wave Propagation by the Finite-Difference Method. Lecture Notes. *Kyoto University*.
- Moczo, P. and P.-Y. Bard, 1993.** Wave diffraction, amplification and differential motion near strong lateral discontinuities. *Bull. Seism. Soc. Am.* 83, 85-106.
- Moczo, P., E. Bystrický, J. Kristek, J. M. Carcione, and M. Bouchon, 1997.** Hybrid modeling of P-SV seismic motion at inhomogeneous viscoelastic topographic structures. *Bull. Seism. Soc. Am.* 87, 1305-1323.
- Moczo, P. and J. Kristek, 2004.** On the rheological models in the time-domain methods for seismic wave propagation. Submitted to *Geophys. Res. Lett.*
- Moczo, P., J. Kristek, and E. Bystrický, 2001.** Efficiency and optimization of the 3D finite-difference modeling of seismic ground motion. *J. Comp. Acoustics* 9, 593-609.
- Moczo, P., J. Kristek, and M. Gális, M., 2004.** Simulation of planar free surface with near-surface lateral discontinuities in the finite-difference modeling of seismic motion. *Bull. Seism. Soc. Am.* 94, 760-768.
- Moczo, P., J. Kristek, and L. Halada, 2000.** 3D 4th-order staggered-grid finite-difference schemes: stability and grid dispersion. *Bull. Seism. Soc. Am.* 90, 587-603.

- Moczo, P., J. Kristek, V. Vavryčuk, R. J. Archuleta, and L. Halada, 2002.** 3D heterogeneous staggered-grid finite-difference modeling of seismic motion with volume harmonic and arithmetic averaging of elastic moduli and densities. *Bull. Seism. Soc. Am.* 92, 3042-3066.
- Moczo, P., P. Labák, J. Kristek, and F. Hron, 1996.** Amplification and differential motion due to an antiplane 2D resonance in the sediment valleys embedded in a layer over the halfspace. *Bull. Seism. Soc. Am.* 86, 1434-1446.
- Moczo, P., M. Lucká, J. Kristek, and M. Kristeková, 1999.** 3D displacement finite differences and a combined memory optimization. *Bull. Seism. Soc. Am.* 89, 69-79.
- Morton, K. W. and D. F. Mayers, 1994.** Numerical Solution of Partial Differential Equations. *Cambridge University Press*.
- Muir, F., J. Dellinger, J. Etgen and D. Nichols, 1992.** Modeling elastic fields across irregular boundaries. *Geophysics* 57, 1189-1193.
- Ohminato, T. and B. A. Chouet, 1997.** A free-surface boundary condition for including 3D topography in the finite-difference method. *Bull. Seism. Soc. Am.* 87, 494-515.
- Olsen, K. B. and G. T. Schuster, 1992.** Seismic hazard analysis in Salt Lake Valley by finite-difference simulation of three dimensional elastic wave propagation. *Scientific Excellence in High Performance Computing: The 1990 IBM Price Papers*, Vol. 1, Sec. 6, Baldwin Press, Athens, Georgia, 135-165.
- Opršal, I. and J. Zahradník, 1999.** Elastic finite-difference method for irregular grids. *Geophysics* 64, 240-250.
- Peng, C. and M. N. Toksöz, 1994.** An optimal absorbing boundary condition for finite difference modeling of acoustic and elastic wave propagation. *J. Acoust. Soc. Am.* 95, 733-745.
- Peng, C. and M. N. Toksöz, 1995.** An optimal absorbing boundary condition for elastic wave modeling. *Geophysics* 60, 296-301.
- Pitarka, A., 1999.** 3D elastic finite-difference modeling of seismic motion using staggered grids with nonuniform spacing. *Bull. Seism. Soc. Am.* 89, 54-68.

- Randall, C. J., 1988.** Absorbing boundary condition for the elastic wave equation. *Geophysics* 53, 611-624.
- Renaut, R. A. and J. Petersen, 1989.** Stability of wide-angle absorbing boundary conditions for the wave equation. *Geophysics* 54, 1153-1163.
- Reynolds, A. C., 1978.** Boundary conditions for the numerical solution of wave propagation problems. *Geophysics* 43, 1099-1110.
- Richtmyer, R. D. and K. W. Morton, 1967.** Difference Methods for Initial Value Problems. J. Wiley & Sons, New York; (reprinted by Kreiger, New York, 1994).
- Robertsson, J. O. A., 1996.** A numerical free-surface condition for elastic/viscoelastic finite-difference modeling in the presence of topography. *Geophysics* 61, 1921-1934.
- Robertsson, J. O. A., J. O. Blanch, and W. W. Symes, 1994.** Viscoelastic finite-difference modeling. *Geophysics* 59, 1444-1456.
- Robertsson, J. O. A. and K. Holliger, 1997.** Modeling of seismic wave propagation near the Earth's surface. *Phys. Earth Planet. Int.* 104, 193-211.
- Rodrigues, D., 1993.** Large scale modelling of seismic wave propagation. PhD. Thesis, *Ecole Centrale Paris*.
- Saenger, E. H., N. Gold, and S. A. Shapiro, 2000.** Modeling the propagation of elastic waves using a modified finite-difference grid. *Wave Motion* 31, 77-92.
- Saenger, E. H. and T. Bohlen, 2004.** Finite-difference modeling of viscoelastic and anisotropic wave propagation using the rotated staggered grid. *Geophysics* 69, 583-591.
- Schoenberg, M. and F. Muir, 1989.** A calculus for finely layered anisotropic media. *Geophysics* 54, 581-589.
- Sochacki, J. S., J. H. George, R. E. Ewing, and S. B. Smithson, 1991.** Interface conditions for acoustic and elastic wave propagation. *Geophysics* 56, 168-181.

- Sochacki, J. S., R. Kubichek, J. H. George, W. R. Fletcher, and S. B. Smithson, 1987.** Absorbing boundary conditions and surface waves. *Geophysics* 52, 60-71.
- Stacey, R., 1988.** Improved transparent boundary formulations for the elastic-wave equation. *Bull. Seism. Soc. Am.* 78, 2089-2097.
- Takeuchi, N. and R. J. Geller, 2000.** Optimally accurate second order time-domain finite difference scheme for computing synthetic seismograms in 2-D and 3-D media. *Phys. Earth Planet. Int.* 119, 99-131.
- Tessmer, E., 2000.** Seismic finite-difference modeling with spatially varying time steps. *Geophysics* 65, 1290-1293.
- Virieux, J., 1984.** SH-wave propagation in heterogeneous media: velocity-stress finite-difference method. *Geophysics* 49, 1933-1957.
- Virieux, J., 1986.** P-SV wave propagation in heterogeneous media: velocity-stress finite-difference method. *Geophysics* 51, 889-901.
- Wang, Y., J. Xu, and G. T. Schuster, 2001.** Viscoelastic wave simulation in basins by a variable-grid finite-difference method. *Bull. Seism. Soc. Am.* 91, 1741-1749.
- Xu, T. and G. A. McMechan, 1995.** Composite memory variables for viscoelastic synthetic seismograms. *Geophys. J. Int.* 121, 634-639.
- Xu, T. and G. A. McMechan, 1998.** Efficient 3-D viscoelastic modeling with application to near-surface land seismic data. *Geophysics* 63, 601-612.
- Yomogida, K. and J. T. Etgen, 1993.** 3-D wave propagation in the Los Angeles basin for the Whittier-Narrows earthquake. *Bull. Seism. Soc. Am.* 83, 1325-1344.
- Zahradník, J., 1995a.** Comment on ‘A hybrid method for estimation of ground motion in sedimentary basins: Quantitative modeling for Mexico City’ by D. Fäh, P. Suhadolc, St. Mueller and G.F. Panza. *Bull. Seism. Soc. Am.* 85, 1268-1270.
- Zahradník, J., 1995b.** Simple elastic finite-difference scheme. *Bull. Seism. Soc. Am.* 85, 1879-1887.

- Zahradník, J. and P. Moczo, 1996.** Hybrid seismic modeling based on discrete-wavenumber and finite-difference methods. *Pageoph* 148, 21-38.
- Zahradník, J. and E. Priolo, 1995.** Heterogeneous formulations of elastodynamic equations and finite-difference schemes. *Geophys. J. Int.*, 120, 663-676.
- Zeng, X., 1996.** Finite difference modeling of viscoelastic wave propagation in a generally heterogeneous medium in the time domain, and a dissection method in the frequency domain. Ph.D. Thesis, *University of Toronto*.
- Zhang, J., 1997.** Quadrangle-grid velocity-stress finite-difference method for elastic-wave-propagation simulation. *Geophys. J. Int.* 131, 127-134.
- Zhu, J., 1999.** A transparent boundary technique for numerical modeling of elastic waves. *Geophysics* 64, 963-966.

The Finite-Difference Method for Seismologists

An Introduction

2004, Peter Moczo, Jozef Kristek, Ladislav Halada

Cover Design by Martin Gális
Published by the Comenius University Bratislava
First Edition, 158 pages, 2 Tables, 13 Figures
Published 2004

ISBN 80-223-2000-5